

Electronic Thesis and Dissertation Repository

---

11-26-2018 1:30 PM

## Transient Analysis of Full Scale and Experimental Downburst Flows

Junayed Chowdhury, *The University of Western Ontario*

Supervisor: Hangan, Horia, *The University of Western Ontario*

A thesis submitted in partial fulfillment of the requirements for the Master of Engineering Science degree in Civil and Environmental Engineering

© Junayed Chowdhury 2018

Follow this and additional works at: <https://ir.lib.uwo.ca/etd>



Part of the [Aerodynamics and Fluid Mechanics Commons](#), [Civil and Environmental Engineering Commons](#), [Environmental Design Commons](#), and the [Mechanical Engineering Commons](#)

---

### Recommended Citation

Chowdhury, Junayed, "Transient Analysis of Full Scale and Experimental Downburst Flows" (2018). *Electronic Thesis and Dissertation Repository*. 5861.  
<https://ir.lib.uwo.ca/etd/5861>

This Dissertation/Thesis is brought to you for free and open access by Scholarship@Western. It has been accepted for inclusion in Electronic Thesis and Dissertation Repository by an authorized administrator of Scholarship@Western. For more information, please contact [wlsadmin@uwo.ca](mailto:wlsadmin@uwo.ca).

# Abstract

Downbursts are highly transient natural phenomena which produce strong downdrafts evolving from a cumulonimbus cloud. They induce an outburst of damaging winds on or near to the ground causing an immense damage to the ground mounted structures and aircrafts. This study investigates the transient nature of downbursts using wind speed records from full scale downburst events employing an objective methodology. This method can detect the abrupt change points in a downburst time series based on statistical parameters such as mean, standard deviation and linear trend. In addition to the analysis of the full scale downburst events, several large scale experimental model downbursts are produced in the Wind Engineering, Energy and Environment (WindEEE) Dome at Western University by varying downdraft jet diameter and jet velocity to comprehensively characterize the downburst flow field. High resolution surface layer data is captured using Cobra probes and dynamics of the downburst vortices is investigated using Particle Image Velocimetry (PIV) Technique. The analysis of wind speed record is carried out deploying the moving mean approach with different averaging times. Statistical analysis on turbulence using reasonable averaging time shows the similarities of experimental model with full scale events. For the first time, an effort has been made to compare the primary vortex structure and its evolution with the limited full scale downburst records obtained using Doppler radar measurements.

## Keywords

Downburst, Full scale events, Change points, Transient features, Cobra probe, PIV, Time averaging, Spectral analysis, Vortex dynamics

## Co-Authorship Statement

Chapter Two will be submitted to the Monthly Weather Review journal for publication under the co-authorship of Romanic D., Junayed C., Jubayer C. and Hangan H.

Romanic D. supervised and organized the manuscript. Junayed C. collected the data, analyzed and produced all the figures to explain the result. Junayed C. also wrote part of the manuscript. Romanic D. analyzed the results and wrote most of the part of the manuscript, interpreted results and conducted literature review. Jubayer C. collected data and helped with writing the result section as well as reviewing the manuscript. Hangan H. framed and supervised overall research and commented on the analysis.

Chapter Three will be submitted to the Journal of Wind Engineering and Industrial Aerodynamics under the co-authorship of Junayed C., Jubayer C., Parvu D., Romanic D., and Hangan H.

Junayed C. conducted the literature review, analyzed the data. Junayed C. also produced the figures and results, wrote the overall manuscript. Jubayer C. and Parvu D. performed Cobra Probe and PIV experiments where Jubayer C. also contributed with the analysis of the cobra probe data and . reviewed the paper. Romanic D. helped with evaluating the results, reviewed and commented on the analysis. Hangan H. supervised the research, recommended the literature review and helped with the discussion of the results.

## Acknowledgments

I would like to express my sincere gratitude to my research supervisor Dr. Horia Hangan for his encouraging support and guidance throughout the course of this research work. His extensive knowledge in wind engineering has encouraged and enlightened me all throughout the completion of my master's degree.

I would also like to thank my thesis examiners Dr. Girma Bitsuamlak, Dr. Han-Ping Hong and Dr. C.T. DeGroot for making some time in between their busy schedule's to evaluate my thesis work.

My sincere thanks to Dr. Jubayer Chowdhury, who has supported me unconditionally and extensively all throughout this thesis. Whenever I had any difficulties with understanding materials in this field of study, I was sure that I would receive the highest assistance from him. I would like to extend my thanks to Dr. Djordje Romanic for helping me understanding critical issues in my thesis particularly with the writing results where his depth of knowledge always provided the best answers to my questions.

I would again like to thank my co-authors of my on-going publications -Dr. Jubayer Chowdhury, Dr. Djordje Romanic, Dan Parvu for sharing their knowledge and time that has made these publications possible.

During this thesis, I was fortunate to have excellent support from my colleagues from my research group. Sharing the same office space with Mohammed Karami and Julien Lotufo, and later on with Arash Ashrafi, we had long research related discussions that helped me to grow my understandings in wind engineering. Especially Mohammed Karami, who helped me with the study materials and learn software's related to this research work. In spite of his busy schedule as a Ph.D. student himself, he was always there to solve any issues that I had with my research. Aya Kassab, Marilena Enus has helped me sharing their thoughts about my thesis during my presentations that helped me to find the critical issues to address in my thesis. I would also like to thank Anant Gairola for reviewing the introduction part of my thesis and providing me with his valuable comments.

I would like to extend my thanks to Gerald Defoe, Dr. Jubayer Chowdhury, Dan Parvu, for conducting the experiments in WindEEE and Julien Lotufo for helping me with the setup procedures for the experiments critically important for this thesis work. I would also like to thank Adrian Costache for all his technical support during the experiments and overall the course of my master's degree.

A special thanks to all the professor whose courses I attended during my Master's degree (Dr. Horia Hangan-Wind Engineering, Wind Energy, Dr. Girma Bitsuamlak-Building Sustainability, Prof. Giovanni Solari-Wind Excited and Aeroelastic Response of Structures, Dr. Ayman El Ansary- Finite Element and Method).

I would like to acknowledge the financial supports from the Department of Civil and Environmental Engineering at Western University and Natural Sciences and Engineering Research Council of Canada (NSERC) Discovery grants.

Lastly and most importantly the support from my family, my parents Jigar Khairun Nafia and Mir Hossain Chowdhury, My sister-in-law Easmine Akter, My brother Jubayer Chowdhury for their encouraging support whenever I was feeling unnerved and shared my thoughts without any hesitation. My three years old niece Zuhaira who has given me strength and peace just even looking at her. And Tanzuma Islam, who was always there for me. Without their support, this thesis work would have been impossible.

# Table of Contents

Abstract .....	i
Keywords .....	i
Co-Authorship Statement.....	ii
Acknowledgments.....	iii
Table of Contents .....	v
List of Tables .....	viii
List of Figures .....	ix
List of Appendices .....	xiii
Nomenclature .....	xiv
Chapter 1 .....	1
1 Introduction .....	1
1.1 General introduction .....	1
1.2 Definition of Downburst .....	1
1.3 Classification of Downburst .....	3
1.4 Literature Review.....	5
1.4.1 Downburst field studies .....	5
1.4.2 Numerical and physical simulations .....	11
1.5 Motivation and purpose of this thesis .....	17
1.6 Organization of this thesis .....	19
1.7 References.....	19
Chapter 2.....	25
2 Investigation of transient nature of downbursts from Europe, United States and Australia through detection of abrupt changes in wind speed records.....	25
2.1 Introduction.....	25
2.2 Data and methods.....	31

2.2.1	Data.....	31
2.2.2	Change points in downburst wind records-theoretical background.....	32
2.3	Results.....	36
2.3.1	Europe.....	37
2.3.2	The US.....	40
2.3.3	Australia.....	43
2.4	Discussion.....	45
2.4.1	Model sensitivity.....	45
2.4.2	Transient characteristics of downburst time series.....	48
2.4.3	Outlook.....	53
2.5	Conclusions.....	54
2.6	Acknowledgements.....	56
2.7	References.....	60
Chapter 3.....		66
3	Parametric characterization of large scale experimentally produced downburst flows	66
3.1	Introduction.....	66
3.2	Experimental setup and test cases.....	70
3.2.1	Test chamber (WindEEE Dome).....	70
3.2.2	Cobra probe setup.....	71
3.2.3	PIV setup.....	73
3.3	Results.....	74
3.3.1	Downburst records analysis and the proper value of moving average period ( $T_{avg}$ ).....	74
3.3.2	Downburst velocity profiles.....	84
3.3.3	Statistical Analysis of Turbulence.....	87
3.3.4	Vortex dynamics using Particle Image Velocimetry.....	94

3.4 Summary and Conclusions .....	102
3.5 References .....	104
Chapter 4 .....	112
4 Conclusions and Recommendations .....	112
4.1 Summary .....	112
4.2 Conclusions .....	113
4.3 Recommendation and future work .....	115
4.4 References .....	116
Appendices .....	118
References .....	122
Curriculum Vitae .....	123



## List of Tables

Table 2.1: Downburst events investigated in this paper. See Fig. 2 for their location on map .....	57
Table 3.1: $Re$ for different jet diameters and fan speeds .....	72
Table 3.2: The maximum instantaneous radial velocity ( $u_{max,i}$ ) and its location for each of the investigated cases.....	75
Table 3.3: Average values of $\mu_{\tilde{u}'}$ , $\sigma_{\tilde{u}'}$ , $\gamma_{\tilde{u}'}$ , $\kappa_{\tilde{u}'}$ from all six cases .....	83
Table 3.4: The maximum value of the time varying mean radial velocity, $u_{max}$ and its location .....	84
Table 3.5: The values of $R$ , $G_{max}$ , $G_{peak}$ using $T_{avg} = 0.1$ s for all $Re$ cases in this study...	93
Table 3.6: The values of $T_{ii}$ , $T_{ei}$ and $T_{int}$ observed at for different values of $Re$ .....	95

# List of Figures

Figure 1.1: Differences in flow structure between downburst (microburst) and tornado (NOAA photo library) ..... 2

Figure 1.2: Illustration of four stages of a Downburst event. Descending of air, air hitting the ground, maturing and spreading out of air radially as runaway vortex rolls (Wolfson, 1988). 3

Figure 1.3: Schematic of a wet and dry microburst (Fujita, 1990). ..... 4

Figure 1.4: Aerial photographs showing the damages by downbursts wind. Trees are blown (left) in a starburst pattern and an outbuilding (right) was damaged by microburst winds (Fujita, 1990). ..... 6

Figure 1.5: Single-Doppler wind data in vertical cross section showing contours of Vertical windspeed (left) Horizontal wind speed (right) of a microburst during the project NIMROD (Fujita, 1992, Wilson and Wakimoto, 2001) ..... 7

Figure 1.6: Photograph of a Microburst outflow observed in Denver, Colorado during JAWS project. Dust ring observed on 15 July, 1982 (left) and Outflow of the microburst from heavy rain shaft on 6 July, 1984 (Right) (Hjelmfelt, 1988). ..... 8

Figure 1.7: Time evolution of a microburst seen during the JAWS project. (Wilson et al., 1984, Hjelmfelt, 1988). ..... 9

Figure 1.8: Simulated microburst vorticity field obtained through the PIV experiment (Alahyari & Longmire, 1994) ..... 13

Figure 1.9: Velocity profile for a full scale event from JAWS experiment (Hjelmfelt, 1988)15

Figure 1.10: Comparison of downburst mean velocity profiles between empirical model, laboratory experiment and typical boundary layer profiles (Kim and Hangan, 2007). ..... 16

Figure 2.1: An hour-long time series of (a) steady atmospheric boundary layer (ABL) wind and (b) transient downburst. Location and date of measured time series shown above plots. 26

Figure 2.2: Location map of downburst events in (a) Europe, (b) United States and (c) Australia .....	31
Figure 2.3: All downburst records investigated in this study .....	36
Figure 2.4: Three segmentation methods applied to a downburst records from Genoa (left panels) and a downburst record from Livorno (right panels). .....	38
Figure 2.5: Same as Figure 2.4 but for one La Spezia event (left panels) and one Livorno event (right panels). Notice that the downburst signatures in this figure and Figure 2.4 are noticeably different; see text for further discussion. ....	40
Figure 2.6: Three segmentation methods applied to a downburst records from Syracuse (left panels) and Pep (right panels).....	42
Figure 2.7: Three segmentation methods applied to a downburst records from Lubbock (left panels) and Washington (right panels). ....	43
Figure 2.8: Three segmentation methods applied to a downburst records from Australia. ....	44
Figure 2.9: The number of detected change points versus $\gamma$ for three different sampling frequencies. ....	46
Figure 2.10: Dependency of $\gamma$ on sampling frequency, $f_s$ , for the mean cost function.....	47
Figure 2.11: (a) Downburst durations determined using M, SD and LT approaches for time records listed in Table 1. (b, c, d) Histograms of downburst durations obtained by M, SD and LT approaches, respectively. ....	49
Figure 2.12: Same as Figure 2.10, but for downburst ramp-up time. ....	50
Figure 2.13: (a) The ratio ( $R_{dp/bp}$ ) of mean wind speeds during downburst peak (dp) and before peak (bp), as well as the ratio ( $R_{dp/ap}$ ) of the mean wind speeds during dp and after peak (ap). (b, c) Histograms of $R_{dp/bp}$ and $R_{dp/ap}$ , respectively. ....	52
Figure 2.14: Same as Figure 2.12, but for the standard deviation. ....	53

Figure 3.1: Schematic of (a) horizontal and (b) vertical sections of the WindEEE Dome downburst mode.....	71
Figure 3.2: (a) Mast equipped with 12 Cobra probes (b) Schematics of the location of the measuring mast and Cobra probes in the WindEEE Dome testing chamber.....	72
Figure 3.3: PIV setup .....	73
Figure 3.4: Radial ( $u$ ), lateral ( $v$ ) and vertical ( $w$ ) components of instantaneous velocity for $Re$ (a) $1.83 \times 10^6$ , (b) $2.62 \times 10^6$ , (c) $4.24 \times 10^6$ , (d) $1.82 \times 10^6$ , (e) $2.68 \times 10^6$ and (f) $4.09 \times 10^6$ .....	75
Figure 3.5: Abrupt changes in the signal (dashed lines) used to determine the initial point of the gust front (first dashed line) for (a) $Re=1.83 \times 10^6$ and (b) $Re=1.82 \times 10^6$ .....	77
Figure 3.6: Time history of the $u$ velocity component and its decomposition for the case of $Re = 1.83 \times 10^6$ and $HD > 1$ obtained by using different values of $T_{avg}$ : (a) 0.01 s, (b) 0.025 s, (c) 0.05 s, (d) 0.1 s, (e) 0.2 s, and (f) 0.3 s. ....	80
Figure 3.7: Derived functions based on the Fourier transform of $u(t)$ and $u'(t)$ , $n F_{\bar{u}} ^2$ , $n F_{u'} ^2$ and $n F_{\bar{u}}  F_{u'} $ , for $Re = 1.83 \times 10^6$ and $H/D > 1$ . The panels indicate different values of $T_{avg}$ that were used to obtain $u(t)$ and $u'(t)$ : (a) 0.01 s, (b) 0.025 s, (c) 0.05 s, (d) 0.1 s, (e) 0.2s and (f) 0.3 s.....	82
Figure 3.8: Downburst radial velocity profiles at the radial location of $u_{max}$ (a) without normalization and (b) normalized.....	85
Figure 3.9: Normalized velocity profiles from full scale events are plotted against the experimentally generated downbursts in the WindEEE Dome.....	86
Figure 3.10: Vertical profiles of $u(t)$ at different time instances in the time series and at the radial location of $u_{max}$ . The investigated case is for $Re=2.62 \times 10^6$ and $H/D > 1$ . (a) Moving mean time series and (b) vertical profiles at different time instances, $t=0.34$ to $0.58$ s (i)–(vii) .....	87

Figure 3.11: PSD of the reduced turbulence fluctuations matched with  $n - 53$  profile (red line) using  $T_{avg} = 0.1$  s for  $Re$ , (a)  $1.82 \times 10^6$ , (b)  $2.62 \times 10^6$ , (c)  $4.09 \times 10^6$ , (d)  $1.83 \times 10^6$ , (e)  $2.68 \times 10^6$  and (f)  $4.24 \times 10^6$ ..... 89

Figure 3.12: PSD of the reduced turbulence fluctuations ( $T_{avg} = 0.1$  s) matched against the analytical model proposed by Solari and Piccardo (2001) (red line) for  $Re$  (a)  $1.83 \times 10^6$ , (b)  $2.62 \times 10^6$ , (c)  $4.24 \times 10^6$ , (d)  $1.82 \times 10^6$ , (e)  $2.68 \times 10^6$  and (f)  $4.09 \times 10^6$  ..... 90

Figure 3.13: PDF of the reduced turbulent fluctuations ( $T_{avg} = 0.1$  s) for  $Re$  (a)  $1.83 \times 10^6$ , (b)  $2.62 \times 10^6$ , (c)  $4.24 \times 10^6$ , (d)  $1.82 \times 10^6$ , (e)  $2.68 \times 10^6$  and (f)  $4.09 \times 10^6$ . Red line represents a Gaussian PDF..... 92

Figure 3.14: PIV vectors and velocity magnitude contours for  $H/D < 1$  and  $Re = 2.68 \times 10^6$  at different time instances. Time interval between two consecutive instances is 0.11s. .... 95

Figure 3.15: (a) Vector plot with velocity magnitude from PIV experiment with the location of the maximum velocity and the centre of the vortex for  $H/D < 1$  and  $Re = 2.68 \times 10^6$ , (b) velocity magnitude plotted against normalized radial distance and (c) schematic of the downburst flow field and the location of the maximum velocity obtained using the full scale data from the JAWS campaign (Hjelmfelt, 1988)..... 97

Figure 3.16: Streamline plots showing the primary vortex at different instances for  $H/D < 1$  and  $Re = 2.68 \times 10^6$  ..... 98

Figure 3.17: Streamlines showing the second vortex after passing of the primary vortex for  $H/D < 1$  and  $Re = 2.68 \times 10^6$  ..... 99

Figure 3.18: Trajectory of the vortex centre for different values of  $Re$ . .... 100

Figure 3.19: Comparison of vortex centre heights from the WindEEE Dome downbursts and full scale events on (a) 16 June 1978 (b) 17 June 1978 (Wakimoto, 1982) ..... 101

Figure 3.20: Normalized vortex trajectories from the WindEEE Dome downbursts compared with full scale event on 17 June, 1978 (Wakimoto, 1982) ..... 102

## List of Appendices

Appendix A: Figures presented here are in support of the Chapter 3.....	118
Appendix B: PIV error correction.....	120

# Nomenclature

## Abbreviations

ABL	Atmospheric Boundary Layer
AGL	Above Ground Level
CS	Cloud Simulation
CLAWS	Classify, Locate and Avoid Wind Shear
CP-3	Coherent Pulsed 3
CMOS	Complementary Metal-Oxide Semiconductor
EF-3	Enhanced Fujita 3
ESDU	Engineering Science Data Unit Standard
GRF	Gust Response Factor
JAWS	Joint Airport Weather Studies
LT	Linear Trend
MIST	Microburst and Severe Thunderstorm Project
M	Mean
NCAR	National Center for Atmospheric Research
NIMROD	National Intensive Meteorological Research on Downbursts
PDF	Probability Density Function
PIV	Particle Image Velocimetry
PSD	Power Spectral Density
RMS	Root Mean Square
RPM	Revolution Per Minute

SD	Standard Deviation
TFI	Turbulent Flow Instrumentation
WindEEE	Wind Engineering Energy and Environment

### Symbols

$D$	Downburst jet diameter	m
FS	Fan speed	%
$f_s$	Sampling frequency	Hz
$F_{\bar{u}}$	Fourier transform of time varying mean	-
$F_{u'}$	Fourier transform of residual fluctuation	-
$G$	Gust factor	-
$G_{max}$	Ratio between maximum instantaneous velocity with maximum moving mean velocity	-
$\hat{G}$	Ratio between 1-s peak velocity with maximum moving mean velocity	-
$g$	Gust response factor	-
$H$	Height of the Downburst	m
$I_u$	Turbulence Intensity	-
$L_v$	Maximum of the moving mean velocity	m/s
$n$	Sampling frequency	Hz
$R$	Radial distance	m
$\hat{R}$	Ratio between maximum instantaneous velocity with 1-s peak velocity	-
$Re$	Reynolds number	-



$R_{cm}$	Radial distance of the vortex core at minimum height	m
$R_{dp/bp}$	Ratio between the mean wind speed during downburst peak and before downburst peak	-
$R_{dp/ap}$	Ratio between the mean wind speed during downburst peak and after downburst peak	-
$S_{\tilde{u}'}$	Power spectral density of $\tilde{u}'$	-
$T_{avg}$	Averaging time	s
$T_{ii}$	Insertion instance of the vortex into the region	s
$T_{ei}$	Ending instance of the vortex passing the region	s
$T_{int}$	Time interval of the instances	s
$t_s$	Sampling time	s
$t$	Time	s
$\hat{U}_{1m}$	1-min maximum wind speed	m/s
$\bar{U}_-$	Pre peak mean wind speed	m/s
$\bar{U}_+$	Post peak mean wind speed	m/s
$u$	Instantaneous radial wind velocity	m/s
$\bar{u}$	Time varying mean of radial velocity component	m/s
$u'$	Residual fluctuation of radial velocity component	m/s
$\tilde{u}'$	Reduced turbulent fluctuation of $u$	-
$\hat{u}$	1-s peak radial wind speed	m/s
$u_{max}$	Maximum instantaneous radial velocity	m/s
$\bar{u}_{max}$	Maximum running mean radial velocity	m/s
$u_{max,i}$	Instantaneous maximum radial velocity	m/s
$\bar{U}_{dp}$	Mean wind speed during downburst peak	m/s

$\bar{U}_{bp}$	Mean wind speed before downburst peak	m/s
$\bar{U}_{ap}$	Mean wind speed after downburst peak	m/s
$u_{co}$	Primary vortex core convective velocity	m/s
$v$	Instantaneous lateral wind velocity	m/s
$v$	Instantaneous wind speed	m/s
$\bar{v}$	Time varying mean wind speed	m/s
$v'$	Residual fluctuation	m/s
$\tilde{v}'$	Reduced turbulent fluctuation	-
$\hat{v}$	Peak response	m/s
$\bar{v}_{TVM}$	Largest response to time varying mean	m/s
$w$	Instantaneous axial (vertical) wind velocity	m/s
$Z$	Height of the cobra probe	m
$Z_{cm}$	Minimum height of the vortex core in vortex trajectory	m
$Z_{max}$	Height of the maximum moving mean velocity	m
$Z_{max,i}$	Height of the maximum instantaneous velocity	m

### Greek Symbols

$\sigma_v$	Slowly varying standard deviation	m/s
$\sigma_u$	Standard deviation of radial velocity component	m/s
$\sigma_{\tilde{u}'}$	Standard deviation of $\tilde{u}'$	-
$\sigma_{dp}$	Standard deviation during downburst peak	m/s
$\sigma_{bp}$	Standard deviation before downburst peak	m/s

$\sigma_{ap}$	Standard deviation after downburst peak	m/s
$\sigma_{dp/bp}$	Ratio between the standard deviation during downburst peak and before downburst peak	-
$\sigma_{dp/ap}$	Ratio between the standard deviation during downburst peak and after downburst peak	-
$\mu_{\tilde{u}'}$	Mean value of $\tilde{u}'$	-
$\gamma_{\tilde{u}'}$	Skewness value of $\tilde{u}'$	-
$\kappa_{\tilde{u}'}$	Kurtosis value of $\tilde{u}'$	-
$\theta_e$	Maximum vertical differential	-
$\tau$	Short time interval	s
$\gamma$	Penalty constant	-

# Chapter 1

## 1 Introduction

### 1.1 General introduction

On June 1975, an aircraft from Eastern Airlines confronted with a rapid diverging wind while attempting to land at New York's John F. Kennedy Airport (JFK) crashed and killed 112 people. This divergent wind pattern was recorded previously while the starburst pattern of fallen trees was visible in an aerial survey from the damages of 'super-outbreak' of 148 tornadoes on 3-4 April 1974 (Fujita, 1974). Similarities in the wind pattern of these two events were found based on the investigation of the recorded data from the aircraft flight data recorder. From all this analysis Fujita termed the event as 'Downburst' and defined it as 'A natural event that occurs due to thunderstorms produced by a cumulonimbus cloud causing a strong downdraft which induces an outburst of damaging winds on or near the ground' (Fujita, 1990). This radially divergent wind with high wind velocity transpires when descending air hits the ground causing immense damage to the ground-mounted structures.

Downburst is defined in the next section followed by the classifications of downbursts. Previous studies on downbursts and their findings as well as limitations are described in the literature review section. This chapter ends with the motivation and organization of the thesis as well as a list of the cited references.

### 1.2 Definition of Downburst

Downbursts were primarily defined exclusively for aviation purposes during 1976 and 1977. Later, it was redefined meteorologically as scientists reveal the scale and nature of this phenomenon (Fujita and Wakimoto, 1981). In nature, downbursts can be identified as an anti-tornado storm. This anti-tornado storm is described as a sudden downfall of slow

rotating air towards the ground. While reaching the ground, this sudden downfall bursts out violently causing an immediate rise in the wind velocity in the lower region of the ground (Fujita, 1990). **Figure 1.1** shows the fundamental differences in flow structure between downburst and tornado.

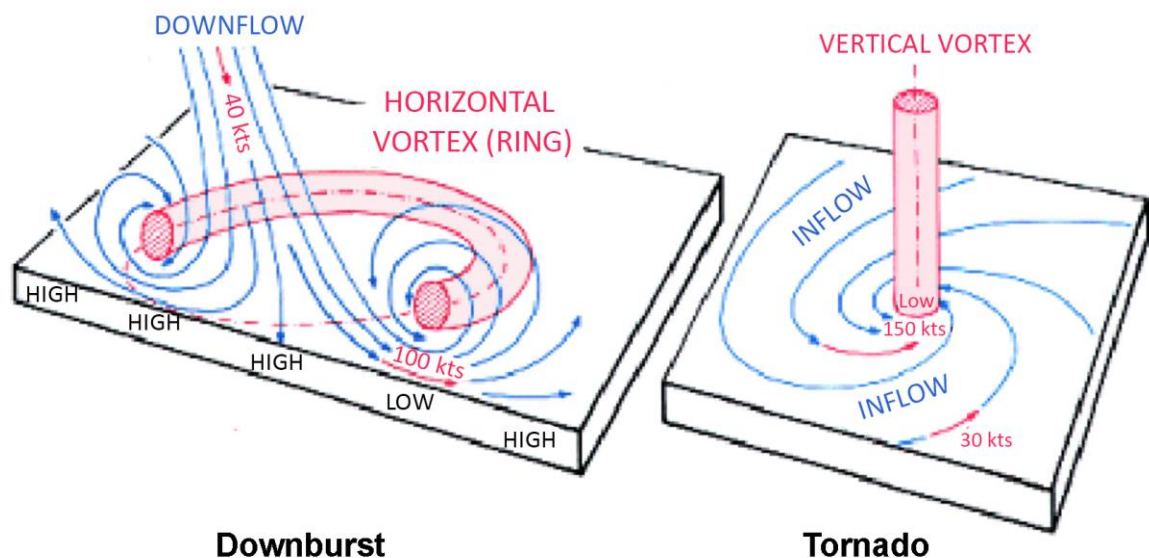


**Figure 1.1: Differences in flow structure between downburst (microburst) and tornado (Adapted from NOAA photo library)**

According to Byers and Braham (1948) a thunderstorm evolves in three stages. During the first stage, air rises vertically. At the second stage, both the rising and sinking air co-exists and in the final stage the cloud breaks up and strong sinking current hits the ground producing downbursts. This rising and sinking currents are termed as 'Updraft' and 'Downdraft' respectively. Formation of a downburst is a density-driven incident in the atmosphere. This density driven incident is caused by thermodynamic cooling associated with the formation of the thunderstorm cloud itself. Inside the thunderstorm cloud, the thermodynamic process causes air density to rise in the volume of clouds which eventually results into a massive downdraft with precipitation in the form of rain, snow, hail and graupel (Wakimoto, 1985). The precipitation sometimes aids in the downdraft to gain greater strength and accelerate the thunderstorm air parcels downward (Wolfson, 1988). Wolfson (1988) described the downburst evolution in four stages (Descending stage:

midair microburst descends, Contact stage: microburst hits the ground, Mature stage: stretching of the ring vortex, Breakup stage: runaway vortex rolls induce burst swaths) and these stages are illustrated in **Figure 1.2**.

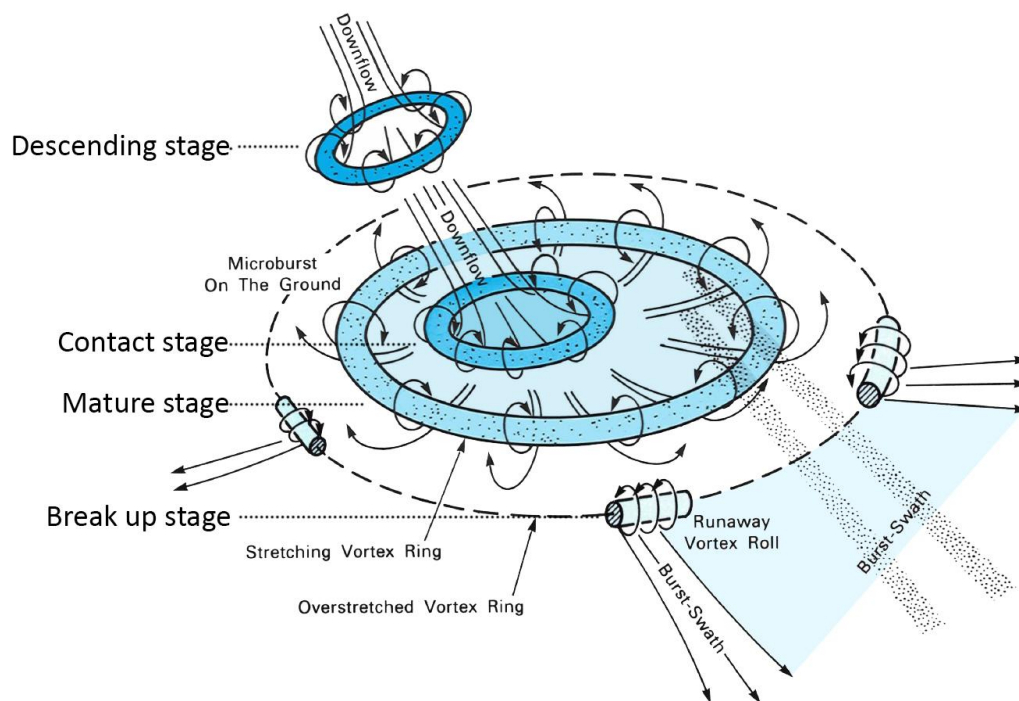


**Figure 1.2: Illustration of four stages of a Downburst event. Descending of air, air hitting the ground, maturing and spreading out of air radially as runaway vortex rolls (Adapted from Wolfson, 1988)**

### 1.3 Classification of Downburst

Primarily Fujita (1990) classified downburst into Microburst and Macroburst. A macroburst is a large-scale downburst which has a damaging wind extending over 4 km (> 2.5 miles) and a microburst is a small downburst which has a damaging wind extending up to 4 km ( $\leq$  2.5 miles) horizontally. Based on the observations and analyses, Fujita (1990) postulated that a microburst can produce wind gusts as high as 75 m/s, whereas a macroburst, due to their more extensive scale, can produce wind speeds up to 60 m/s. A

microburst can last for about 2-5 minutes, on the other hand, a macroburst can last up to 30 minutes.

Due to its short span in time and high intensity, the maximum wind speed of microbursts is expected to be higher than that of macroburst (Fujita, 1974). The intensity of a downburst is usually much less than that of a tornado, but sometimes their intensity may reach as high as F3. Of the 142 downbursts that Fujita observed during his survey in between 1976 and 1978, 98.6% were F2 or weaker, none were F4 or stronger, but 1.4% were as strong as F3 (Fujita, 1978).

Additional classification of downburst emerged while several full scale projects were conducted to understand its character. While pursuing the projects NIMROD (Northern Illinois Meteorological Research on Downbursts) (Fujita, 1978), JAWS (Joint Airport Wind Shear) (Wilson et al., 1984; Hjelmfelt, 1988) and MIST (Microburst and Severe Thunderstorm) (Fujita, 1990), three types of downburst were detected and observed. During JAWS, strong microburst winds were recorded without sufficient rainfall on the ground and was classified as dry microburst (Fujita, 1990). Cloud base in the MIST project near Huntsville, AL was at a very low elevation and the downburst was accompanied by heavy rain. Fujita classified this event as a wet microburst. A schematic of this classification is shown in **Figure 1.3**.

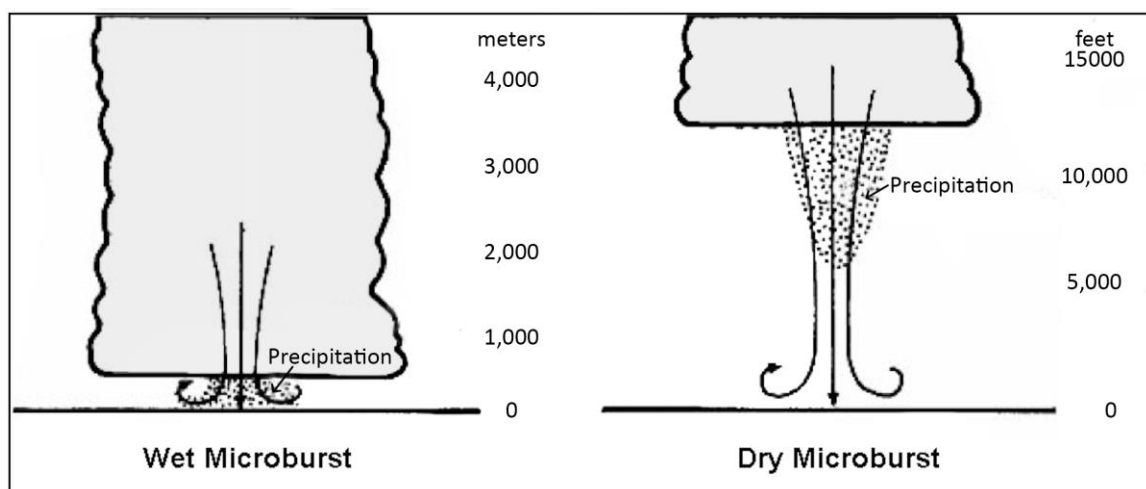


**Figure 1.3: Schematic of a wet and dry microburst (Adapted from Fujita, 1990).**

According to the damage patterns, downbursts were again classified into five scales (Fujita and Wakimoto, 1981). Downburst swaths can have lengths from tens of meters to several hundred kilometers. From the downbursts that occurred on 16 July 1980, five different meteorological scales were classified. Based on the damage pattern these scales were classified as a family of Downbursts clusters (Meso-BETA scale), Downburst cluster (Meso-ALPHA scale), Downburst (Meso-BETA scale), Microburst (Meso-ALPHA scale) and Burst swath (Meso-BETA scale). These five categories are branched under the two significant sub-categories which are ‘Masoscale’ and ‘Misoscale’. Each of these scales are also divided into ALPHA (larger) and BETA (smaller) scales for subscale identification (Fujita and Wakimoto, 1981).

## 1.4 Literature Review

In this section previous studies on downbursts and their flow characteristics are discussed. These studies can be divided into three main categories, field measurements of full scale downbursts, experiments with model scale downbursts and numerical simulations. In Section 1.4.1, projects capturing full scale downburst events and their major findings are discussed. Section 1.4.2 presents different experimental and numerical techniques to simulate downbursts and how these techniques vary from one another. The importance and effects of downbursts related to wind engineering are also explained here.

### 1.4.1 Downburst field studies

Fujita first identified downbursts back in 1976 from a set of aerial photographs. Investigating the damages in the wake of the super out-break of tornadoes on 3-4 April 1974, Fujita found a strange pattern which changed his vision towards the damages by the storm. He found that the trees were blown out in a starburst pattern, which is similar to the damage caused by a jet of descending air as it hits the ground and bursts out violently. From these aerial photographs (**Figure 1.4**) Fujita confirmed the existence of downbursts which



is a strong downdraft inducing an outburst of damaging winds on or near the ground (Fujita, 1978).

A series of field studies were conducted during the 1970s and 1980s to know more about the characteristics of downbursts. The first field study was the project NIMROD during the spring and summer of 1978. The primary objective of NIMROD was to study and validate the existence of downbursts and to collect meteorological data on a nationwide scale. After the crash of an Airliner short of the runway of John F. Kennedy Airport, New York on June 24, 1975, the National Transportation Safety Board called for an investigation to prevent further sinking of airplanes due to the sharp wind changes under thunder showers.

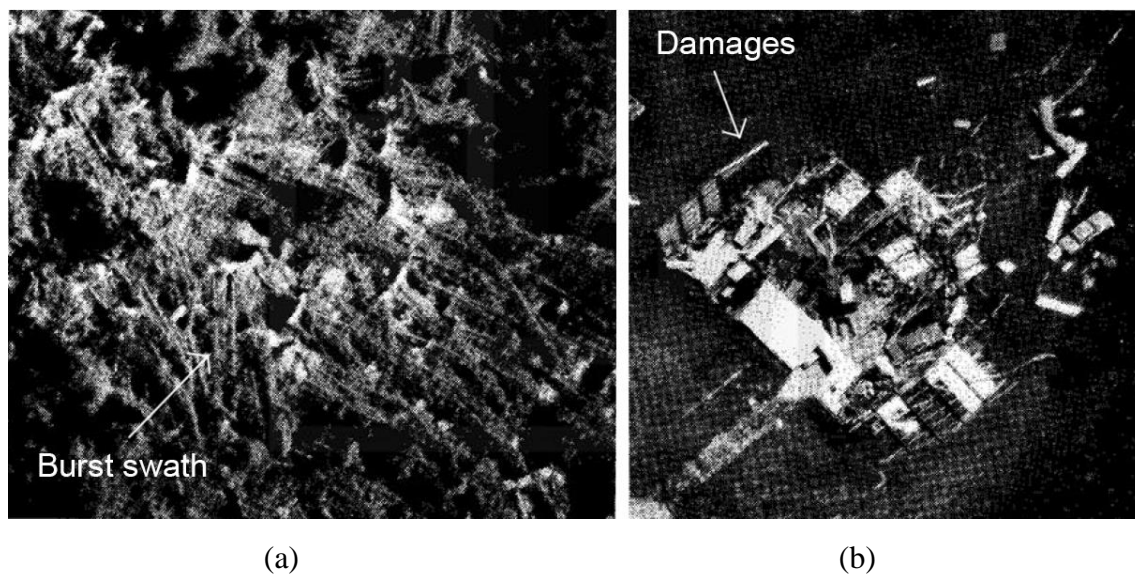


**Figure 1.4: Aerial photographs showing the damages by downbursts wind. (a) Trees are blown in a starburst pattern and (b) an outbuilding was damaged by microburst winds (Adapted from Fujita, 1990).**

The Project NIMROD starts with the operation of a Triple-Doppler Network in Northern Illinois in May and June of 1978. Three Doppler radars were placed in the site in close proximity in order to determine the three-dimensional structure of the downburst airflow. But to prove the existence of downbursts and increase the likelihood of capturing more events, Fujita (1978) decided to increase the distance between two radars which set the radar triangle with a length of 60 km for each leg. The Doppler radars measured a high

wind speed of 31 m/s above 45 m from ground in the western suburbs of Chicago (Wilson et al., 1984; Fujita, 1990). Approximately 50 downbursts were detected during the project NIMROD proving their existence and high frequency of occurrence in nature (Wilson and Wakimoto, 2001). **Figure 1.5** shows the horizontal and vertical cross sections of one of the downburst events captured during NIMROD.

Right after the project NIMROD, researchers like Fujita, Serafin, Wilson and John McCarthy decided to conduct more experiments to have a better understanding of the structure, evolution and cause of microbursts over the high plains. As a result Project JAWS was conducted for 86 days from 15 May to 13 August, 1982 in Colorado, Denver. The same Doppler radars from NIMROD were used but this time the radars were laid out to capture the three dimensional wind field of the life cycle of a microburst. The spacing between the two radar was 15, 18 and 28 km, which was much tighter than NIMROD project (Wilson and Wakimoto, 2001). A total of 186 downbursts were captured during this time.

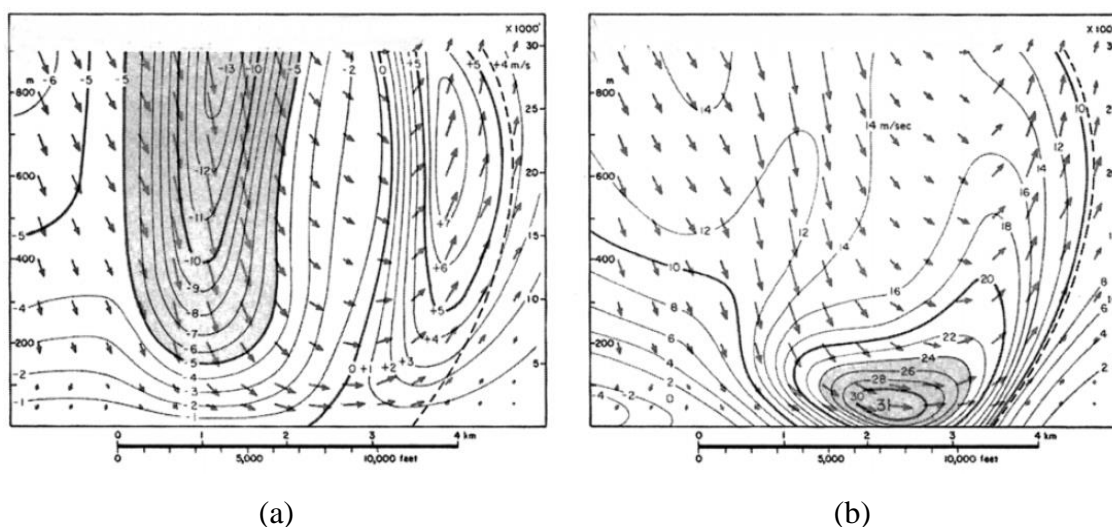


**Figure 1.5: Single-Doppler wind data in vertical cross section showing contours of (a) Vertical wind speed and (b) Horizontal wind speed of a microburst during the project NIMROD (Adapted from Fujita, 1992, Wilson and Wakimoto, 2001)**

One of the major findings of JAWS project was that strong downdrafts were not only associated with shafts of heavy rainfall (a wet microburst), as it was thought in the

beginning, but could also occur in the absence of any significant rain activity at all. Proctor (1988) analyzed the environmental conditions of June 30, 1982 downburst event and described how microburst downdraft was initiated by the distribution of precipitation at the top of the boundary layer. Srivastava (1985, 1987), based on his analytical model, explained that the equality in sub cloud environmental lapse rate and dry-adiabatic rate, or even relatively light rainfall can be a reason to produce intense downdrafts which eventually produce no rain near the ground. This type of event is termed as a dry microburst. Out of 186 microburst events during the JAWS experiment, 151 were identified as dry microbursts and the rest were wet microbursts. **Figure 1.6** shows the microburst outflow observed in Denver, Colorado on 15 July 1982. The effect of snow and hail at the top of the boundary layer to create downdraft is explained later by Proctor (1988).

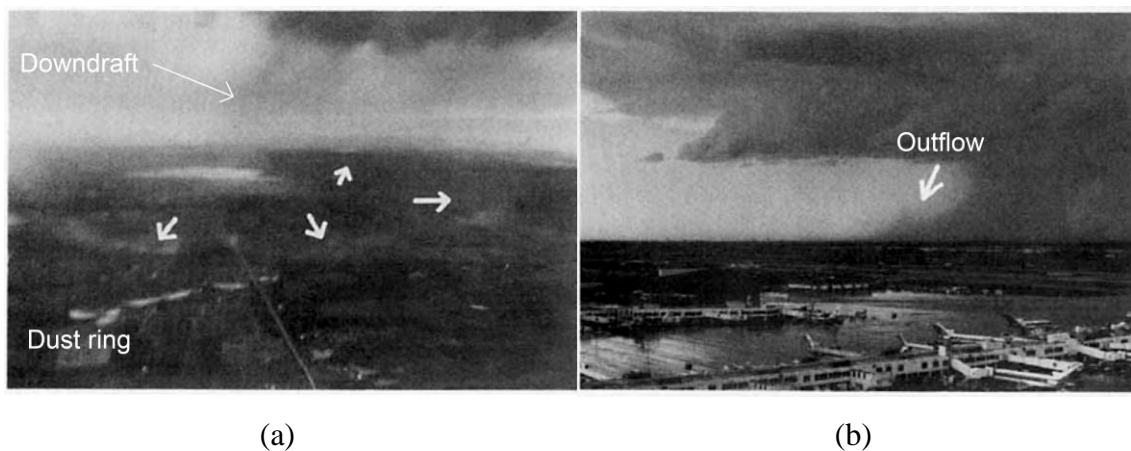


**Figure 1.6: Photograph of a Microburst outflow observed in Denver, Colorado during JAWS project. (a) Dust ring observed on 15 July, 1982 and (b) Outflow of the microburst from heavy rain shaft on 6 July, 1984 (Adapted from Hjelmfelt, 1988).**

Downbursts are accompanied by the formation of an annular vortex developing as a result of the shear between the descending flow and the still surrounding air mass. The spreading of microburst after reaching the ground surface was seen by Fujita (1985) in his laboratory model. In full scale, this radial expansion of outflow happens near the ground (<1 km) with the maximum gust in less than 100 m from the ground (Wilson et al., 1984; Hjelmfelt,

1988; Fujita, 1990; Mason et al., 2005). Wilson et al. (1984), from the analysis of doppler radar data from the JAWS project, postulated that the maximum differential wind speed occurs at a height of approximately 75 m from the ground. This surface layer is of critical importance for wind engineering. However, the full scale data in the near surface region is very limited and has very low spatial and temporal resolution. In **Figure 1.7** the development and dissipation of microburst are shown in time.

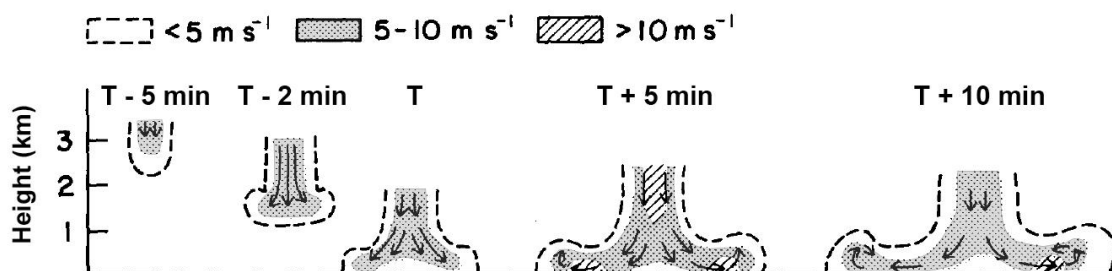


**Figure 1.7: Time evolution of a microburst seen during the JAWS project (Adapted from Wilson et al., 1984, Hjelmfelt, 1988).**

Most of the full scale downburst data found in the literature are either from the United States (Wakimoto, 1982; Wilson et al., 1984; Hjelmfelt, 1988; Holmes et al., 2008; Gunter and Schroeder, 2015) or from Europe (Järvi et al., 2007; Solari et al., 2015; Burlando et al., 2017). There are few downburst datasets available from Asia (Choi and Hidayat, 2002) and Australia (Sherman, 1987). In comparison to synoptic boundary layer winds, thunderstorm downburst winds are highly transient in nature. To detect this transient nature, different methodologies have been proposed (Gomes and Vickery, 1978; Cook et al., 2003). Gomes and Vickery (1978) proposed the method of applying the extreme-value analysis method to separate the extreme wind events. Choi and Hidayat (2002) used the gust factor analysis to separate thunderstorm from non-thunderstorm winds for wind engineering applications. In Chapter 2 of the thesis, an analysis on separating downburst winds from synoptic boundary layer winds is discussed in detail.

As a downburst is a non-stationary process, the typical way of using a fixed averaging time to analyze stationary synoptic wind events, is not appropriate for downburst time series. Therefore, a moving time average method has been adopted by Choi and Hidayat, (2002),

Chen and Letchford (2004), Holmes et al. (2008), McCullough et al. (2014), Lombardo et al. (2014) and Solari et al. (2015). Hong (2016) proposed a model to represent nonstationary winds using the decomposition of instantaneous power spectrum. Choi and Hidayat (2002) proposed a running mean approach for thunderstorm winds which provides more accurate results for the prediction of peak response factor of a structure. In this process Choi and Hidayat (2002) decomposed the instantaneous wind velocity ( $v$ ) into a time varying mean part ( $\bar{v}$ ) and residual fluctuation ( $v'$ ) using different averaging time ( $t$ ). This can be expressed as Eq. (1.1).

$$v(t) = \bar{v}(t) + v'(t) \quad (1.1)$$

Based on this method and calculating the spectra of the  $v'$  for a averaging time ranging from 10 s to 120 s Choi and Hidayat (2002) postulated an averaging time of 60 s for downburst events recorded in Tuas, Singapore. Using the similar approach from the dataset of Lubbock Reese downdraft, Holmes et al. (2008) suggested 40 seconds as the averaging time for thunderstorm downbursts. Holmes used the criteria of retaining the main features of downburst time history and near zero mean value for residual fluctuation ( $v'$ ) as criteria to determine the averaging time. Lombardo et al. (2014) followed the 2<sup>nd</sup> criteria suggested by Holmes et al. (2008), which states that  $v'$  should have a near zero mean value, to obtain the averaging time. Twenty different averaging time ranging from 1.1 s to 723 s were applied on downburst events recorded at Reese Technology Center in Lubbock, Texas, USA. Using additional criteria and based on the analysis on 96 downburst events on ports of Italy, Solari et al. (2015) used 30 seconds as the averaging time to analyze downburst events. To find the averaging time Solari et al. (2015) also decomposed the wind velocity into a slowly varying mean and residual fluctuation which is dealt as a non-stationary random process. In addition to decomposing the instantaneous wind speeds ( $v$ ) into  $\bar{v}$  and  $v'$ , Solari et al. (2015) introduced the analysis of reduced turbulent fluctuation ( $\tilde{v}'$ ) via Eq. (1.2) which is dealt as a rapidly varying random Gaussian process with a near zero mean value and unit standard deviation and expressed by Standard deviation of residual fluctuation ( $\sigma_v$ ).

$$v'(t) = \sigma_v(t)\tilde{v}'(t) \quad (1.2)$$

Solari et al. (2015) also defined three wind speed ratios of importance to loading and response of structures to downburst winds, i.e:

$$\hat{R} = \frac{v_{max}}{\hat{v}} \quad (1.3)$$

$$G_{max} = \frac{v_{max}}{\bar{v}_{max}} \quad (1.4)$$

$$\hat{G} = \frac{\hat{v}}{\bar{v}_{max}} \quad (1.5)$$

Here,  $v_{max}$  is the instantaneous maximum of the downburst wind speed,  $\hat{v}$  is the 1-s peak wind speed and  $\bar{v}_{max}$  is the maximum of the running mean which is a function of averaging time,  $t$ .

Field measurements are the most relevant way to study downburst characteristics. However, it is important to note that capturing full scale downburst events is a challenging process as duration of downbursts are very short in nature and also difficult to forecast. Accurate flow visualization near the ground region is sometimes difficult to obtain by doppler radar technology (Alahyari and Longmire, 1994). Also, as mentioned previously, data within the surface layer, which is the most critical region for wind engineering applications, is very limited with low spatial and temporal resolutions. Considering these difficulties, numerical models (Kim and Hangan, 2007; Mason et al. 2009; Vermeire et al., 2011; Zhang et al., 2013; Orf et al., 2014) and scaled experimental models (Fujita, 1985; Alahyari and Longmire, 1994; Mason et al., 2005; Xu and Hangan, 2008; Sengupta and Sarkar, 2008; Jesson et al., 2013, Zhang et al., 2013) have been developed to study downbursts. A brief summary of these numerical and experimental studies along with their significant findings are presented in the following section.

#### 1.4.2 Numerical and physical simulations

For wind engineering purposes, downbursts can be modelled physically and numerically. Zhang et al. (2013) classified physical and numerical microburst modeling methods into

three categories: ring-vortex, cooling source and impinging jet modeling. Ring vortex model is used primarily to understand the main features of the flow field around the primary vortex in a downburst (Ivan, 1986; Schultz, 1990; Jesson and Sterling, 2018) In the ring-vortex model, the descending air is modeled as annular vortex ring prior to touching the ground (Chen and Letchford, 2004). Although the ring vortex model qualitatively captures the features of primary downburst vortex, impinging jet models have shown to be better in predicting the radial outflow of downbursts (Holmes and Oliver, 2000; Savory et al., 2001).

In the cooling source (CS) model, negative buoyancy is used for the dynamic development of the simulated downburst (Vermeire et al., 2011; Orf et al., 2014). Physically this is done by releasing heavier fluids into lighter fluids which is termed as liquid drop release method (Lundgren et al., 1992; Alahyari and Longmire, 1994; Yao and Lundgren, 1996). Yao and Lundgren (1996) modelled an isolated dynamic downburst by releasing salt water solution from higher elevation into fresh water. This experimental model identified the divergent flow with vortex ring dissipating from a central impact point. Similar results on the vortex formation is seen from the experimental model by Fujita (1985). Here it is important to note that, the experimental model, Yao and Lundgren (1996) showed the presence of a counter rotating vortex (secondary vortex) at the leading edge of the vortex and very close to the surface. The reason of development of this counter rotating vortex is the friction between the shear layer of wind and steady ground surface. In recent experiments Mason et al. (2005) presented the similar concept of counter rotating vortex. From the experiment by Lundgren et al. (1992) Yao and Lundgren (1996) Reynolds number dependency in the model microburst was found only at low Reynolds number and it was noticed that large-scale turbulent (i.e. primary vortex, secondary vortex) motions are not dominated by Reynolds number effects.

First successful application of particle image velocimetry (PIV) in a variable density flow was demonstrated by Alahyari and Longmire (1994). One of the major reasons to turn to PIV experiments was to capture the microburst wind flow field with higher spatial resolution and less intrusively compared to conventional hot wire anemometry in use at that time. From the experimental model Lundgren et al. (1992) considered microburst events as independent of Reynolds number when Reynolds number was greater than 3000.

Maximum velocity was found at  $R/D = 1$  where  $R$  is the radial distance and  $D$  is the jet diameter (Alahyari and Longmire, 1994). **Figure 1.8** shows the descending phase and generation of vortex from the PIV experiment.

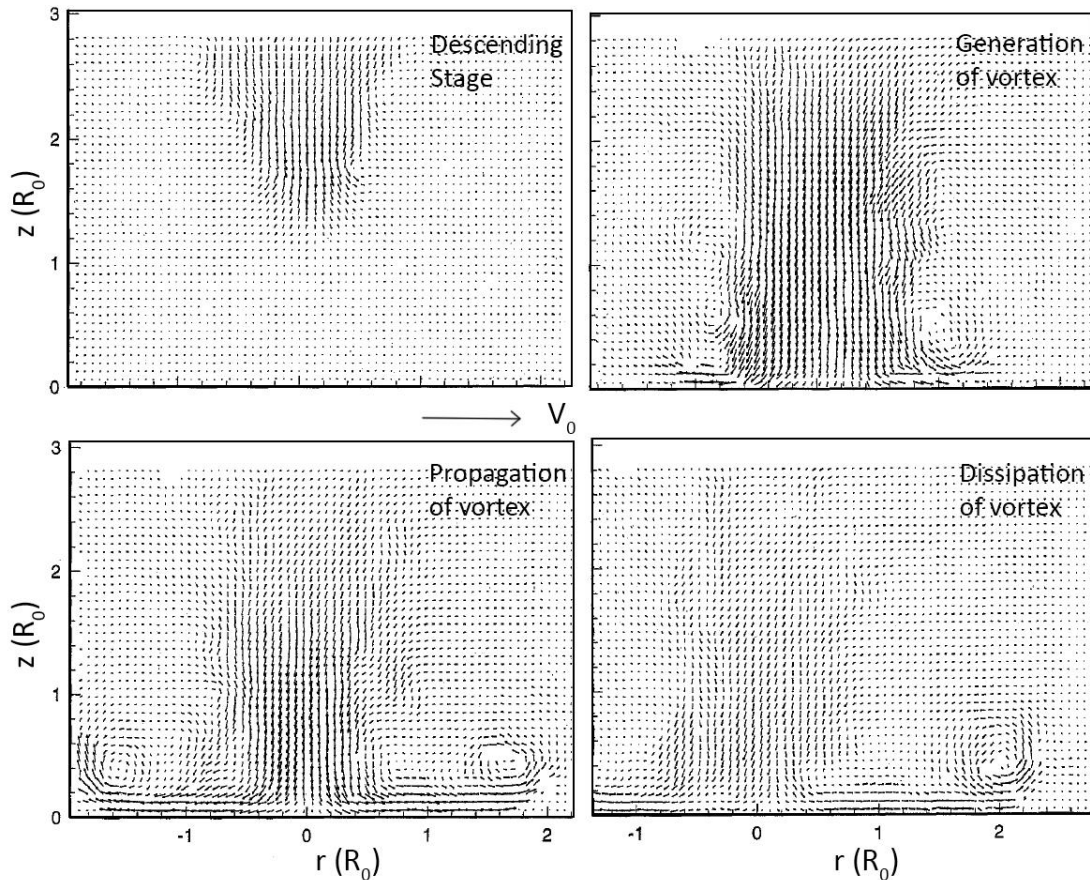


**Figure 1.8: Simulated microburst vorticity field obtained through the PIV experiment (Adapted from Alahyari & Longmire, 1994)**

Numerically, negatively-buoyant CS model has been used by Mason et al. (2009), Vermeire et al. (2011), Zhang et al. (2013) and Orf et al. (2014). Numerical CS models use thermodynamic cooling from a pre-defined cooling source forcing function that produces a similar type of downdrafts observed in nature. While these models come closer to reproducing the physics of real downdrafts, they usually run heavy simulations on large domains and do not emphasize on the details of the surface layer which is of crucial importance to wind engineering.



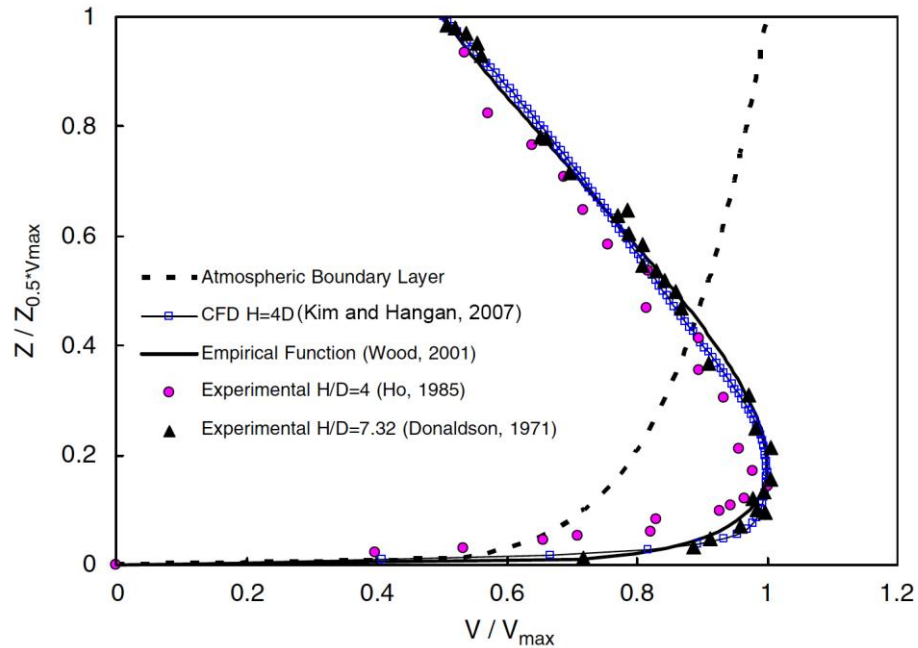
Impinging jets models have been widely adopted by researchers to investigate microburst outflow as its relatively simple and has the ability to produce the proper vortex flow structure and to provide reasonable resolution in the surface layer (Xu and Hangan, 2008; Zhang et al., 2013). Though the evolution of downbursts in nature is a very complex process, in laboratory, physical and numerical downbursts are modelled by axi-symmetric, continuous or impulsively driven circular impinging jets (Letchford and Chay, 2002; Kim and Hangan, 2007; Xu and Hangan, 2008; Zhang et al., 2013). Fujita (1985) was in fact the first to hypothesize this type of mechanism in laboratory to simulate downburst. Later on, using impinging jet method, Landreth and Adrian (1990) measured the velocity field of a impinging circular flow onto a flat surface. Selvam and Holmes (1992) were one of the firsts to use impinging jet model numerically. Kim and Hangan (2007) also employed numerical simulations to successfully reproduce the dynamic vortex structure of impinging jets with application to downburst. In recent years, many researchers have adopted impinging jet model to physically investigate downburst flow field (Wood et al., 2001; Chay and Letchford, 2002; Mason et al., 2005; McConville et al., 2009; Xu and Hangan, 2008; Zhang et al., 2013). Despite all these studies, scaling of the impinging jet model of downburst remained limited making it difficult for the researchers to understand the wind loading on reasonably scaled building models (Zhang et al., 2013). Numerical simulations have brought some contributions, but when it comes to estimating design wind speeds for structures for wind engineering applications, physical experiments are at the end the ones that can produce detailed results and are historically trusted.

Based on laboratory model, Fujita (1990) was the first one to describe five stages of a microburst outflow. Fujita termed the stages as: Descending stage, Contact stage, Touchdown stage, Spreading stage and Ring vortex stage. Similar kind of experiment was conducted by Yao and Lundgren (1996), where the evolution of microburst simplified to three stages: Descending stage, interaction stage and outflow stage. According to Fujita, the leading edge of the ring vortex is the most intense point in a downburst outflow with wind speed reaching its maximum value beneath the primary ring vortex (Fujita 1985; Alahyari and Longmire, 1994).



Hangan (2007). The height of the peak downburst velocity increases with the increase in radial distance (Wood et al., 2001; McConville et al., 2009). Recent experiments McConville et al. (2009) and Zhang et al. (2013) confirmed the peak velocity of a downburst occurring at  $R/D \approx 1$ .

Vertical profiles of downburst flows near the ground are different from synoptic boundary



layer winds.

**Figure 1.10** shows an example of normalized thunderstorm downburst velocity profile compared with boundary layer winds (Kim and Hangan, 2007). Wood et al. (2001) also investigated the velocity profiles of downbursts at different radial locations from the downdraft centre. Similarities were found when compared with full scale data from JAWS and NIMROD projects.

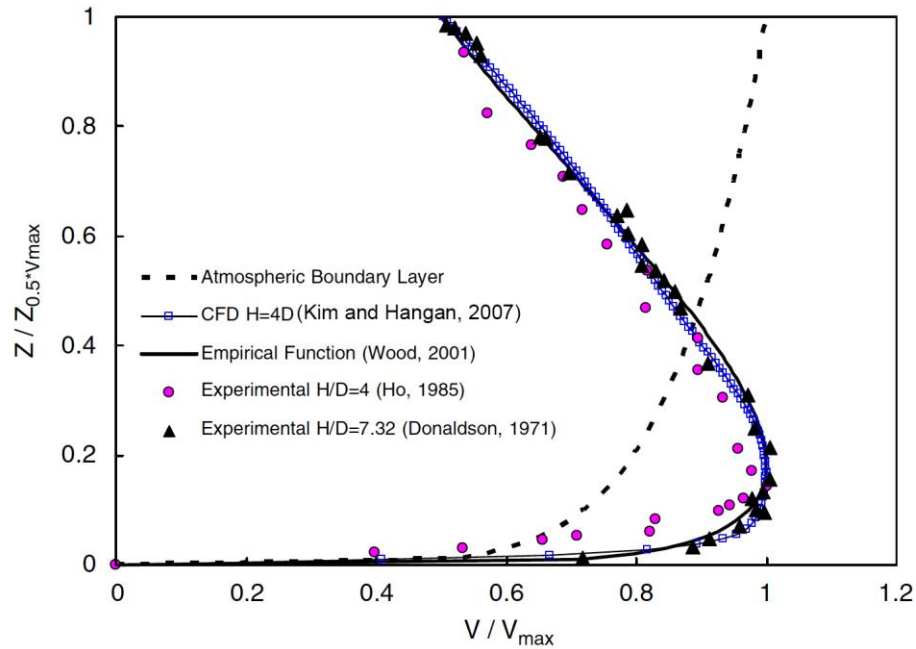


**Figure 1.10: Comparison of downburst mean velocity profiles between empirical model, laboratory experiment and typical boundary layer profiles (Adapted from Kim and Hangan, 2007)**

Aside from the three techniques (ring-vortex, cooling source and impinging jet) to simulate downburst identified by Zhang et al. (2013), another approach, namely wall jets (also referred to as slot jets), has also been adopted by researchers (Lin and Savory, 2006; Lin et al., 2007; Lin and Savory, 2010). This technique employs a secondary strong flow through a slot on the floor of traditional boundary layer wind tunnel to model the downburst outflow (Lin and Savory, 2006). While they are relatively simple to implement and provide good resolution in the surface region, these models do not reproduce the accurate vortex structure, as they concentrate on generating vorticity through a wall jet mechanism. As a result, the primary vortex structure lifts from the surface and does not produce a proper dynamic separation reattachment (Mason et al., 2005). Impinging jet technique, where the entire three dimensional flow structures of downbursts are modelled, provide better simulations compared to wall jet technique (Lin and Savory, 2006).

In the present study, downbursts are simulated using an impinging jet technique at the WindEEE dome to characterize the downburst outflow. This study, for the first time,

analyzes the downburst wind speed time history similar to an approach used for full scale downburst records (Solari et al., 2015) as well as compares the important turbulence characteristics (Spectra, probability density function, gust factor) relevant to wind loading of structures with full scale downburst events. In addition, particle image velocimetry (PIV) measurement technique is employed to analyze the vortex dynamics. Details of this analysis is presented in Chapter 3 of this thesis.

## 1.5 Motivation and purpose of this thesis

Downbursts are highly transient in nature and therefore one of the primary targets of this research is to investigate this transient nature using an objective method. A useful methodology to analyze transient signals has been used previously by researchers (Lavielle, 2005; Killick et al., 2012) for signal processing but never used on downburst signals to separate thunderstorm period from mean ABL flow. In addition, time series analysis is used to understand the typical downburst duration as well as the partition of full scale downburst events based on a variety of events worldwide.

The current research also focuses on the characterization of the downbursts turbulent flow field at high spatial and temporal resolutions. A large scale impinging jet approach is employed, as it is the best compromise between reproducing the vortex dynamics corresponding to real events and providing sufficient surface layer resolution. The large scale WindEEE Dome at Western University (Hangan et al., 2017) is used to characterize the turbulent flow field from simulated downbursts with high spatial and time resolution.

First, a time analysis of the velocity field is conducted based on Cobra probe measurements and using a similar approach to full scale analysis previously conducted by Solari et al. (2015). This allows the comparison of not only the mean but most importantly the turbulence between full scale and experimental downbursts.

Secondly, a large scale PIV analysis is conducted in order to investigate the vortex dynamics in experimentally produced downburst and to relate this to full scale events.

Considering all these different aspects, the following are the motivations of this thesis:

- To identify an objective method that can separate different stages of downbursts from a thunderstorm time history record
- To analyze the transient characteristics of downburst events from different parts of the world to obtain a perception of downburst characteristics around the world
- To investigate the downburst characteristics for different flow and geometrical parameters in an experimental simulator, which in turn would lead to recreating full scale downburst events in a laboratory environment
- To analyze the downburst flow in the surface layer with comparison to ABL flow
- To characterize the statistical parameters of turbulence in a downburst and how they relate to full scale downburst events
- To understand the structure and evolution of the primary downburst vortex and compare it with available full scale data

## 1.6 Organization of this thesis

This thesis follows the ‘Integrated article’ format as per thesis submission requirement of Western University. The thesis contains two articles described in Chapter 2 and Chapter 3 respectively.

Chapter 1 provides a brief introduction of thunderstorm downbursts and discusses the previous projects capturing full scale data. This section also includes a review of downburst characteristics obtained from laboratory experiments as well as numerical simulations by previous researchers.

Chapter 2 presents and analyzes the full scale downburst events from 3 different continents: Europe, US and Australia. 37 downburst records from 14 downburst events analyzed to identify a method to segment different stages of downburst in a thunderstorm wind record.

Chapter 3 focuses on the parametric characterization of large scale laboratory simulated downbursts in the unique three dimensional wind testing chamber, the WindEEE Dome. A moving time averaging method is employed to decompose the downburst time history for wind engineering application following the criteria set by Holmes (2008) and Solari et al. (2015). Turbulent characteristics and notable wind ratios ( $R, G_{max}, \hat{G}$ ) from the downburst flow are compared with previous full scale downburst events. Analysis on the primary vortex structure (primary vortex formulation, vortex trajectory) were carried out by PIV experiment explaining in the latter part of this chapter.

Chapter 4 provides the conclusions and an overall summary of the thesis. This section also recommends the scope of future works from this current study.

## 1.7 References

- Alahyari, A., Longmire, E.K., 1994. Particle image velocimetry in a variable density flow: application to a dynamically evolving microburst. *Experiments in Fluids* 17, 434–440. <https://doi.org/10.1007/BF01877047>
- Burlando, M., Romanić, D., Solari, G., Hangan, H., Zhang, S., 2017. Field Data Analysis and Weather Scenario of a Downburst Event in Livorno, Italy, on 1 October 2012. *Monthly Weather Review* 145, 3507–3527. <https://doi.org/10.1175/MWR-D-17-0018.1>
- Byers, H.R., Braham, R.R., 1948. Thunderstorm structure and circulation. *J. Meteor.* 5, 71–86. [https://doi.org/10.1175/1520-0469\(1948\)005<0071:TSAC>2.0.CO;2](https://doi.org/10.1175/1520-0469(1948)005<0071:TSAC>2.0.CO;2)
- Chay, M.T., Letchford, C.W., 2002. Pressure distributions on a cube in a simulated thunderstorm downburst—Part A: stationary downburst observations. *Journal of Wind Engineering and Industrial Aerodynamics* 90, 711–732. [https://doi.org/10.1016/S0167-6105\(02\)00158-7](https://doi.org/10.1016/S0167-6105(02)00158-7)
- Chen, L., Letchford, C.W., 2004. A deterministic–stochastic hybrid model of downbursts and its impact on a cantilevered structure. *Engineering Structures* 26, 619–629. <https://doi.org/10.1016/j.engstruct.2003.12.009>
- Choi, E.C.C., Hidayat, F.A., 2002. Gust factors for thunderstorm and non-thunderstorm winds. *Journal of Wind Engineering and Industrial Aerodynamics, Fifth Asia-Pacific Conference on Wind Engineering* 90, 1683–1696. [https://doi.org/10.1016/S0167-6105\(02\)00279-9](https://doi.org/10.1016/S0167-6105(02)00279-9)

- Cook, N.J., Ian Harris, R., Whiting, R., 2003. Extreme wind speeds in mixed climates revisited. *Journal of Wind Engineering and Industrial Aerodynamics* 91, 403–422. [https://doi.org/10.1016/S0167-6105\(02\)00397-5](https://doi.org/10.1016/S0167-6105(02)00397-5)
- Fujita, 1978. Manual of downburst identification for Project NIMROD. SMRP Res. Paper, 156 104.
- Fujita, T., 1990. Downbursts: meteorological features and wind field characteristics. *Journal of Wind Engineering and Industrial Aerodynamics, The Sixth U.S. National Conference on Wind Engineering* 36, 75–86. [https://doi.org/10.1016/0167-6105\(90\)90294-M](https://doi.org/10.1016/0167-6105(90)90294-M)
- Fujita, T.T., 1985. *The Downburst: Microburst and MacRoburst*. University of Chicago.
- Fujita, T.T., 1974. Jumbo Tornado Outbreak of 3 April 1974. *Weatherwise* 27, 116–126. <https://doi.org/10.1080/00431672.1974.9931693>
- Fujita, T.T., Wakimoto, R.M., 1981. Five Scales of Airflow Associated with a Series of Downbursts on 16 July 1980. *Mon. Wea. Rev.* 109, 1438–1456. [https://doi.org/10.1175/1520-0493\(1981\)109<1438:FSOAAW>2.0.CO;2](https://doi.org/10.1175/1520-0493(1981)109<1438:FSOAAW>2.0.CO;2)
- Gomes, L., Vickery, B.J., 1978. Extreme wind speeds in mixed wind climates. *Journal of Wind Engineering and Industrial Aerodynamics* 2, 331–344. [https://doi.org/10.1016/0167-6105\(78\)90018-1](https://doi.org/10.1016/0167-6105(78)90018-1)
- Gunter, W.S., Schroeder, J.L., 2015. High-resolution full-scale measurements of thunderstorm outflow winds. *Journal of Wind Engineering and Industrial Aerodynamics* 138, 13–26. <https://doi.org/10.1016/j.jweia.2014.12.005>
- Hangan, H., Refan, M., Jubayer, C., Parvu, D., Kilpatrick, R., 2017. Big Data from Big Experiments. *The WindEEE Dome, in: Whither Turbulence and Big Data in the 21st Century?* Springer, Cham, pp. 215–230. [https://doi.org/10.1007/978-3-319-41217-7\\_12](https://doi.org/10.1007/978-3-319-41217-7_12)
- Hjelmfelt, M.R., 1988. Structure and Life Cycle of Microburst Outflows Observed in Colorado. *J. Appl. Meteor.* 27, 900–927. [https://doi.org/10.1175/1520-0450\(1988\)027<0900:SALCOM>2.0.CO;2](https://doi.org/10.1175/1520-0450(1988)027<0900:SALCOM>2.0.CO;2)
- Holmes, J.D., Hangan, H.M., Schroeder, J.L., Letchford, C.W., Orwig, K.D., 2008. A forensic study of the Lubbock-Reese downdraft of 2002. *Wind and Structures* 11, 137–152. <https://doi.org/10.12989/was.2008.11.2.137>
- Holmes, J.D., Oliver, S.E., 2000. An empirical model of a downburst. *Engineering Structures* 22, 1167–1172. [https://doi.org/10.1016/S0141-0296\(99\)00058-9](https://doi.org/10.1016/S0141-0296(99)00058-9)
- Hong, H.P., 2016. Modeling of Nonstationary Winds and Its Applications. *Journal of Engineering Mechanics* 142, 04016004. [https://doi.org/10.1061/\(ASCE\)EM.1943-7889.0001047](https://doi.org/10.1061/(ASCE)EM.1943-7889.0001047)



- Järvi, L., Punkka, A.-J., Schultz, D.M., Petäjä, T., Hohti, H., Rinne, J., Pohja, T., Kulmala, M., Hari, P., Vesala, T., 2007. Micrometeorological observations of a microburst in southern Finland, in: *Atmospheric Boundary Layers*. Springer, New York, NY, pp. 187–203. [https://doi.org/10.1007/978-0-387-74321-9\\_13](https://doi.org/10.1007/978-0-387-74321-9_13)
- Jesson, M., Haines, M., Singh, N., Sterling, M., Taylor, I., 2013. Numerical and Physical Simulation of a Thunderstorm Downburst. Research Publishing Services, pp. 1139–1148. [https://doi.org/10.3850/978-981-07-8012-8\\_P3](https://doi.org/10.3850/978-981-07-8012-8_P3)
- Jesson, M., Sterling, M., 2018. A simple vortex model of a thunderstorm downburst – A parametric evaluation. *Journal of Wind Engineering and Industrial Aerodynamics* 174, 1–9. <https://doi.org/10.1016/j.jweia.2017.12.001>
- Killick, R., Fearnhead, P., Eckley, I.A., 2012. Optimal Detection of Changepoints With a Linear Computational Cost. *Journal of the American Statistical Association* 107, 1590–1598. <https://doi.org/10.1080/01621459.2012.737745>
- Kim, J., Hangan, H., 2007. Numerical simulations of impinging jets with application to downbursts. *Journal of Wind Engineering and Industrial Aerodynamics* 95, 279–298. <https://doi.org/10.1016/j.jweia.2006.07.002>
- Landreth, C.C., Adrian, R.J., 1990. Impingement of a low Reynolds number turbulent circular jet onto a flat plate at normal incidence. *Experiments in Fluids* 9, 74–84. <https://doi.org/10.1007/BF00575338>
- Lavielle, M., 2005. Using penalized contrasts for the change-point problem. *Signal Processing* 85, 1501–1510. <https://doi.org/10.1016/j.sigpro.2005.01.012>
- Letchford, C.W., Chay, M.T., 2002. Pressure distributions on a cube in a simulated thunderstorm downburst. Part B: moving downburst observations. *Journal of Wind Engineering and Industrial Aerodynamics* 90, 733–753. [https://doi.org/10.1016/S0167-6105\(02\)00163-0](https://doi.org/10.1016/S0167-6105(02)00163-0)
- Letchford, C.W., Mans, C., Chay, M.T., 2002. Thunderstorms—their importance in wind engineering (a case for the next generation wind tunnel). *Journal of Wind Engineering and Industrial Aerodynamics, Fifth Asia-Pacific Conference on Wind Engineering* 90, 1415–1433. [https://doi.org/10.1016/S0167-6105\(02\)00262-3](https://doi.org/10.1016/S0167-6105(02)00262-3)
- Lin, W.E., Orf, L.G., Savory, E., Novacco, C., 2007. Proposed large-scale modelling of the transient features of a downburst outflow. *Wind and Structures* 10, 315–346. <https://doi.org/10.12989/was.2007.10.4.315>
- Lin, W.E., Savory, E., 2010. Physical modelling of a downdraft outflow with a slot jet. *Wind and Structures* 13, 385–412. <https://doi.org/10.12989/was.2010.13.5.385>
- Lin, W.E., Savory, E., 2006. Large-scale quasi-steady modelling of a downburst outflow using a slot jet. *Wind and Structures* 9, 419–440. <https://doi.org/10.12989/was.2006.9.6.419>

- Lombardo, F.T., Smith, D.A., Schroeder, J.L., Mehta, K.C., 2014. Thunderstorm characteristics of importance to wind engineering. *Journal of Wind Engineering and Industrial Aerodynamics* 125, 121–132. <https://doi.org/10.1016/j.jweia.2013.12.004>
- Lundgren, T.S., Yao, J., Mansour, N.N., 1992. Microburst modelling and scaling. *Journal of Fluid Mechanics* 239, 461–488. <https://doi.org/10.1017/S002211209200449X>
- Mason, M.S., Letchford, C.W., James, D.L., 2005. Pulsed wall jet simulation of a stationary thunderstorm downburst, Part A: Physical structure and flow field characterization. *Journal of Wind Engineering and Industrial Aerodynamics* 93, 557–580. <https://doi.org/10.1016/j.jweia.2005.05.006>
- Mason, M.S., Wood, G.S., Fletcher, D.F., 2009. Numerical simulation of downburst winds. *Journal of Wind Engineering and Industrial Aerodynamics* 97, 523–539. <https://doi.org/10.1016/j.jweia.2009.07.010>
- McConville, A.C., Sterling, M., Baker, C.J., 2009. The physical simulation of thunderstorm downbursts using an impinging jet. *Wind and Structures An International Journal* 12, 133–149. <https://doi.org/10.12989/was.2009.12.2.133>
- McCullough, M., Kwon, D.K., Kareem, A., Wang, L., 2014. Efficacy of Averaging Interval for Nonstationary Winds. *Journal of Engineering Mechanics* 140, 1–19. [https://doi.org/10.1061/\(ASCE\)EM.1943-7889.0000641](https://doi.org/10.1061/(ASCE)EM.1943-7889.0000641)
- Orf, L.G., Oreskovic, C., Savory, E., Kantor, E., 2014. Circumferential analysis of a simulated three-dimensional downburst-producing thunderstorm outflow. *Journal of Wind Engineering and Industrial Aerodynamics* 135, 182–190. <https://doi.org/10.1016/j.jweia.2014.07.004>
- Panneer Selvam, R., Holmes, J.D., 1992. Numerical simulation of thunderstorm downdrafts. *Journal of Wind Engineering and Industrial Aerodynamics, Special Issue 8th International Conference on Wind Engineering 1991* 44, 2817–2825. [https://doi.org/10.1016/0167-6105\(92\)90076-M](https://doi.org/10.1016/0167-6105(92)90076-M)
- Proctor, F.H., 1988. Numerical Simulations of an Isolated Microburst. Part I: Dynamics and Structure. *J. Atmos. Sci.* 45, 3137–3160. [https://doi.org/10.1175/1520-0469\(1988\)045<3137:NSOAIM>2.0.CO;2](https://doi.org/10.1175/1520-0469(1988)045<3137:NSOAIM>2.0.CO;2)
- Schultz, T.A., 1990. Multiple vortex ring model of the DFW microburst. *Journal of Aircraft* 27, 163–168. <https://doi.org/10.2514/3.45913>
- Sengupta, A., Sarkar, P.P., 2008. Experimental measurement and numerical simulation of an impinging jet with application to thunderstorm microburst winds. *Journal of Wind Engineering and Industrial Aerodynamics* 96, 345–365. <https://doi.org/10.1016/j.jweia.2007.09.001>

- Sherman, D.J., 1987. The Passage of a Weak Thunderstorm Downburst over an Instrumented Tower. *Mon. Wea. Rev.* 115, 1193–1205. [https://doi.org/10.1175/1520-0493\(1987\)115<1193:TPOAWT>2.0.CO;2](https://doi.org/10.1175/1520-0493(1987)115<1193:TPOAWT>2.0.CO;2)
- Solari, G., Burlando, M., De Gaetano, P., Repetto, M.P., 2015. Characteristics of thunderstorms relevant to the wind loading of structures. *Wind and Structures* 20, 763–791. <https://doi.org/10.12989/was.2015.20.6.763>
- Srivastava, R.C., 1985. A Simple Model of Evaporatively Driven Downdraft: Application to Microburst Downdraft [WWW Document]. [http://dx.doi.org/10.1175/1520-0469\(1985\)042<1004:ASMOED>2.0.CO;2](http://dx.doi.org/10.1175/1520-0469(1985)042<1004:ASMOED>2.0.CO;2). URL [https://journals.ametsoc.org/doi/abs/10.1175/1520-0469\(1985\)042%3C1004:ASMOED%3E2.0.CO%3B2](https://journals.ametsoc.org/doi/abs/10.1175/1520-0469(1985)042%3C1004:ASMOED%3E2.0.CO%3B2) (accessed 8.6.18).
- Srivastava, R.C., Srivastava, R.C., 1987. A Model of Intense Downdrafts Driven by the Melting and Evaporation of Precipitation [WWW Document]. [http://dx.doi.org/10.1175/1520-0469\(1987\)044<1752:AMOIDD>2.0.CO;2](http://dx.doi.org/10.1175/1520-0469(1987)044<1752:AMOIDD>2.0.CO;2). URL [https://journals.ametsoc.org/doi/abs/10.1175/1520-0469\(1987\)044%3C1752:AMOIDD%3E2.0.CO;2](https://journals.ametsoc.org/doi/abs/10.1175/1520-0469(1987)044%3C1752:AMOIDD%3E2.0.CO;2) (accessed 8.6.18).
- Vermeire, B.C., Orf, L.G., Savory, E., 2011. Improved modelling of downburst outflows for wind engineering applications using a cooling source approach. *Journal of Wind Engineering and Industrial Aerodynamics* 99, 801–814. <https://doi.org/10.1016/j.jweia.2011.03.003>
- Wakimoto, R.M., 1985. Forecasting Dry Microburst Activity over the High Plains. *Mon. Wea. Rev.* 113, 1131–1143. [https://doi.org/10.1175/1520-0493\(1985\)113<1131:FDMAOT>2.0.CO;2](https://doi.org/10.1175/1520-0493(1985)113<1131:FDMAOT>2.0.CO;2)
- Wakimoto, R.M., 1982. The Life Cycle of Thunderstorm Gust Fronts as Viewed with Doppler Radar and Rawinsonde Data. *Mon. Wea. Rev.* 110, 1060–1082. [https://doi.org/10.1175/1520-0493\(1982\)110<1060:TLCOTG>2.0.CO;2](https://doi.org/10.1175/1520-0493(1982)110<1060:TLCOTG>2.0.CO;2)
- Wilson, J.W., Roberts, R.D., Kessinger, C., McCarthy, J., 1984. Microburst Wind Structure and Evaluation of Doppler Radar for Airport Wind Shear Detection. *J. Climate Appl. Meteor.* 23, 898–915. [https://doi.org/10.1175/1520-0450\(1984\)023<0898:MWSAEO>2.0.CO;2](https://doi.org/10.1175/1520-0450(1984)023<0898:MWSAEO>2.0.CO;2)
- Wilson, J.W., Wakimoto, R.M., 2001. The Discovery of the Downburst: T. T. Fujita's Contribution. *Bulletin of the American Meteorological Society* 82, 49–62. [https://doi.org/10.1175/1520-0477\(2001\)082<0049:TDOTDT>2.3.CO;2](https://doi.org/10.1175/1520-0477(2001)082<0049:TDOTDT>2.3.CO;2)
- Wolfson, M.M., 1988. Characteristics of Microbursts in the Continental United States.
- Wood, G.S., Kwok, K.C.S., Motteram, N.A., Fletcher, D.F., 2001. Physical and numerical modelling of thunderstorm downbursts. *Journal of Wind Engineering and Industrial Aerodynamics* 89, 535–552. [https://doi.org/10.1016/S0167-6105\(00\)00090-8](https://doi.org/10.1016/S0167-6105(00)00090-8)

- Xu, Z., Hangan, H., 2008. Scale, boundary and inlet condition effects on impinging jets. *Journal of Wind Engineering and Industrial Aerodynamics* 96, 2383–2402. <https://doi.org/10.1016/j.jweia.2008.04.002>
- Yao, J., Lundgren, T.S., 1996. Experimental investigation of microbursts. *Experiments in Fluids* 21, 17–25. <https://doi.org/10.1007/BF00204631>
- Zhang, Y., Hu, H., Sarkar, P.P., 2013. Modeling of microburst outflows using impinging jet and cooling source approaches and their comparison. *Engineering Structures* 56, 779–793. <https://doi.org/10.1016/j.engstruct.2013.06.003>

## Chapter 2

### 2 Investigation of the transient nature of downbursts from Europe, United States and Australia through detection of abrupt changes in wind speed records

This chapter investigates the transient nature of 14 downburst events from around the world—9 from Europe, 4 from the United States, and 1 from Australia. Since most of the events were recorded by several anemometers, a total of 37 downburst wind speed records are used in the analysis. The transient features of downbursts were examined by introducing an objective method for detection of change points in the time series. The methodology divides the time series into different segments, each characterized with a statistically significant different property compared to the two adjacent segments. The point between two adjacent segments is called a change point. The segmentation is based on the following properties of the isolated segments: mean (M), the standard deviation (SD) and the linear trend (LT). The three segmentation approaches gave a similar range of downburst duration (<5 minutes) in 72.97% of cases for M, 45.94% for SD and 62.16% for LT. On average, the downburst duration was 6.5 minutes. The ramp-up time, defined as the time between the start of the downburst and the peak wind speed, was below 1 min in 56.8% cases for M, 35.1% for SD and 64.9% for LT. The typical number of segments in the downburst time series is 3–4 using the M and LT approaches and 2–3 employing the SD method. In many cases, the SD method isolates the whole thunderstorm-related segment from the rest of the time series, while the M and LT methods tend to further subdivide the thunderstorm portion of the time series into different parts. Several prospects for further development of this methodology are also outlined.

#### 2.1 Introduction

Downbursts are highly transient wind phenomena associated with thunderstorms. Velocity in a downburst outflow changes rapidly in the radial direction, with height, and in time. In

addition, this spatiotemporal variability applies to all wind components as well as the wind direction making the flows highly three-dimensional. As such, downburst winds have a particular signature in the wind velocity records (**Figure 2.1**). This study focuses on the investigation of downburst signatures by analyzing a cross sample of measured downbursts from several places around the globe. The transient nature of a downburst in comparison to ABL winds is depicted in **Figure 2.1**. Besides steadiness, the ABL winds in **Figure 2.1a** (Lareau et al. 2013) are also characterized by smaller turbulent fluctuations than downburst outflows.

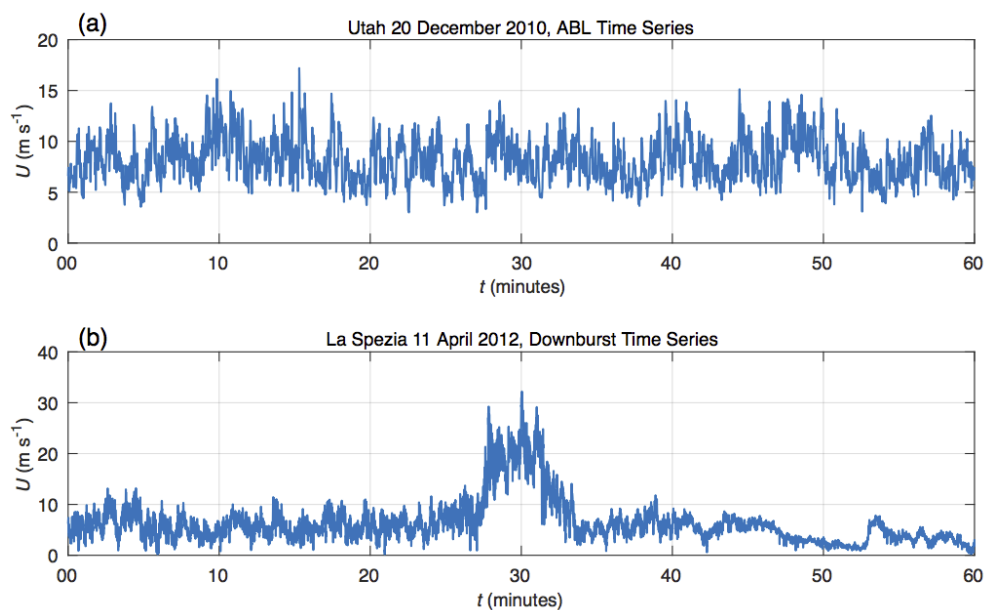


**Figure 2.1: An hour-long time series of (a) steady atmospheric boundary layer (ABL) wind and (b) transient downburst. Location and date of measured time series shown above plots.**

Several methodologies for classification of winds into different types have been proposed over the years. For example, a number of techniques exist to separate extra-tropical cyclone winds from tropical cyclone winds (e.g., Thom 1967; Gomes and Vickery 1978; Cook et al. 2003) in order to estimate wind actions on structures. These methods were proposed after Davenport (1961) developed the wind loading model for extra-tropical cyclones. However, methodologies that separate thunderstorm from non-thunderstorm winds (e.g.,

Riera and Nanni 1989; Choi and Hidayat 2002; Kasperski 2002; Durañona et al. 2007; Lombardo 2009; Lombardo et al. 2014; Gunter et al. 2017) are more relevant to this article.

Fujita (1985) proposed an algorithm for downburst detection from measured wind speed data based on the 1-min mean wind speed ( $\bar{U}_{1\text{min}}$ ), 1-min maximum wind speed ( $\hat{U}_{1\text{min}}$ ), as well as the pre-peak mean wind speed ( $\bar{U}_-$ ) and post-peak mean wind speed ( $\bar{U}_+$ ). The last two ( $\bar{U}_-, \bar{U}_+$ ) are calculated from seven 1-min segments prior to and after the central peak, respectively, with the first minute before and after the peak being excluded from the analysis. According to Fujita (1985), the following conditions have to be satisfied simultaneously in order for an event to be classified as downburst: (1)  $\hat{U}_{1\text{min}} > 10 \text{ m s}^{-1}$ , (2)  $\hat{U}_{1\text{min}} > \bar{U}_+ + 5$  and  $\hat{U}_{1\text{min}} > \bar{U}_- + 5$ , (3)  $\hat{U}_{1\text{min}} > 1.25\bar{U}_+$  and  $\hat{U}_{1\text{min}} > 1.25\bar{U}_-$ , and lastly (4)  $\bar{U}_+ \leq 1.5\bar{U}_-$ . Fujita (1985) applied this algorithm to 5 million wind time histories and extracted 579 downbursts from NIMROD (Northern Illinois Meteorological Research on Downburst) and JAWS (Joint Airport Weather Studies) field campaigns combined.

Lombardo et al. (2009) put forward a methodology to separate thunderstorm from non-thunderstorm winds from the hourly Automated Surface Observing System (ASOS) data. The ASOS network of automated weather stations covers most of the continental United States (US; e.g., see Romanic et al. 2018). Due to the coarse time resolution of ASOS data, only the hourly peak values of thunderstorm winds and their duration were obtained and analyzed. Since the method was applied to a large set of data, the research was focused on the underlying statistical distribution of extremes. The individual time series were not investigated in detail. De Gaetano et al. (2014) implemented an automated procedure for extraction of three classes of winds from anemometer records: (1) stationary and Gaussian, (2) non-stationary and non-Gaussian, and (3) stationary and non-Gaussian winds. The second class of winds belongs to thunderstorm winds classified as downbursts. The separation methodology of De Gaetano et al. (2014) is implemented through a sequential algorithm that uses 10-min and 1-hour values of various statistical parameters averaged over 1-s and 1-min intervals, respectively. The considered parameters over a 10-min interval are peak and mean velocities ( $\hat{U}_{10\text{min}}$  and  $\bar{U}_{10\text{min}}$ , respectively), mean wind direction ( $\theta_{10\text{min}}$ ), gust factor ( $G_{10\text{min}} = \hat{U}_{10\text{min}}/\bar{U}_{10\text{min}}$ ), turbulence intensity ( $I_{10\text{min}}$ ),

skewness ( $\gamma_{10\text{min}}$ ) and kurtosis ( $k_{10\text{min}}$ ), as well as the same set of parameters for a 1-hour interval (with the exception of the peak velocity). If  $\hat{U}_{10\text{min}} \geq 15 \text{ m s}^{-1}$ , the wind record is a candidate to be a thunderstorm wind. In addition, if  $G_{10\text{min}}/G_{10\text{min\_ref}} > 1.25$  ( $G_{10\text{min\_ref}}$  is the reference gust factor obtained from the Engineering Sciences Data Unit standard, ESDU 1993), then the event is either non-stationary and non-Gaussian (i.e., thunderstorm wind) or stationary and non-Gaussian. Lastly, whether the event is thunderstorm or not is determined qualitatively. De Gaetano et al. (2014) applied their method to a large set of wind data obtained through the field measurement campaigns “Wind and Ports” (Solari et al. 2012) and “Wind, Ports and Sea” (Repetto et al. 2017), which were carried out between 2009 and 2015 in the Mediterranean, and extracted more than 150 thunderstorm wind events. Most downburst data examined in this paper are obtained from these two databases.

Of particular importance for this paper are the research studies by Lombardo (2009), Lombardo et al. (2014) and Gunter et al. (2017). Those studies also investigated individual time series of thunderstorm winds by analyzing abrupt changes in wind speed (Lombardo 2009; Lombardo et al. 2014) and wind direction (Gunter et al. 2017) data. The segmentation method proposed by Lombardo et al. (2014) identified potential abrupt changes in the wind speed time series by inspecting statistically significance changes in variance using the reverse arrangement test (NIST, 2006) and run test (Bendat and Piersol, 2000). The beginning of each time series was split into eighteen 3-s segments and the segments were subjected to stationarity testing. If the test statistics of this portion of the time series was stationary, the algorithm would include the following 3-s interval and repeat the stationary testing. This addition of the following 3-s portion to the previous length of the segment is carried out until one or both of the above-mentioned tests indicated non-stationarity. The occurrence of non-stationarity is deemed as a change point in the time series. More recently, Gunter et al. (2017) separated the time series of thunderstorm winds into five segments identified in a 40-s moving average of wind direction time history. Their method is based on identifying the zero-derivative points on either sides of the abrupt change in the moving average time series. The physical justification of the method follows from the studies of Goff (1976) and Wakimoto (1982).



Since downbursts are particularly dangerous for aircrafts in their landing and take-off stages of flights (Fujita and Byers 1977), many studies looked into the methodologies of detection and analysis of downbursts from radars and anemometers installed at airports and elsewhere (e.g., Wilson et al. 1984; Qiu and Xu 1996; Geerts 2001; Pryor and Ellrod 2004; Smith et al. 2004; Vasiloff and Howard 2009; De Meutter et al. 2014; Gunter and Schroeder 2015; Pryor 2015; Wang et al. 2015; Adachi et al. 2016; Baldini et al. 2018). These days a near real-time warnings of downburst occurrence can be issued to pilots using the products obtained from Doppler weather radars, Doppler Lidars, the Low-Level Windshear Alert System (Wolfson et al. 1995) and wind profilers and sodars (Ellrod et al. 2000). Some of the widely known downburst forecasting products are WINDEX (McCann 1994), dry microburst index (Ellrod and Nelson 1999) and maximum vertical  $\theta_e$  differential, where  $\theta_e$  is the equivalent potential temperature. An overview of downburst prediction methods is given in Pryor (2015).

Notice that there is a pronounced difference between these studies and the articles described in the previous paragraphs. Namely, the latter articles are meteorological studies that investigate downbursts using not only wind data, but also taking into account various information about atmospheric pressure, air temperature and potential temperature, radar echo, cloud structure and precipitation, among other factors. Therefore, statistical and signal properties of the wind velocity time series in meteorological studies are commonly overlooked. At the same time, wind engineering studies focus on the signal and spectral characteristics of downbursts without investigating the deeper physical background of the phenomena. A recent study by Burlando et al. (2017) attempts to merge wind engineering and meteorological approaches of analyzing downbursts.

This article investigates abrupt changes in wind speed records of downbursts with the goal to quantitatively describe the transient nature of the phenomena using objective procedures in order to facilitate automated data analysis. The introduced methodology, however, could be applied to the analysis of time series of other downburst parameters (Lompar et al. 2018), and not just wind speed. **Figure 2.1b** portrays a typical downburst time series. The prominent features of the anemometer record are the separation of downburst outflow from background winds that precede and proceed the downburst, downburst ramp up, and

decline of wind speed after the main velocity peak. In some cases, a second peak in velocity, which is typically weaker than the first peak, also exists if the thunderstorm moves over the weather station (Chay et al. 2006; Burlando et al. 2017). Although these features are well-known facets of downburst time series, there is no quantitative and mathematically rigorous technique that objectively determines downburst duration (e.g., the exact times of the start and end of the event) and duration of different stages of downburst outflow. For instance, the beginning of downburst ramp-up is typically answered by subjectively selecting a point on the time series that “seem” to be a good candidate (Chay et al., 2006; Holmes et al., 2008; McConville et al., 2009). However, those approaches are subjective and therefore not suitable for any kind of automated analysis of downburst time series. This is in particular the case for large sets of data or in situations when near real-time downburst forecasting is needed.

Therefore, the goal of the present study is to introduce a mathematical technique for detection of abrupt changes in downburst velocity records and to investigate the transient nature of downbursts. The methodology adopted in this paper is borrowed from the signal processing research carried out in the fields of speech analysis and brain research (Basseville and Nikiforov 1993; Darkhovski 1994; Lavielle 2005), as well as geosciences (Killick et al. 2012). Chen and Letchford (2004), (2006) as well as Burlando et al. (2017) reported that turbulent fluctuations in downbursts are more pronounced than in the winds prior to and after the event. While this feature of downburst winds is portrayed in **Figure 1.1c**, this article attempts to further quantify the relationship between turbulent fluctuations before and after the downburst. The methodology for downburst segmentation is applied to 14 downburst events out of which 9 are from Europe, 4 from the US, and 1 from Australia. Similarities and differences between downbursts from different parts of the world are therefore objectively examined.

## 2.2 Data and methods

### 2.2.1 Data

Downburst data used in this study come from a variety of sources and cover three continents: Europe (9), North America (4), and Australia (1). Eight downbursts from Europe come from two European Union projects “Wind and Ports” (Solari et al. 2012) and “Wind, Ports and Sea” (Repetto et al. 2017). The goal of these projects was to provide a high-quality field measurements of thunderstorm winds in the Ligurian Sea and the north Tyrrhenian Sea, in the Mediterranean (**Figure 2.2a**). Out of eight events from this region (Italy), one event was recorded in Genoa, five were measured in La Spezia, and three come from Livorno. Notice that some events were captured with several anemometers making the number of analyzed velocity records larger than the number of considered events. Anemometer characteristics and site coordinates are provided in Table 2.1 and **Figure 2.2a**. The remaining event from Europe was observed in Finland (Järvi et al. 2007) in 2004 (Table 2.1 and **Figure 2.2a**). Notice that the events from the Mediterranean correspond to downbursts that originated above sea, while the event in Finland is a downburst that took place above a forest area. Thus, there is a large difference between surface roughness of two regions in addition to the pronouncedly different climatological characteristics of Finland (northeast Europe) and the Mediterranean coast of Italy (south Europe).



**Figure 2.2: Location map of downburst events in (a) Europe, (b) United States and (c) Australia**

**Figure 2.2b** shows the location of downbursts investigated in the US. Two events were recorded in Texas—one in Pep (Gunter et al. 2017) and another in Lubbock (Orwig and Schroeder 2007; Holmes et al. 2008). The Lubbock downburst was recorded by twelve anemometers (six masts) which makes it the best documented downburst event in this study. Anemometer characteristics for all US events are also listed in Table 2.1. Another event from the US was recorded in Syracuse, Kansas, (Gunter and Schroeder 2015) and one in the Andrews Air Force Base (AAFB) in Washington, Maryland (Fujita 1985) (**Figure 2.2b** and Table 2.1). It is important to point out here that the raw data for the Washington event (Fujita 1985) were not available to the authors and therefore the published time series in Fujita (1985) was digitized in order to obtain wind speed data. Therefore, the uncertainty of digitalized data records is inevitably larger than for the raw data that were kindly supplied to the authors. However, the introduced uncertainty due to the digitalization is deemed not to influence the validity of obtained results because this study is mostly concerned with the investigation of breakpoints (i.e., abrupt changes) in velocity time series. Also note that all downbursts from the US emerged above land.

The single downburst event from Australia was observed by Sherman (1987) in the suburban region of Brisbane (**Figure 2.2c**). Although the event was captured by four anemometers (Table 2.1), the raw data were not available and thus the analyzed time series were digitalized in order to obtain wind speeds. Notice that anemometers in Table 2.1 are labelled by the first two letters of the site, e.g., LI3 is Livorno anemometer 3 and BR4 is Brisbane anemometer 4, and so on. Lastly, combining the number of anemometers and the number of downbursts, the total number of analyzed downburst time series in this paper is 37.

### 2.2.2 Change points in downburst wind records-theoretical background

Informally, change points represent the points in the time series at which statistical properties of a segment of observations change. Formally, a change point can be defined as follows. Consider a time series  $U_t = (U_1, U_2, \dots, U_T)$  of velocity data (e.g., **Figure 2.1**),

where  $T$  is the total number of velocity readings. That is,  $T = \Delta T \cdot f_s$ , where  $\Delta T$  is the length of measurements (in s) and  $f_s$  is the sampling frequency (in Hz). A change point occurs if there exist a time,  $\tau \in \{1, 2, \dots, T - 1\}$ , at which some statistical properties of  $\{U_1, \dots, U_\tau\}$  and  $\{U_{\tau+1}, \dots, U_T\}$  are different. The above definition can readily be extended to a set of change points,  $m$ , with their respective positions being  $1 < \tau_1 < \tau_2 < \dots < \tau_m < T$ .

In the change point detection problems, the goal is to minimize the expression (Lavielle 1999); 2005; Killick et al. 2012):

$$\sum_{i=1}^{m+1} [\mathcal{C}(U_{(\tau_{i-1}+1):\tau_i}) + \gamma], \quad (2.1)$$

where  $\mathcal{C}(\cdot)$  is a cost function for a segment  $\tau_{i-1}$  and  $\tau_i$ , and  $\gamma$  is a penalty function against overfitting. In this study, the minimization is performed using a recursive approach (Killick et al. 2012):

$$F(s) = \min_{t < s} [F(t) + \mathcal{C}(U_{(t+1):s}) + \gamma], \quad (2.2)$$

where  $F(s)$  is the optimal partitioning of the points  $U_1, U_2, \dots, U_s$  ( $s = 1, 2, \dots, T$ ) and  $F(t)$  is the optimal partitioning of the points  $U_1, U_2, \dots, U_t$ , where  $t < s$  and  $F(0) = -\gamma$ . The details of this computational algorithm—the so-called the optimal partitioning method—are described in (Jackson et al. 2005)) and (Lavielle 2005), with certain computational improvements using the prude exact linear time method proposed by Killick et al. (2012). Eq. (2.2) shows that the penalty constant,  $\gamma$ , is a “balance” between the cost function and the number of change points. If  $\gamma = 0$ , there is no penalty for adding a change point to the model and therefore the data are segmented in as many segments as possible, i.e.,  $T - 1$  segments. The relationship between  $\gamma$  and  $m$  depends on the data and it will be discussed more in section 4 based on the results obtained from the analyzed downbursts. In general terms, however, Eq. (2.2) demonstrates that a larger  $\gamma$  results in fewer change points and thus smaller variance of the model  $F(s)$ . Since the variance describes the sensitivity of the

model to input data, the small variance also results in a larger bias of the model. So, in other words,  $\gamma$  is a tradeoff between bias and variance of  $F(s)$ .

The next step is to describe the cost functions used in this study. Let us again consider the time series  $U_t = (U_1, U_2, \dots, U_T)$  and, supported by the central limit theorem, let us further assume that the time series is a result of an independent normal stochastic process (Chen and Gupta 2012). Therefore,  $v_t$  can be modelled as:

$$U_i = c_{0,j} + c_{1,j}t_i + \varepsilon_i, \quad (2.3)$$

where  $t_i$  ( $i = 1, 2, \dots, T$ ) is the time record,  $\varepsilon_i$  is the noise (error term with zero mean and unit variance), and  $c_{0,j}$  and  $c_{1,j}$  are the linear regression coefficients of the segment  $j$ . In other words,  $U_i$  is a subset of a random variable  $\mathcal{U}_i$  whose Gaussian probability density function ( $f_{\mathcal{U}_i}$ ) is:

$$f_{\mathcal{U}_i}(U_i | t_i, c_{0,j}, c_{1,j}, \sigma_j^2) = \frac{1}{\sqrt{2\pi\sigma_j^2}} e^{-\frac{(U_i - c_{0,j} - c_{1,j}t_i)^2}{2\sigma_j^2}}, \quad (2.4)$$

where  $\sigma^2$  is the variance. Invoking the assumption of data independency once more, the likelihood function ( $L$ ) of all data  $U_t = (U_1, U_2, \dots, U_T)$  is the product of the  $f_{\mathcal{U}_i}$ 's, i.e.:

$$L(\bar{C}_0, \bar{C}_1, \bar{\sigma}^2) = \prod_{j=1}^{m+1} \prod_{i=\tau_{j-1}+1}^{\tau_j} \frac{1}{\sqrt{2\pi\sigma_j^2}} e^{-\frac{(U_i - c_{0,j} - c_{1,j}t_i)^2}{2\sigma_j^2}} \quad (2.5)$$

where  $\bar{C}_0 = (c_{0,1}, c_{0,2}, \dots, c_{0,m+1})$ ,  $\bar{C}_1 = (c_{1,1}, c_{1,2}, \dots, c_{1,m+1})$  and  $\bar{\sigma}^2 = (\sigma_1^2, \sigma_2^2, \dots, \sigma_{m+1}^2)$ . The unbiased maximum likelihood estimates of the unknown parameters in Eq. (2.5) are the solution of the following system of algebraic equations (Neter et al. 1996):

$$\hat{C}_{0,j} = \bar{U}_i - \hat{C}_{1,j}\bar{t}_i, \quad (2.6)$$

$$\hat{C}_{1,j} = \frac{\sum_{i=\tau_{j-1}+1}^{\tau_j} (t_i - \bar{t}_i)^2 (U_i - \bar{U}_i)^2}{\sum_{i=\tau_{j-1}+1}^{\tau_j} (t_i - \bar{t}_i)^2}, \quad (2.7)$$

$$\hat{\sigma}_j^2 = \frac{1}{\tau_j - \tau_{j-1} - 2} \sum_{i=\tau_{j-1}+1}^{\tau_j} (U_i - c_{0,j} - c_{1,j}t_i)^2, \quad (2.8)$$

where  $\bar{t}_i = \frac{1}{\tau_j - \tau_{j-1}} \sum_{i=\tau_{j-1}+1}^{\tau_j} t_i$  and  $\bar{U}_i = \frac{1}{\tau_j - \tau_{j-1}} \sum_{i=\tau_{j-1}+1}^{\tau_j} U_i$ . It is beneficial to introduce twice the negative log-likelihood function as a choice of the cost function in order to directly (and easily) add segment costs to the overall cost. Therefore, we cast Eq. (2.5) in the form:

$$c(U_{(\tau_{j-1}): \tau_j}) = -2 \ln[L(\hat{C}_{0,j}, \hat{C}_{1,j}, \hat{\sigma}_j^2)] \quad (2.9)$$

or after expanding the right-hand side:

$$c(U_{(\tau_{j-1}): \tau_j}) = (\tau_j - \tau_{j-1}) \ln(2\pi\hat{\sigma}_j^2) + 2 \sum_{i=\tau_{j-1}+1}^{\tau_j} \frac{(U_i - \hat{c}_{0,j} - \hat{c}_{1,j}t_i)^2}{2\hat{\sigma}_j^2}. \quad (2.10)$$

Eq. (2.10) represents the likelihood linear regression cost function. Setting  $\hat{c}_1 = 0$ , we retrieve the likelihood mean cost function, i.e.:

$$c(U_{(\tau_{j-1}): \tau_j}) = -(\tau_j - \tau_{j-1}) \ln(2\pi\hat{\sigma}_j^2) + 2 \sum_{i=\tau_{j-1}+1}^{\tau_j} \frac{(U_i - \hat{c}_{0,j})^2}{2\hat{\sigma}_j^2}. \quad (2.11)$$

When analyzing the abrupt changes in the mean wind speed, the standard deviation ( $\sigma$ , square root of variance, or r.m.s) is a fixed constant in the above expression. Similarly, when investigating the change points through  $\sigma$ , the mean is a fixed constant. Recall that constant terms do not contribute to the result of minimization or maximization problems, so the exact value of any constant is irrelevant. This study for the introduces the methodology for detection of abrupt changes in wind data with application to downburst analysis.

## 2.3 Results

**Figure 2.3** shows time histories of all 37 downburst records analyzed in this paper. Horizontal lines marked the peak wind speed for time series from Europe, the US and Australia. The strongest downburst investigated in this paper is from the US (Fujita 1985) with the maximum wind speed reaching  $68 \text{ m s}^{-1}$ . The strongest downburst from Europe was recorded on 26 October 2012 in Livorno and the wind speed was near  $40 \text{ m s}^{-1}$ . The Andrews Air Force Base downburst captured by Fujita (1985) still remains one of the most vigorous downburst events recorded by an anemometer. The following three subsections describe the main characteristics of the analyzed downbursts from Europe, the US and Australia.

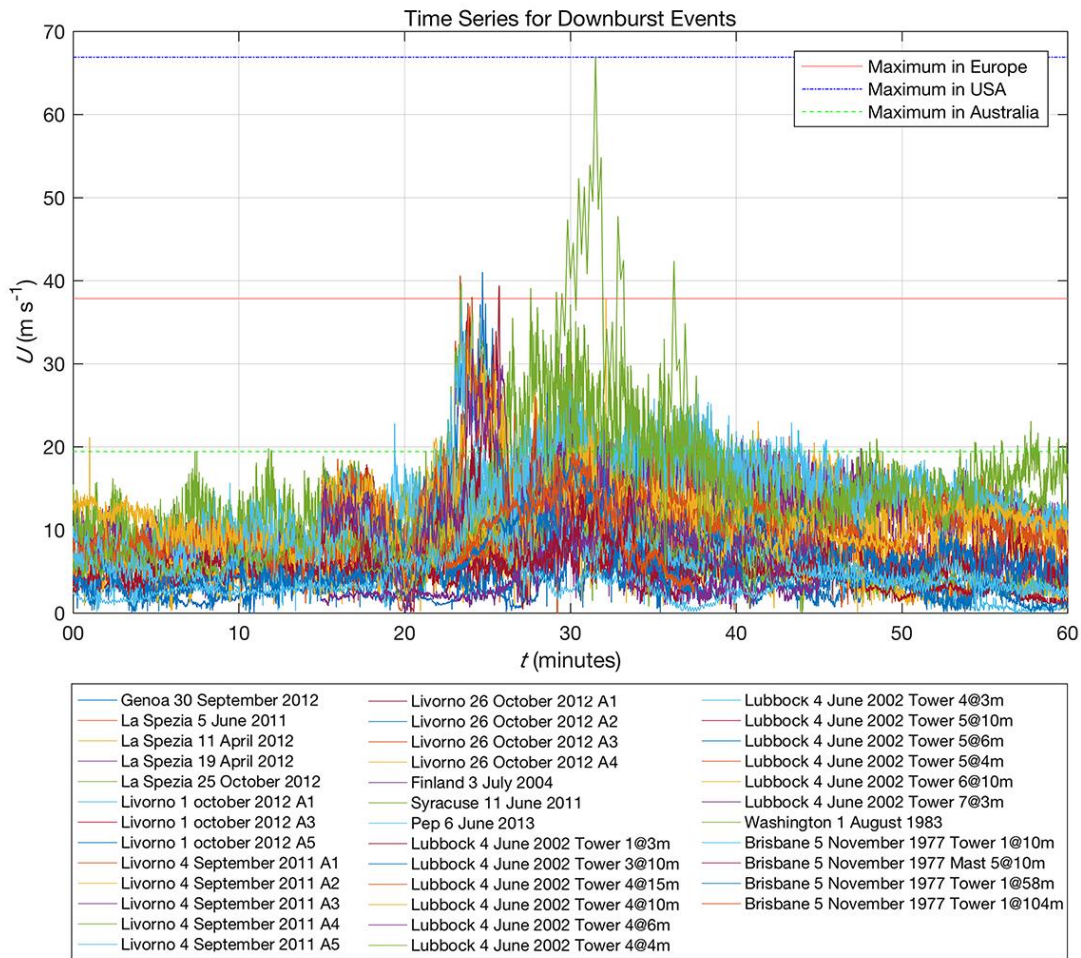


**Figure 2.3:** All downburst records investigated in this study



### 2.3.1 Europe

**Figure 2.4** shows two downburst events in Italy, one in Genoa and one in Livorno. In both cases anemometers were installed along the coast and recorded downbursts which occurred above sea and moved inland (wind direction not shown). It is important to note that the projects “Wind and Ports” (Solari et al. 2012) and “Wind, Ports and Sea” (Repetto et al. 2017) contain a unique data of downbursts spawned above sea (Burlando et al. 2017). Other downburst records are from inland stations and the downburst winds are therefore influenced by the higher surface roughness, roughness changes, orography and obstacles that might exist around the measuring tower. This is not the case with the analyzed downbursts from the Mediterranean.

The introduced segmentation method objectively distinguishes between different stages of each downburst (**Figure 2.4**). In this case, the standard deviation (SD) and mean (M) methods similarly divided the time series in four segments in Genoa and five segments in Livorno. An additional segment in Livorno is due to the steady increase of wind speed prior to the downburst event. It is worth mentioning that this Livorno downburst was analyzed in details in a recent study by (Burlando et al. 2017). This steady increase of wind speed is sometimes referred to as a gust front, although the difference between gust front and downburst is somewhat blurry in literature. Anyhow, the duration of this segment is 3 min 17 s and 5 min 6 s according to the M and SD methods, respectively. In this case, however, it seems that the M approach provides better results at isolating the central downburst peak. The steady increase of wind speed prior to downburst is typically observed only at lower heights (Droegemeier and Wilhelmson 1987; Mueller and Carbone 1987; Burlando et al. 2017). The heights of the anemometers in Genoa and Livorno are 61.4 m and 20 m above ground, respectively.

The Other four segments in the M and SD approaches (**Figure 2.4**) correspond to the ABL winds before the thunderstorm, the first downburst peak, the second downburst peak, and the ABL winds after the downburst event. The segments M2 and SD2 in Genoa and M3 and SD3 in Livorno are the main downburst signatures characterized by a sudden increase of wind speed when the anemometers are located in the fastest region of the downburst flow (Hjelmfelt 1988), decrease of the wind speed as the anemometers are in the stagnation

region of the downburst (Chay et al. 2006). The second downburst peak (M3 and SD3 in Genoa and M4 and SD4 in Livorno) are associated with an abrupt shift in wind direction as the thunderstorm moves away from the anemometers (Wakimoto 1982; Fujita 1985; Sherman 1987; Burlando et al. 2017).

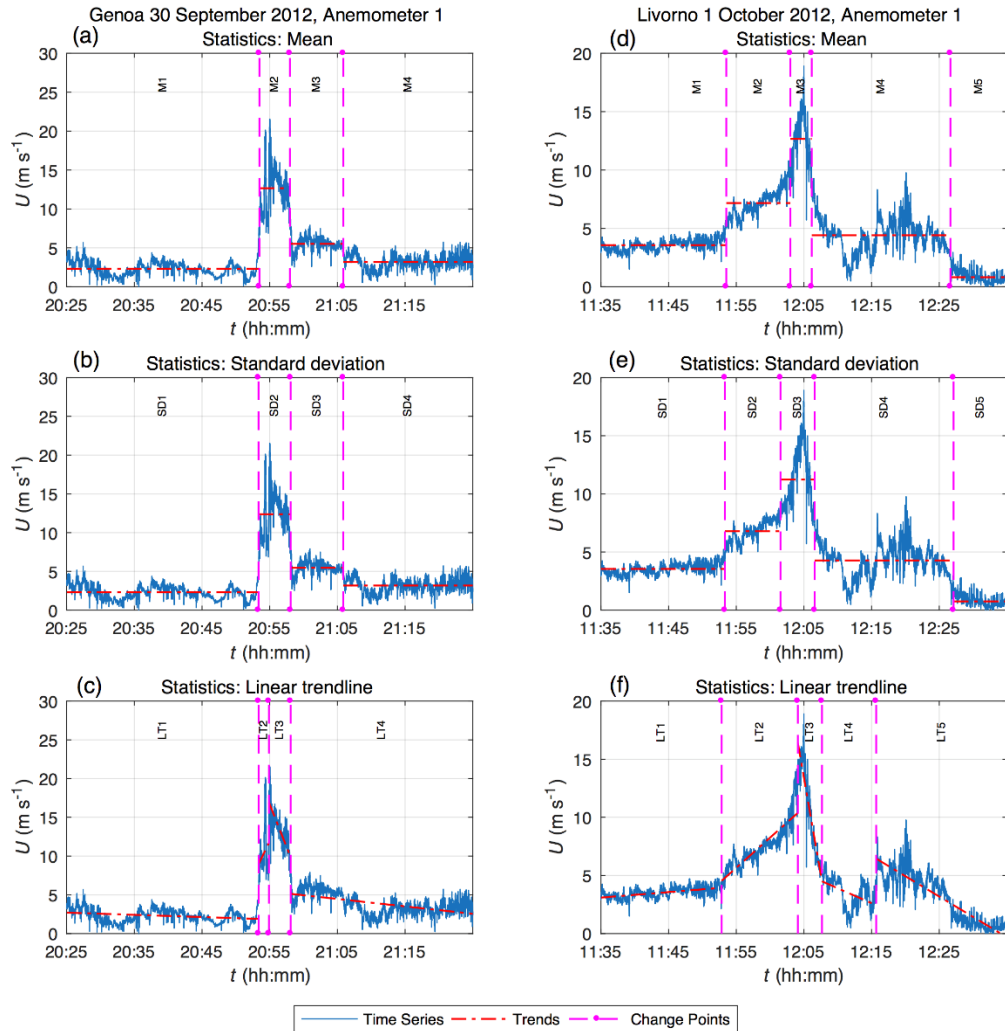


**Figure 2.4: Three segmentation methods applied to a downburst records from Genoa (left panels) and a downburst record from Livorno (right panels).**

This peak is not observed in all downburst records as it depends on the relative position between thunderstorm and anemometer. The last segments in the downburst time series correspond to the background ABL winds that proceed downburst. In most cases, these

winds are weaker than the ones that precede the downburst, but not always as in the Genoa case (**Figure 2.4**).

**Figure 2.5** shows two downburst records with very different signatures compared to the ones in **Figure 2.4**. Namely, downbursts in **Figure 2.5** are characterized by a broad main peak and they lack a pronounced signature of the second peak that is observed in both downburst records in **Figure 2.4**. In both cases in **Figure 2.5**, the increase/decrease of wind speed is rather gradual, i.e., typical for the anemometers at lower heights. Anemometer height for both of the events here are 15.5 m and 20 m respectively. Here, the M and SD approaches differently segment the time series. In La Spezia (**Figure 2.5**), the M3 segment is very narrow and could probably be merged with the ~15-min-long segment M4; similar to the M3 segmentation of the Livorno time series in the same figure. Notice that the La Spezia downburst is accurately isolated from the background winds using the SD method (downburst duration is 18 min 7.7 s).

Once again, the LT method provides noticeably different results from either the M or SD partitioning. Interestingly though, the LT approach might indicate the existence of the second peak (LT4) in the La Spezia event. If this event is a two-peak downburst, the first downburst peak is characterized with the segments LT2 and LT3 and the second peak with the segments LT4 and LT5. However, a possibility that LT4 is a pronounced turbulent fluctuation cannot be excluded since its existence is not confirmed via either M or SD methods. Observing the Livorno time series (**Figure 2.5**), on the other hand, it might seem that all segments from LT3 to LT6 could be assign the same LT. Notice that the segment LT6 is also detected using the M and SD methods, which demonstrates that the statistical properties (i.e., M, SD and LT) of this part of the time series indeed significantly differ from the rest of the record. Appendix A shows few more segmented time histories of full scale events from Europe.

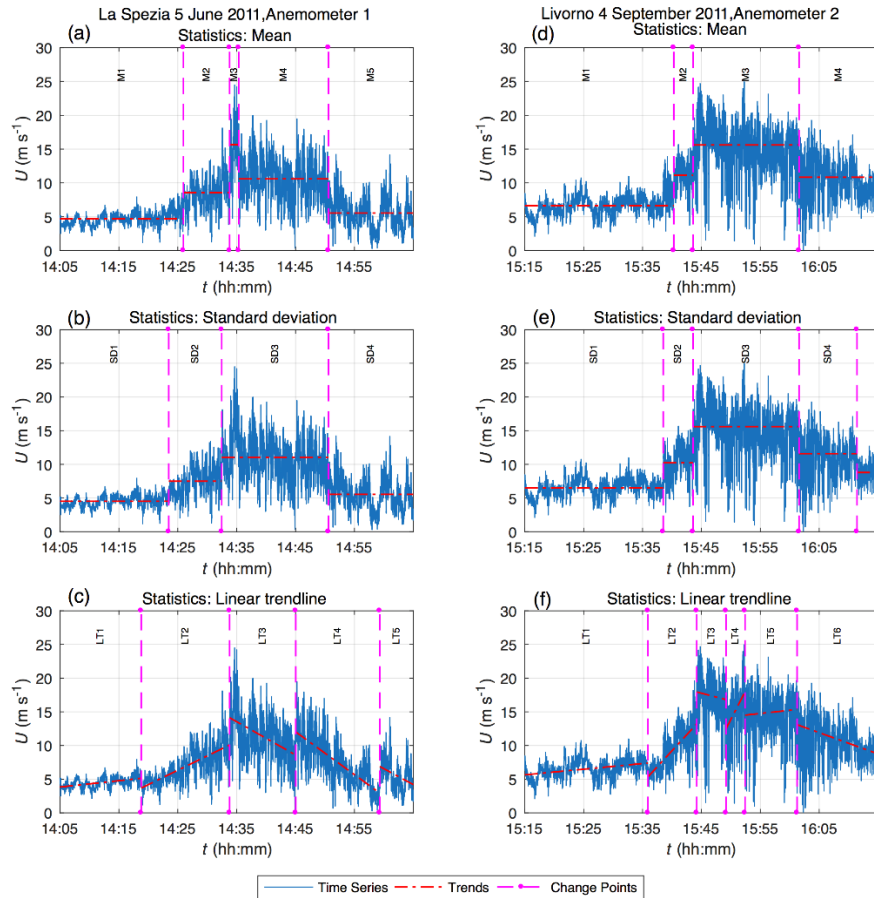


**Figure 2.5:** Same as Figure 2.4 but for one La Spezia event (left panels) and one Livorno event (right panels). Notice that the downburst signatures in this figure and Figure 2.4 are noticeably different; see text for further discussion.

### 2.3.2 The US

Performances of the segmentation method on downburst records from the US are depicted in **Figure 2.6**. Qualitatively, these two events are similar to downbursts in **Figure 2.4**, all characterized by sharp ramp-up and slowdown of winds in contrast to the time series in **Figure 2.5** where the occurrence of the downburst is more progressive. A short calm prior to the main downburst peak is observed in both US records—M2 and SD2 segments in the Syracuse time series and around 14:24 h into the Pep event. However, due to its short duration this feature in the Pep event is not identified as an abrupt change in the velocity

record. (Mahoney 1988) concluded that the rapid decrease of wind speed prior to downburst takes place when downburst winds propagate into strong opposing winds. According to (Wakimoto 1982), however, the calm is related to the sudden non-hydrostatic pressure jump at the boundary between the cold downburst and warm environmental air (Lompar et al. 2018). Similar findings are reported by Pistotnik et al. (2011).

The mean downburst peak in the Syracuse event is segmented into three parts using the M cost function, while the SD approach considers those three segments as one. Indeed, the Syracuse event is accurately divided into two portions of background winds (SD1 and SD4), the downburst peak (SD3), and the calm before downburst (SD2). The similar segmentation took place in the case of Pep downburst. The existence of the localized peak prior to the strongest downburst peak in the Pep record (around 14:25 h; i.e., M2 segment) is in accordance with the (Hjelmfelt 1988) model of downburst in which the localized peak is associated with the main vortex ring that precedes the strong inflow current that feeds the radially advancing downburst rolling vortex. The height of the leading vortex (Droegemeier and Wilhelmson 1987) is approximately two times the height of the inflow current (Simpson 1969), which partially explains the stronger velocities in the inflow current. Indeed, the existence of the leading-vortex peak can also be observed in the Syracuse event as the M3 segment in the time series. Furthermore, since both peaks are associated with the same downburst flow, their fluctuating properties are similar, thus both fall in a single SD segment.

**Figure 2.7** shows the segmented time series for the Lubbock (Orwig and Schroeder 2007; Holmes et al. 2008) and the Washington (AAFB; Fujita 1985) downbursts. It is important to notice that the sampling frequencies in these two cases are 1 Hz and around 0.1 Hz, respectively. We intentionally say “around 0.1 Hz” as the AAFB record was manually digitalized from Fujita (1985) and therefore a degree of sampling error is introduced. The M and SD methods equally divided the Lubbock downburst into four segments each representing the background winds prior to downburst, the first downburst peak, the second downburst peak and the background winds after the event. Although the LT method also results in four segments, these are not identical to the one obtained using the M and SD cost functions.

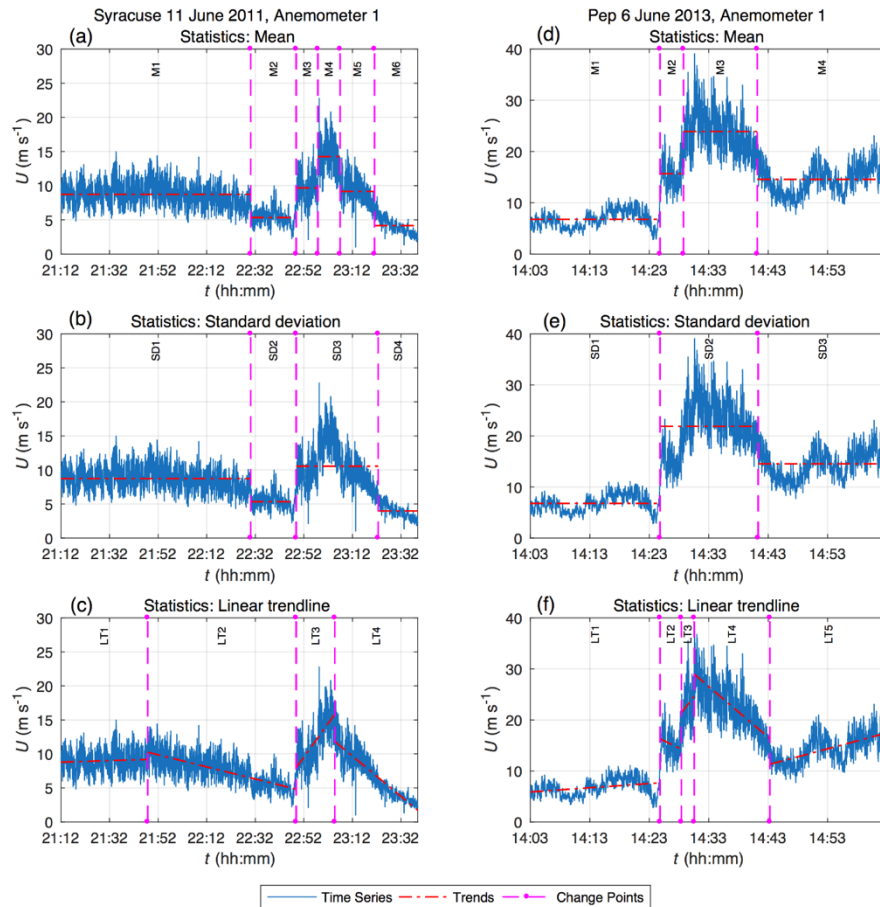


**Figure 2.6: Three segmentation methods applied to a downburst records from Syracuse (left panels) and Pep (right panels).**

The dip in background winds immediately prior to the downburst is accurately represented deploying the LT approach. This finding is similar to the Syracuse record in **Figure 2.6c**. The strongest investigated downburst in this paper—the AAFB event—is also separated into three segments using the M and SD methods (**Figure 2.7d,e**).

Once again, these segments represent the background winds, the first, and the second downburst peaks. In this case, however, the time series after the downburst is too short in order to identify the background winds after the second peak.

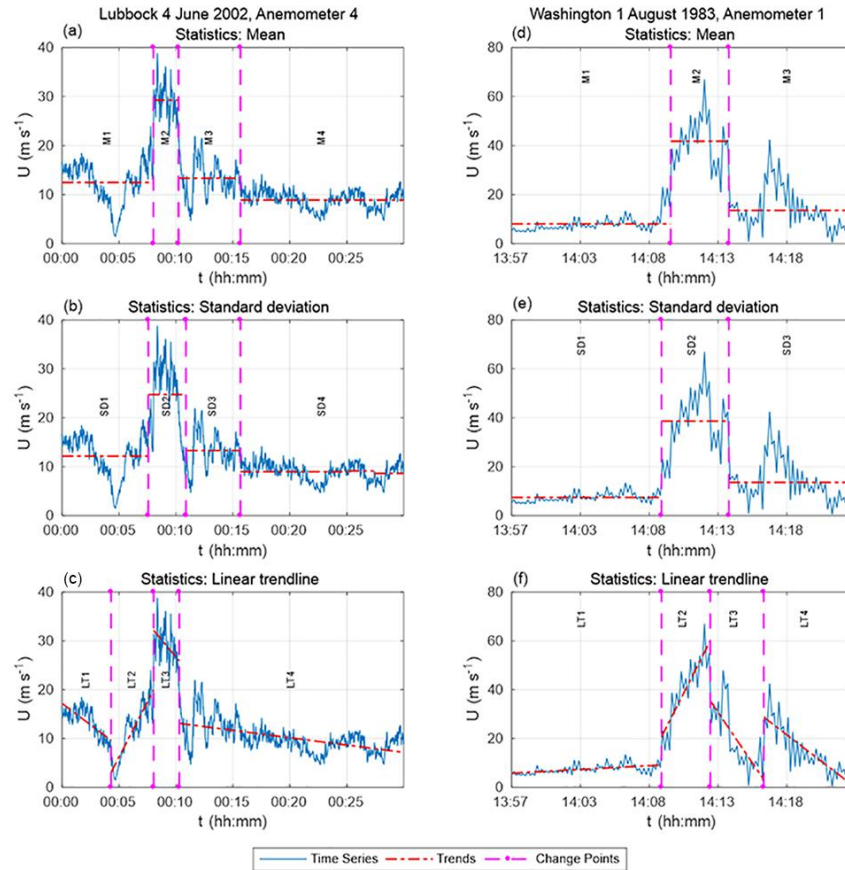


**Figure 2.7: Three segmentation methods applied to a downburst records from Lubbock (left panels) and Washington (right panels).**

### 2.3.3 Australia

**Figure 2.8** shows the downburst event in Brisbane captured by two anemometers positioned on adjacent towers of different heights. Similar to the event in Syracuse and Pep (**Figure 2.6**), the segment M2 at tower 1 shows the localized peak prior to the strongest downburst spike. Also similar to the previous examples, the SD method isolates the whole thunderstorm-related segment of the time series from the background wind (SD2 at both tower 1 and mast 5). Notice that concatenated M2 and M3 are similar to SD2 in terms of the total duration of the downburst, confirming the previous statement that SD method typically tends to reduce the number of segments in comparison to M and LT approaches. For the mast 5, the M and SD methods resulted in the same segmentation.

The existence of the steady increase of wind speed prior to downburst is also observed at the tower 1 and mast 5 (similar to La Spezia and Livorno records from Europe, among others), although the increase is more abrupt on tower 1. In both cases, the LT method introduces an additional segment into the time series. Although the existence of LT3 on tower 1 is not very clear, the same segment on mast 5 is associated with the wind speed spike at around 20:21 h. Notice that the same spike appears in the time series from tower 1 at approximately the same time, but its existence is somewhat masked due to the longer duration of the time series. This finding also shows that the number of segments is also a function of the time series duration.

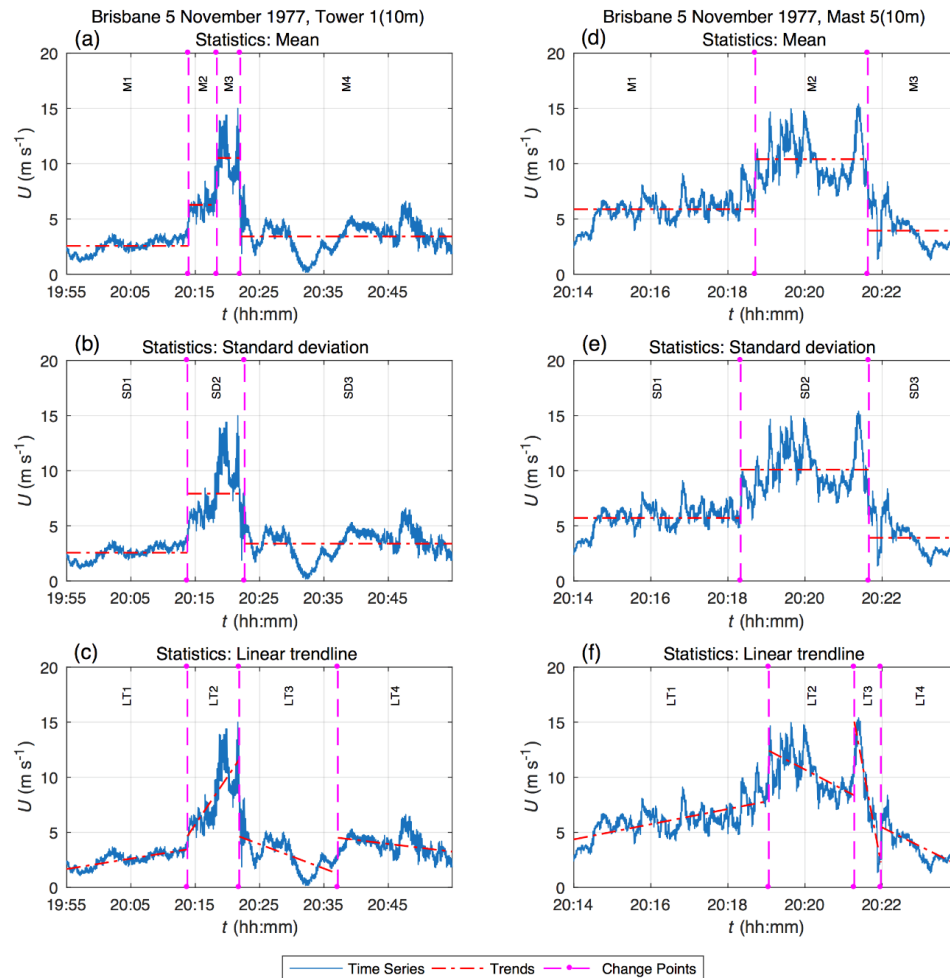


**Figure 2.8: Three segmentation methods applied to a downburst records from Australia.**



## 2.4 Discussion

**Section 2.3** demonstrated that the proposed methodology is overall accurate at isolating the main features of downburst signal. However, different cost functions sometimes produce inconsistent results (e.g., **Figure 2.6**). Also, the number of change points in the downburst time series is sensitive to the value of the penalty constant ( $\gamma$ ) in Eq. (2.2). Lastly, due to the large number of analyzed records, section 3 only presents the detailed results for several downburst events. The above queries and generalization of the results for the whole database will be addressed in this section.

### 2.4.1 Model sensitivity

The introduced model for detection of change points in downburst records is robust because the number of change points depends only on the value of  $\gamma$  in Eq. (2.2). Larger  $\gamma$  results in fewer change points. Therefore, a challenge was to determine  $\gamma$  in such a way to separate time series into physically meaningful segments, but at the same time to find a unique value of  $\gamma$  that would be the same or at least similar for all analyzed records. The second objective was imposed in order to make the model as general as possible for downburst analysis. **Figure 2.9** portrays the relationship between  $\gamma$  for the mean cost function and the number of change points in three investigated records with different  $f_s$ . Recall that the number of segments is the number of change points plus unity. The Genoa event that is investigated in **Figure 2.9** was recorded with a sonic anemometer with  $f_s = 10$  Hz and the time series is analyzed in **Figure 2.4a**. Four segments in the time series correspond to (1) background winds prior to downburst, (2) first downburst peak, (3) second downburst peak, and (4) background winds after downburst. The proper segmentation of this time series is obtained for  $\gamma \cong 6000$  and further increase of  $\gamma$  does not reduce the number of segments. However, the model is sensitive on the value of  $\gamma$ , in the cases when  $\gamma < 5000$ . The Lubbock downburst was captured by an anemometer with  $f_s = 1$  Hz and the time series with change points is depicted in **Figure 2.7a–c**. In comparison to the Genoa downburst characterized with higher  $f_s$ , the  $\gamma$  for the Lubbock downburst takes fewer discrete values prior to 3010 that provides the accurate number of change points (3). This behavior is even more

pronounced for the Brisbane time series which has the lowest  $f_s$  of around 0.2 Hz (**Figure 2.9**).

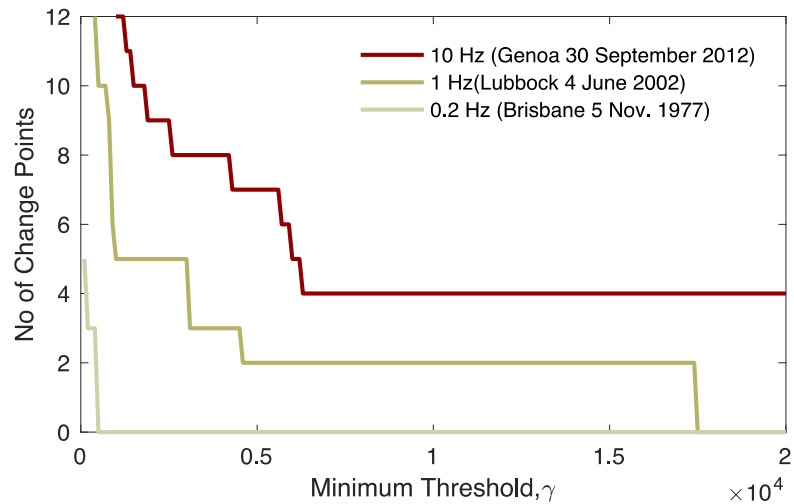


**Figure 2.9: The number of detected change points versus  $\gamma$  for three different sampling frequencies.**

That is, by increasing  $f_s$ , the model is more sensitive to the value of  $\gamma$  prior to the critical value after which the number of change points remains the same with further increase of  $\gamma$ . Our analysis performed on a large set of downbursts shows that  $\gamma = 12400 - 15000$ ,  $\gamma = 3000 - 8000$  and  $\gamma = 9000 - 11000$  are the values that provide accurate segmentation of downburst time series with  $f_s = 10$  Hz using M, SD and LT methods, respectively. The segmentation is deemed to be accurate since each of the identified segments is characterized with M, SD and LT statistically significantly different from the two adjacent segments, thus portraying a transient wind record.

The following analysis further investigates the relationship between  $\gamma$  and  $f_s$ . In **Figure 2.10**, decimation is used in order to synthetically reduce  $f_s$ . The deployed decimation uses a low-pass filter, in this case Chebyshev Type I Infinite Impulse Response filter of order 8 (Parks and Burrus 1987), to reduce the signal bandwidth and guard against aliasing (Jackson 1996). The algorithm for the decimation and further details on this signal analysis technique are provided in (Digital signal processing committee of the IEEE acoustics, speech, and signal processing society 1979).

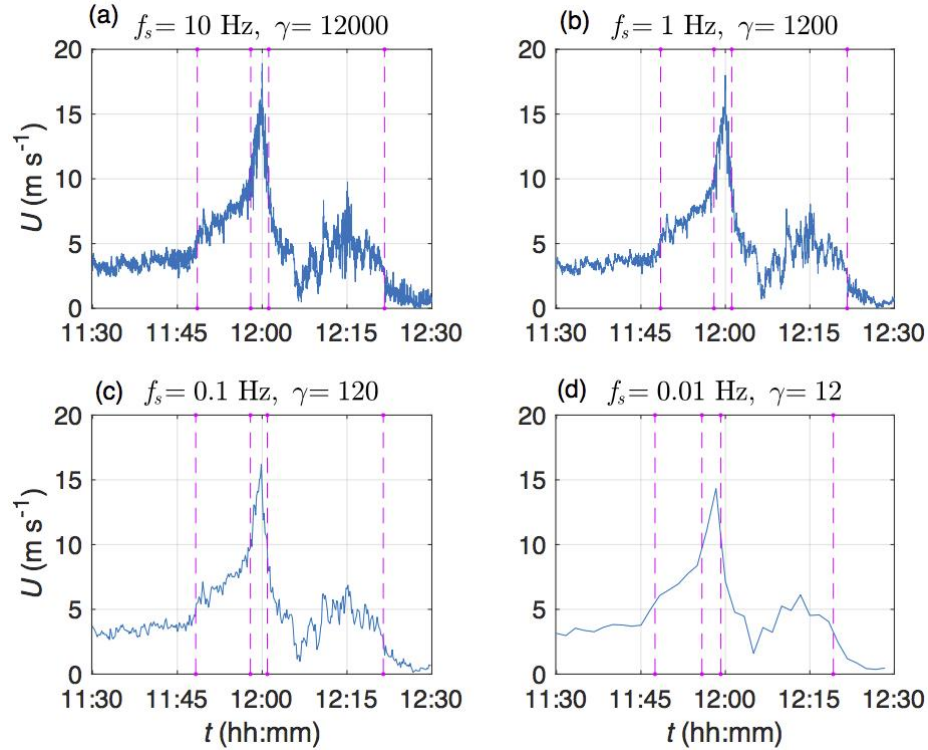


**Figure 2.10: Dependency of  $\gamma$  on sampling frequency,  $f_s$ , for the mean cost function.**

As can be seen from **Figure 2.10**, the value of  $\gamma$  needs to be changed with decreasing  $f_s$  in order to preserve the same number and location of change points in the time series. Clearly, the relationship between  $\gamma$  and  $f_s$  is linear with a positive slope, i.e.:

$$\gamma = 1200f_s \quad (12)$$

Based on the records analyzed here (Table 2.1), it can be inferred that for a specific  $f_s$ , the values of  $\gamma$  are of the same order for different events. For example, most of the downburst events in Europe had a sampling frequency of 10 Hz, for which  $\gamma$  ranged from 12,000 to 15,000 for the mean cost function. This relationship between  $\gamma$  and  $f_s$  depicted in **Figure 2.10** could be one of the criteria for approximating the proper value of  $\gamma$  in downburst time series.

## 2.4.2 Transient characteristics of downburst time series

In this subsection, downburst duration and ramp-up time are discussed for all the downburst events listed in Table 2.1 based on the three statistical approaches used for detecting the change points in the velocity time history: mean (M), standard deviation (SD) and linear trend (LT). Downburst duration is defined as the length of segment that encompasses only the first downburst peak since some of the downbursts in this study lack the second peak. The ramp-up time is the time between the first change point prior to the peak velocity and the first downburst peak velocity. **Figure 2.11a** shows the downburst durations for the events listed in Table 2.1 as well as the percentage of downburst events for different ranges of downburst durations (**Figure 2.11b–d**). In general, using SD approach resulted in larger downburst durations compared to the other two approaches. As noticed earlier (e.g., Syracuse and Brisbane cases in **Figure 2.6** and **Figure 2.8**, respectively), the SD method typically incorporates the steady increase of winds prior to the downburst peak as a part of the downburst event, while the same part of the time series is a separate segment in the M approach. Therefore, the duration time in the case of SD method can be looked at in many instances as the time interval from the beginning of thunderstorm winds until the downburst end. Interestingly, all three approaches produced similar downburst duration for the cases in the US and Australia, which could be attributed to the lower sampling frequencies of these records and in some instances the absence of the steady wind speed increase prior to the downburst.

As can be seen from **Figure 2.11**, downbursts in general are very short lived. In almost all cases, their duration is less than 20 min regardless of the method. In fact, downbursts (i.e., the first downburst peaks) were shorter than 5 min in around 70% of the cases using the M approach (Fig. 11b). Based on the SD method, the thunderstorm event recorded at Syracuse, US, on 11 June 2011 had the longest duration of 34 min out of all the events listed in Table 2.1.

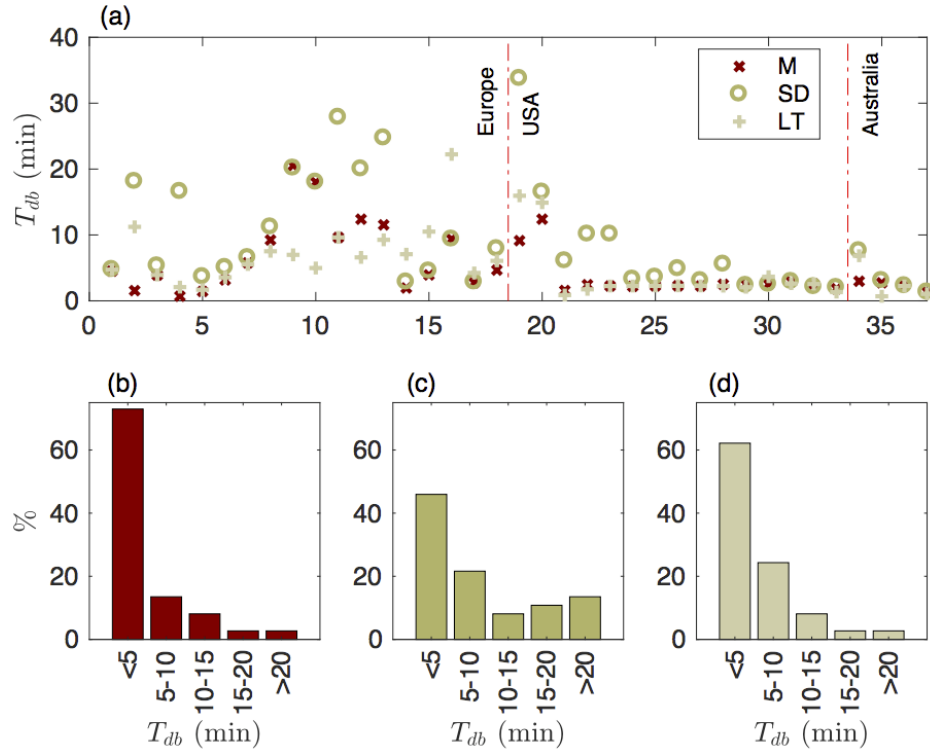


**Figure 2.11: (a) Downburst durations determined using M, SD and LT approaches for time records listed in Table 2.1. (b, c, d) Histograms of downburst durations obtained by M, SD and LT approaches, respectively.**

Similarly, to the downburst duration, the longer ramp-up time was found in general using SD approach compared to M and LT approaches (**Figure 2.12**). Whereas the duration for most of the downburst events was less than 20 min, the ramp-up time for majority of the events was below 4 min. This finding shows that the flow acceleration to the peak wind speed is significantly faster compared to the deceleration from the peak. In most instances, the ramp-up time was even less than 1 min. Although there is a variability in estimating the ramp-up time using the time series segmentation method proposed here, for 20 out of 37 records the differences between the three approaches were less than a minute.

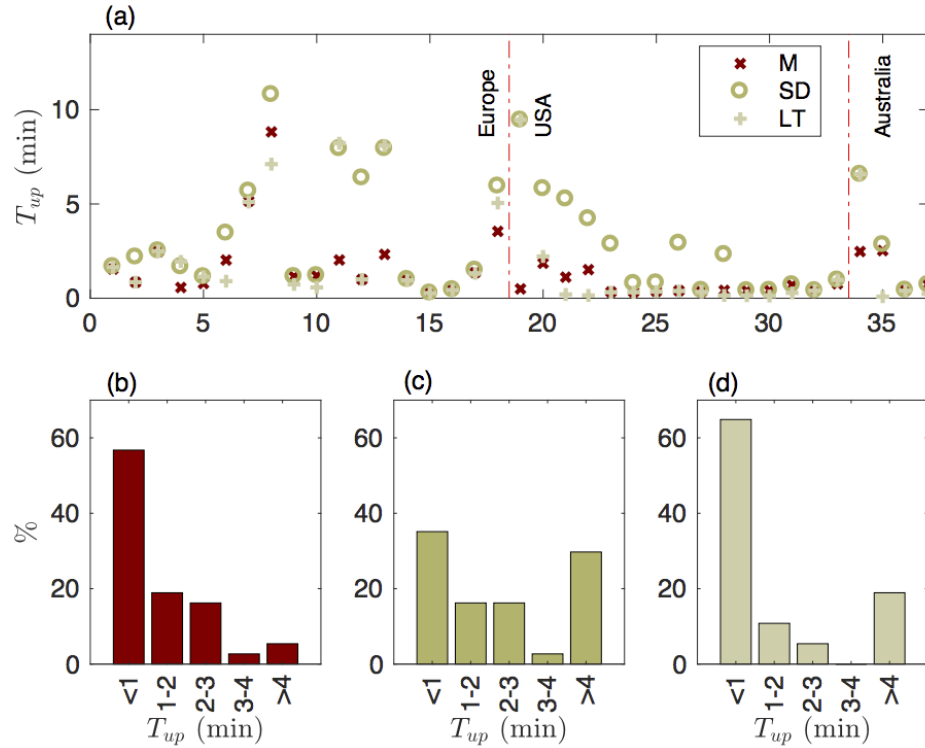


**Figure 2.12: Same as Figure 2.10, but for downburst ramp-up time.**

**Figure 2.13** and **Figure 2.14** analyze the abrupt changes in mean wind speed and standard deviation prior to, during and after the first downburst peak. The ratios of mean wind speeds,  $R_{dp/bp,ap}$ , are defined as:

$$R_{dp/bp,ap} = \begin{cases} \frac{\bar{U}_{dp}}{\bar{U}_{bp}}, & \text{downburst peak vs. background wind before downburst peak,} \\ \frac{\bar{U}_{dp}}{\bar{U}_{ap}}, & \text{downburst peak vs. background wind after downburst peak,} \end{cases} \quad (1, 3)$$

where  $\bar{U}_{dp}$  is the mean wind speed during the first downburst peak and  $\bar{U}_{bp}$  and  $\bar{U}_{ap}$  are the mean wind speeds before and after the downburst peak, respectively. Similarly, the ratios of standard deviations are:

$$S_{dp/bp,ap} = \begin{cases} \frac{\sigma_{dp}}{\sigma_{bp}}, & \text{downburst peak vs. background wind before downburst peak,} \\ \frac{\sigma_{dp}}{\sigma_{ap}}, & \text{downburst peak vs. background wind after downburst peak.} \end{cases} \quad (14)$$

In approximately 60% of the analyzed records,  $\bar{U}_{dp}$  is 2 to 3 times larger than  $\bar{U}_{bp}$  (**Figure 2.13b**), while the larger variability is observed between the ratio of  $\bar{U}_{dp}$  and  $\bar{U}_{ap}$  (**Figure 2.13c**). In Europe, only approximately half of the events have  $R_{dp/bp} < R_{dp/ap}$ , whereas this relationship is observed for almost all the events from the US and Australia. Therefore, for the majority of analyzed downbursts (62.16%), we observe  $\bar{U}_{ap} < \bar{U}_{bp}$ , and in those cases, on average,  $\bar{U}_{bp} = 1.27\bar{U}_{ap}$ .

Turbulent fluctuations in the downburst peak are higher than in the background winds prior and after the downburst (e.g., Chen and Letchford 2004; Chen and Letchford 2006; Burlando et al. 2017). For instance, Chen and Letchford (2004) combined turbulent and a non-turbulent downburst wind fields by applying the evolutionary power spectral density method. In their approach, the amplitude modulation factor in modelling turbulence fluctuations is proportional to the mean wind speed, i.e.:  $0.25\bar{U}(x, y, z, t)$ . However, in a subsequent paper Chen and Letchford (2006) proposed the proportionality constant to be between 0.08 and 0.11. In any case, their method assumes higher values of turbulence fluctuations during the downburst.

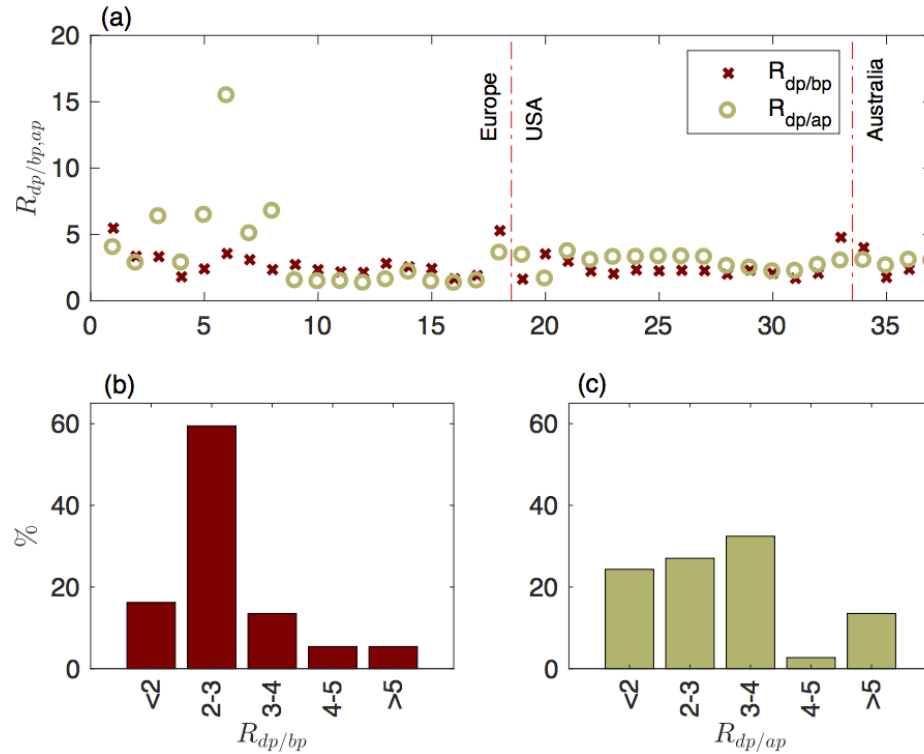


**Figure 2.13: (a) The ratio ( $R_{dp/bp}$ ) of mean wind speeds during downburst peak (dp) and before peak (bp), as well as the ratio ( $R_{dp/ap}$ ) of the mean wind speeds during dp and after peak (ap). (b, c) Histograms of  $R_{dp/bp}$  and  $R_{dp/ap}$ , respectively.**

Our analysis in **Figure 2.14b** shows that the SD during the downburst peak is between 1 and 2 times larger than prior to the peak in approximately 35% of the investigated downburst records. The ratio is even higher for the rest of the cases (**Figure 2.14b**). Similar relationship is observed between the fluctuations during the downburst peak and fluctuations in the background winds after the downburst (**Figure 2.14c**).

The ratios for all the events in Table 2.1 are given in **Figure 2.14a**. Notice that the ratio is only once below 1; that is, the background winds have the lower level of turbulence than downbursts in effectively all cases. Histograms in **Figure 2.14a** and b are similar indicating that on average the SD in background winds prior and after the downburst is also similar.



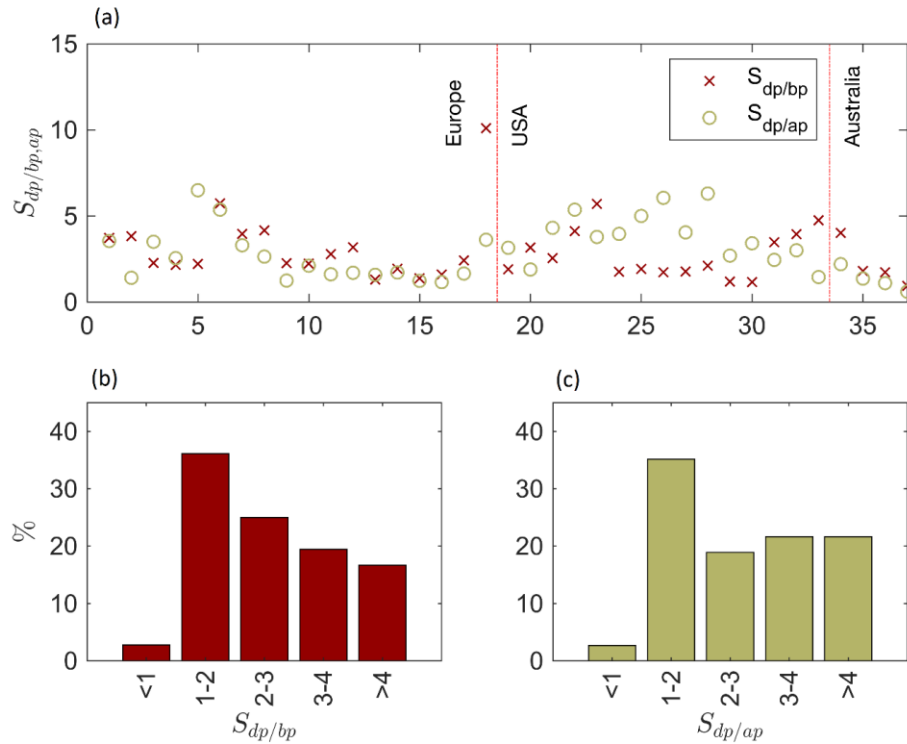


**Figure 2.14: Same as Figure 2.12, but for the standard deviation.**

### 2.4.3 Outlook

In the future work, the method will be coupled with a downburst detection algorithm in order to automatically extract and analyze downburst characteristics such as ramp-up and downburst durations. The algorithm developed for high-frequency anemometer data by De Gaetano et al. (2014) is particularly suitable for the proposed coupling. The high-frequency data enable a meaningful analysis of standard deviation and other higher order statistics.

Ongoing research is also focused on extending the cost functions to higher order statistics such as kurtosis and skewness. That way the model will detect statistically significant changes of kurtosis and skewness in the anemometer records. This improvement of the methodology will enable the objective separation of Gaussian from non-Gaussian winds which is of particular importance in wind energy (Lange et al. 2017) and wind engineering (Solari 2016). For example, the structural responses to transient winds need to be evaluated

using the response spectrum technique (Solari 2016), whereas the structural response to ABL winds is typically analyzed through the gust response factor technique (e.g., Davenport 1961; Solari 1983). In addition, the changepoint detection method is applied only to wind speed data in the present study. The method could be further tested with wind direction data. Other meteorological variables such as temperature, pressure and humidity also experience transient behavior during downburst passage and therefore the method will be used to study their abrupt changes too. Analyzing different penalty functions (Killick et al. 2012) and extending the model beyond the constant penalty are also worth considering.

Finally, the method can be used as one possible method for scaling downburst events. The duration and/or the ramp up time between simulated and real downbursts can produce a suitable time scale. The velocity scale can be extracted comparing the first downburst peak velocity in simulated and real downburst events. A length scale can then be derived based on the time and velocity scales.

## 2.5 Conclusions

This study introduces an objective methodology for the analysis of transient downburst wind events. The method seeks for change points in time series based on the statistical properties of different segments of time series (Lavielle 2005; Killick et al. 2012). The investigated statistics in this paper are the mean (M), standard deviation (SD), and linear trend (LT). That is, the segments of the downburst time series with statistically significant constant values of M, SD, and LT are separated.

In addition, this paper investigated 37 wind speed records from 14 downburst events. 8 events (17 records) were from Italy (Solari et al. 2012; Repetto et al. 2017), one event from Finland (Järvi et al. 2007), 4 events (15 records) from the United States (US; Fujita 1985; Holmes et al. 2008) Gunter and Schroeder 2015; Gunter et al. 2017), and one event (4 records) from Australia (Sherman 1987). The summary of all events is provided in Table 2.1, while the performances of the proposed method are critically discussed in section 4. The downburst in Washington reported by Fujita (1985) is still one of the strongest

downburst events ever recorded, if not the strongest, with the peak velocity of  $68 \text{ m s}^{-1}$  at only 4.9 m above ground.

In brief, the main conclusions of this study are highlighted below:

- The typical number of segments in the downburst time series is 3–4 using the M and LT approaches and 2–3 using the SD method. These segments physically correspond to the ramp-up, the first peak, sometimes the second peak and the ramp down of the wind speed. In many cases, the SD method isolates the whole thunderstorm segment without subdividing downburst multiple peaks from the rest of the time series. The M and LT models, on the other hand, tend to further sub-divide the thunderstorm section into different segments such as the first and second downburst peaks.
- In most cases, all three methods divided the thunderstorm records into physically meaningful segments. The best results using the M method are achieved by choosing the penalty constant function,  $\gamma$ , to be 12400–15000 for the sampling frequency,  $f_s = 10 \text{ Hz}$ , 2600–3160 for  $f_s = 1 \text{ Hz}$  and 400 for  $f_s < 1 \text{ Hz}$ . Similarly, using the SD method, a good choice for  $\gamma$  is 3000–8000, 300–1250 and 250 if  $f_s = 10 \text{ Hz}$ ,  $1 \text{ Hz}$  or  $f_s < 1 \text{ Hz}$ , respectively. Lastly, the appropriate  $\gamma$  values for the LT method for the above-defined frequency ranges are 9000–11000, 1220–1970 and 250, respectively.
- For the M model, the relation between  $\gamma$  and anemometer sampling frequency,  $f_s$ , is linear with the proportionately constant being 1200.
- In the analyzed records, the first downburst peak is typically shorter than 5 min, whereas the ramp-up time is generally below 1 min. The ramp-up time is defined as the interval between the start of the downburst and the moment of peak velocity. It was shown that the ramp-up time is much shorter than the slowdown time of downburst winds after the peak velocity is reached.
- In about 60% of the analyzed cases, the background winds prior to downburst are 2–3 times weaker than the mean wind speed during the downburst peak. In addition, the mean wind speed after the downburst is below the mean wind speed prior to the downburst, on average. This relationship was particularly pronounced for the downburst records from the US and Australia.
- The standard deviation of wind speed during the downburst peak is about two times larger than the same quantity before and after the event. Turbulence fluctuations in background winds are always smaller than during the downburst event.

- A number of prospects for further improvement of the introduced method for detection of abrupt changes of statistical properties in downburst velocity signals are also discussed.

## 2.6 Acknowledgements

The authors would like to thank many people for kindly providing us with downburst data that were analyzed in this study. Prof. Giovanni Solari from the University of Genoa, Italy, openhandedly provided the data on all downburst events from Italy. These anemometer data were recorded by the wind monitoring network of two European Union projects “Wind and Ports” and “Wind, Ports and Sea” funded by the “Italy France Maritime 2007–2013” Cross-border Cooperation Programme. Dr. Leena Järvi from the University of Helsinki, Finland, generously shared with us the downburst time series from Finland. Prof. John Schroeder from Texas Tech University and Dr. Scott Gunter from Columbus State University kindly provided us with downburst records from Pep, Texas and Syracuse, Kansas, United States. These anemometer data are collected within the scope of the project SCOUT (Severe Convective Outflow in Thunderstorms) and funded by the National Science Foundation Grant CMMI 1000160. The atmospheric boundary layer data in **Figure 2.1a** are provided by NCAR/EOL (National Center for Atmospheric Research/Earth Observing Laboratory) under the sponsorship of the National Science Foundation (<https://data.eol.ucar.edu/>).

**Table 2.1: Downburst events investigated in this paper. See Fig. 2 for their location on map**

Serial	Country	Location	Downburst date	Geographical coordinates ( $\lambda, \phi$ ) (°N, °E)	Position	Land use	Height above ground (m)	Sampling frequency (Hz)
1	Italy	Genoa	30 September 2012	(44.399, 8.924)	Tower	Coast(sea)	61.4	10
2		La Spezia	5 June 2011	(44.106, 9.829)	Building	Urban	15.5	
3			11 April 2012					
4			19 April 2012					
5			25 October 2011					
6		Livorno 1	1 October 2012	(43.569, 10.301)	Tower	Coast(sea)	20	
7		Livorno 2		(43.582, 10.307)				
8		Livorno 3		(43.557, 10.290)				
9		Livorno 1	4 September 2011	(43.569, 10.301)	Tower	Coast(sea)	20	
10		Livorno 2		(43.582, 10.307)				
11		Livorno 3		(43.557, 10.290)				
12		Livorno 4		(43.541, 10.293)				

13		Livorno 5		(43.580, 10.318)	Building	Urban	75			
14		Livorno 1	26 October 2012	(43.569, 10.301)	Tower	Coast(sea)	20			
15		Livorno 2		(43.582, 10.307)						
16		Livorno 3		(43.557, 10.290)						
17		Livorno 4		(43.541, 10.293)						
18	Finland	Hyytiälä		3 July 2004					(61.850, 24.283)	Forest
19	US	Syracuse	11 June 2011	(37.827, 258.239)		Grass field	14.4		5	
20		Pep	6 June 2013	(33.771, 257.431)		Fields	10		10	
21		Lubbock 1	4 June 2002	(33.593, 257.971)		Tower	Airport		3	1
22		Lubbock 2							10	
23		Lubbock 3							15	
24		Lubbock 4							10.1	
25		Lubbock 5							6.1	
26		Lubbock 6							4	
27		Lubbock 7							2.1	
28		Lubbock 8							10	
29		Lubbock 9			6					
30		Lubbock 10			4					
31		Lubbock 11			10					
32	Lubbock 12	3								

33		Washington	1 August 1983	(38.796, 283.117)			4.9	0.1
34	Australia	Brisbane 1	5 November 1977	(27.313 S, 153.017)		Suburb	10	0.2
35		Brisbane 2					10	1.12
36		Brisbane 3					58	1
37		Brisbane 4					104	1.15

## 2.7 References

- Adachi, T., K. Kusunoki, S. Yoshida, K. Arai, and T. Ushio, 2016: High-speed volumetric observation of a wet microburst using X-band phased array weather radar in Japan. *Mon. Wea. Rev.*, **144**, 3749–3765, doi:10.1175/MWR-D-16-0125.1.
- Baldini, L., N. Roberto, M. Montopoli, and E. Adirosi, 2018: Ground-based weather radar to investigate thunderstorms. *Remote Sensing of Clouds and Precipitation*, Springer Remote Sensing/Photogrammetry, Springer, Cham, 113–135 [https://link.springer.com/chapter/10.1007/978-3-319-72583-3\\_4](https://link.springer.com/chapter/10.1007/978-3-319-72583-3_4) (Accessed April 24, 2018).
- Basseville, M., and I. V. Nikiforov, 1993: *Detection of Abrupt Changes: Theory and Application*. Prentice Hall, Englewood Cliffs, N.J, 528 pp.
- Bendat, J. S., and A. G. Piersol, 2010: *Random Data: Analysis and Measurement Procedures*. 4 edition. Wiley, Hoboken, N.J, 640 pp.
- Burlando, M., D. Romanić, G. Solari, H. Hangan, and S. Zhang, 2017: Field data analysis and weather scenario of a downburst event in Livorno, Italy, on 1 October 2012. *Mon. Wea. Rev.*, **145**, 3507–3527, doi:10.1175/MWR-D-17-0018.1.
- Chay, M. T., F. Albermani, and R. Wilson, 2006: Numerical and analytical simulation of downburst wind loads. *Eng. Struct.* **28**, 240–254, doi:10.1016/j.engstruct.2005.07.007.
- Chen, J., and A. K. Gupta, 2012: *Parametric Statistical Change Point Analysis: With Applications to Genetics, Medicine, and Finance*. 2nd ed. Birkhäuser Basel, [//www.springer.com/gp/book/9780817648008](http://www.springer.com/gp/book/9780817648008) (Accessed April 30, 2018).
- Chen, L., and C. W. Letchford, 2004: A deterministic–stochastic hybrid model of downbursts and its impact on a cantilevered structure. *Eng. Struct.*, **26**, 619–629, doi:10.1016/j.engstruct.2003.12.009.
- Chen, L., and C. W. Letchford, 2006: Multi-scale correlation analyses of two lateral profiles of full-scale downburst wind speeds. *J. Wind Eng. Ind. Aerodyn.*, **94**, 675–696, doi:10.1016/j.jweia.2006.01.021.
- Choi, E. C. C., and F. A. Hidayat, 2002: Gust factors for thunderstorm and non-thunderstorm winds. *J. Wind Eng. Ind. Aerodyn.*, **90**, 1683–1696, doi:10.1016/S0167-6105(02)00279-9.
- Cook, N. J., R. Ian Harris, and R. Whiting, 2003: Extreme wind speeds in mixed climates revisited. *J. Wind Eng. Ind. Aerodyn.*, **91**, 403–422, doi:10.1016/S0167-6105(02)00397-5.



- Darkhovski, B. S., 1994: Nonparametric methods in change-point problems: a general approach and some concrete algorithms. Institute of Mathematical Statistics, <https://projecteuclid.org/euclid.lnms/1215463117> (Accessed December 13, 2017).
- Davenport, A. G., 1961: The application of statistical concepts to the wind loading of structures. *Proc. Inst. Civil Eng.*, **19**, 449–472, doi:10.1680/iicep.1961.11304.
- De Gaetano, P., M. P. Repetto, T. Repetto, and G. Solari, 2014: Separation and classification of extreme wind events from anemometric records. *J. Wind Eng. Ind. Aerodyn.*, **126**, 132–143, doi:10.1016/j.jweia.2014.01.006.
- De Meutter, P., L. Gerard, G. Smet, K. Hamid, R. Hamdi, D. Degrauwe, and P. Termonia, 2014: Predicting small-scale, short-lived downbursts: Case study with the NWP limited-area ALARO model for the Pukkelpop thunderstorm. *Mon. Wea. Rev.*, **143**, 742–756, doi:10.1175/MWR-D-14-00290.1.
- Digital signal processing committee of the IEEE acoustics, speech, and signal processing society, 1979: *Programs for digital signal processing*. New York, N. Y., IEEE Press, 1979,.
- Droegemeier, K. K., and R. B. Wilhelmson, 1987: Numerical simulation of thunderstorm outflow dynamics. Part I: Outflow sensitivity experiments and turbulence dynamics. *J. Atmos. Sci.*, **44**, 1180–1210, doi:10.1175/1520-0469(1987)044<1180:NSOTOD>2.0.CO;2.
- Durañona, V., M. Sterling, and C. J. Baker, 2007: An analysis of extreme non-synoptic winds. *J. Wind Eng. Ind. Aerodyn.*, **95**, 1007–1027, doi:10.1016/j.jweia.2007.01.014.
- Ellrod, G. P., and J. P. Nelson, 1999: Experimental microburst image products derived from GOES sounder data. 16th Conference on Weather Analysis and Forecasting, Phoenix, AZ, American Meteorological Society, 43–45.
- Ellrod, G. P., J. P. Nelson, M. R. Witiw, L. Bottos, and W. P. Roeder, 2000: Experimental GOES sounder products for the assessment of downburst potential. *Wea. Forecasting*, **15**, 527–542, doi:10.1175/1520-0434(2000)015<0527:EGSPFT>2.0.CO;2.
- ESDU, 1993: *Computer Program for Wind Speeds and Turbulence Properties: Flat or Hill Sites in Terrain with Roughness Changes*. Engineering Sciences Data Unit (ESDU), London, UK.
- Fujita, T. T., 1985: *The downburst: microburst and macroburst*. Satellite and Mesometeorology Research Project, Department of the Geophysical Sciences, University of Chicago, Chicago, IL, United States, 136 pp.

- Fujita T.T, and H. R. Byers, 1977: Spearhead echo and downburst in the crash of an airliner. *Mon. Wea. Rev.*, **105**, 129–146, doi:10.1175/1520-0493(1977)105<0129:SEADIT>2.0.CO;2.
- Geerts, B., 2001: Estimating downburst-related maximum surface wind speeds by means of proximity soundings in New South Wales, Australia. *Wea. Forecasting*, **16**, 261–269, doi:10.1175/1520-0434(2001)016<0261:EDRMSW>2.0.CO;2.
- Goff, R. C., 1976: Vertical structure of thunderstorm outflows. *Mon. Wea. Rev.*, **104**, 1429–1440, doi:10.1175/1520-0493(1976)104<1429:VSOTO>2.0.CO;2.
- Gomes, L., and B. J. Vickery, 1978: Extreme wind speeds in mixed wind climates. *J. Wind Eng. Ind. Aerodyn.*, **2**, 331–344, doi:10.1016/0167-6105(78)90018-1.
- Gunter, W. S., and J. L. Schroeder, 2015: High-resolution full-scale measurements of thunderstorm outflow winds. *J. Wind Eng. Ind. Aerodyn.*, **138**, 13–26, doi:10.1016/j.jweia.2014.12.005.
- Gunter, W. S., C. C. Weiss, and E. C. Bruning, 2017: Surface measurements of the 5 June 2013 damaging thunderstorm wind event near Pep, Texas. *Wind Struct.*, **24**, 185–204, doi:10.12989/was.2017.24.2.185.
- Hjelmfelt, M. R., 1988: Structure and life cycle of microburst outflows observed in Colorado. *J. Appl. Meteor.*, **27**, 900–927, doi:10.1175/1520-0450(1988)027<0900:SALCOM>2.0.CO;2.
- Holmes, J. D., H. M. Hangan, J. L. Schroeder, C. W. Letchford, and K. D. Orwig, 2008: A forensic study of the Lubbock-Reese downdraft of 2002. *Wind Struct.*, **11**, 137–152, doi:10.12989/was.2008.11.2.137.
- Jackson, B., and Coauthors, 2005: An algorithm for optimal partitioning of data on an interval. *IEEE Signal Process. Lett.*, **12**, 105, doi:10.1109/LSP.2001.838216.
- Jackson, L. B., 1996: *Digital Filters and Signal Processing*. Springer Science+Business Media, LLC., New York.
- Järvi, L., and Coauthors, 2007: Micrometeorological observations of a microburst in southern Finland. *Boundary-Layer Meteorol.*, **125**, 343–359, doi:10.1007/s10546-007-9204-7.
- Kasperski, M., 2002: A new wind zone map of Germany. *J. Wind Eng. Ind. Aerodyn.*, **90**, 1271–1287, doi:10.1016/S0167-6105(02)00257-X.
- Killick, R., P. Fearnhead, and I. A. Eckley, 2012: Optimal detection of changepoints with a linear computational cost. *J. Am. Stat. Assoc.*, **107**, 1590–1598, doi:10.1080/01621459.2012.737745.

- Lange, J., and Coauthors, 2017: For wind turbines in complex terrain, the devil is in the detail. *Environ. Res. Lett.*, **12**, 094020, doi:10.1088/1748-9326/aa81db.
- Lareau, N. P., E. Crosman, C. D. Whiteman, J. D. Horel, S. W. Hoch, W. O. J. Brown, and T. W. Horst, 2013: The persistent cold-air pool study. *Bull. Amer. Meteor. Soc.*, **94**, 51–63, doi:10.1175/BAMS-D-11-00255.1.
- Lavielle, M., 1999: Detection of multiple changes in a sequence of dependent variables. *Stoch. Process. Their Appl.*, **83**, 79–102, doi:10.1016/S0304-4149(99)00023-X.
- Lavielle, M., 2005: Using penalized contrasts for the change-point problem. *Signal Process.* **85**, 1501–1510, doi:10.1016/j.sigpro.2005.01.012.
- Lombardo, F.T., 2009. Analysis and Interpretation of Thunderstorm Wind Flow on a Bluff Body. Ph.D. Dissertation. Texas Tech University, 259 pp.
- Lombardo, F.T., F. T., J. A. Main, and E. Simiu, 2009: Automated extraction and classification of thunderstorm and non-thunderstorm wind data for extreme-value analysis. *J. Wind Eng. Ind. Aerodyn.*, **97**, 120–131, doi:10.1016/j.jweia.2009.03.001.
- Lompar, M., M. Ćurić, and D. Romanic, 2018: Implementation of a gust front head collapse scheme in the WRF numerical model. *Atmos. Res.*, **203**, 231–245, doi:10.1016/j.atmosres.2017.12.018.
- Mahoney, W. P., 1988: Gust front characteristics and the kinematics associated with interacting thunderstorm outflows. *Mon. Wea. Rev.*, **116**, 1474–1492, doi:10.1175/1520-0493(1988)116<1474:GFCATK>2.0.CO;2.
- McCann, D. W., 1994: WINDEX—A new index for forecasting microburst potential. *Wea. Forecasting*, **9**, 532–541, doi:10.1175/1520-0434(1994)009<0532:WNIFFM>2.0.CO;2.
- McConville, A.C., Sterling, M., and Baker, C.J., 2009: The physical simulation of thunderstorm downbursts using an impinging jet. *Wind Struct.* **12**: 133–149. DOI: 10.12989/was.2009.12.2.133.
- Mueller, C. K., and R. E. Carbone, 1987: Dynamics of a thunderstorm outflow. *J. Atmos. Sci.*, **44**, 1879–1898, doi:10.1175/1520-0469(1987)044<1879:DOATO>2.0.CO;2.
- Neter, J., M. Kutner, W. Wasserman, and C. Nachtsheim, 1996: Applied Linear Statistical Models. 4 edition. McGraw-Hill/Irwin, Chicago, 1408 pp.
- NIST, 2006: Trend Test. National Institute of Standards and Technology. <https://www.itl.nist.gov/div898/handbook/apr/section2/apr234.htm>. [Accessed: 19 October 2018].

- Orwig, K. D., and J. L. Schroeder, 2007: Near-surface wind characteristics of extreme thunderstorm outflows. *J. Wind Eng. Ind. Aerodyn.*, **95**, 565–584, doi:10.1016/j.jweia.2006.12.002.
- Parks, T. W., and C. S. Burrus, 1987: *Digital Filter Design*. John Wiley & Sons, New York.
- Pistotnik, G., A. M. Holzer, R. Kaltenböck, and S. Tschannett, 2011: An F3 downburst in Austria—A case study with special focus on the importance of real-time site surveys. *Atmos. Res.*, **100**, 565–579, doi:10.1016/j.atmosres.2010.10.011.
- Pryor, K. L., 2015: Progress and developments of downburst prediction applications of GOES. *Wea. Forecasting*, **30**, 1182–1200, doi:10.1175/WAF-D-14-00106.1.
- Pryor, K. L., and G. P. Ellrod, 2004: Recent improvements to the GOES microburst products. *Wea. Forecasting*, **19**, 582–594, doi:10.1175/1520-0434(2004)019<0582:RITTGM>2.0.CO;2.
- Qiu, C.-J., and Q. Xu, 1996: Least squares retrieval of microburst winds from single-doppler radar data. *Mon. Wea. Rev.*, **124**, 1132–1144, doi:10.1175/1520-0493(1996)124<1132:LSROMW>2.0.CO;2.
- Repetto, M. P., M. Burlando, G. Solari, P. De Gaetano, M. Pizzo, and M. Tizzi, 2017: A web-based GIS platform for the safe management and risk assessment of complex structural and infrastructural systems exposed to wind. *Adv. Eng. Softw.*, doi:10.1016/j.advengsoft.2017.03.002.
- Riera, J. D., and L. F. Nanni, 1989: Pilot study of extreme wind velocities in a mixed climate considering wind orientation. *J. Wind Eng. Ind. Aerodyn.*, **32**, 11–20, doi:10.1016/0167-6105(89)90012-3.
- Romanic, D., D. Parvu, M. Refan, and H. Hangan, 2018: Wind and tornado climatologies and wind resource modelling for a modern development situated in “Tornado Alley.” *Renew. Energy*, **115**, 97–112, doi:10.1016/j.renene.2017.08.026.
- Sherman, D. J., 1987: The passage of a weak thunderstorm downburst over an instrumented tower. *Mon. Wea. Rev.*, **115**, 1193–1205, doi:10.1175/1520-0493(1987)115<1193:TPOAWT>2.0.CO;2.
- Simpson, J. E., 1969: A comparison between laboratory and atmospheric density currents. *Q.J.R. Meteorol. Soc.*, **95**, 758–765, doi:10.1002/qj.49709540609.
- Smith, T. M., K. L. Elmore, and S. A. Dulin, 2004: A damaging downburst prediction and detection algorithm for the WSR-88D. *Wea. Forecasting*, **19**, 240–250, doi:10.1175/1520-0434(2004)019<0240:ADDPAD>2.0.CO;2.
- Solari, G., 1983: Analytical estimation of the alongwind response of structures. *J. Wind Eng. Ind. Aerodyn.*, **14**, 467–477, doi:10.1016/0167-6105(83)90047-8.

- Solari, G., 2016: Thunderstorm response spectrum technique: Theory and applications. *Eng. Struct.*, **108**, 28–46, doi:10.1016/j.engstruct.2015.11.012.
- M. P. Repetto, M. Burlando, P. De Gaetano, M. Pizzo, M. Tizzi, and M. Parodi, 2012: The wind forecast for safety management of port areas. *J. Wind Eng. Ind. Aerodyn.* **104–106**, 266–277, doi:10.1016/j.jweia.2012.03.029.
- Thom, H. C. , 1967: Toward a universal climatological extreme wind distribution. The 2nd International Conference on Wind Effects on Buildings and Structures, Ottawa, Canada, 669–683.
- Vasiloff, S. V., and K. W. Howard, 2009: Investigation of a severe downburst storm near Phoenix, Arizona, as seen by a mobile Doppler radar and the KIWA WSR-88D. *Wea. Forecasting*, **24**, 856–867, doi:10.1175/2008WAF2222117.1.
- Wakimoto, R. M., 1982: The life cycle of thunderstorm gust fronts as viewed with Doppler radar and rawinsonde data. *Mon. Wea. Rev.*, **110**, 1060–1082, doi:10.1175/1520-0493(1982)110<1060:TLCOTG>2.0.CO;2.
- Wang, L., M. Wei, and T. Yang, 2015: An advanced algorithm for recognizing wind shear using airborne Doppler weather radar. *Proc. Inst. Mech. Eng. G*, **229**, 2547–2558, doi:10.1177/0954410015580653.
- Wilson, J. W., R. D. Roberts, C. Kessinger, and J. McCarthy, 1984: Microburst wind structure and evaluation of doppler radar for airport wind shear detection. *J. Climate Appl. Meteor.*, **23**, 898–915, doi:10.1175/1520-0450(1984)023<0898:MWSAEO>2.0.CO;2.
- Wolfson, M. M., R. L. Delanoy, B. E. Forman, R. G. Hallowell, M. L. Pawlak, and P. D. Smith, 1995: Automated microburst wind-shear prediction. *Lincoln Lab. J.*, **7**, 399–426.

## Chapter 3

### 3 Flow field dynamics of large scale experimentally produced downburst flows

This chapter characterizes the mean and turbulent flow fields resulting from several large-scale downbursts simulated in the Wind Engineering Energy and Environment (WindEEE) Dome at Western University. Detailed three-component velocity Cobra probe measurements are conducted for several Reynolds numbers and downburst height to diameter ratios. The wind speed records at a comprehensive number of heights and radial distances are analyzed using a moving average approach similar to the ones employed in some full scale campaigns. A proper averaging time is determined and the analysis of the turbulent flow is carried out using first and second order statistics and the similarities with full scale data is presented. Moreover, Particle Image Velocimetry (PIV) measurements are carried out in order to investigate the dynamics of downburst vortices for the same Reynolds numbers and the same downburst height to diameter ratios as in the Cobra probe measurements. The structure and evolution of the primary downburst vortex from PIV are compared with the available full scale data.

#### 3.1 Introduction

Downburst is a column of air descending towards the ground typically from thunderstorm clouds. Fujita (1990) defined these events as sudden and strong downdrafts of cold air originating from a cumulonimbus cloud which upon reaching the ground surface develop intense gusts near the ground. Due to their vigorous nature, downbursts can cause fatal airliner accidents, such as the crash of Boeing 727 in 1975, when 112 people were killed (Fujita and Byers, 1977). Downbursts are also known to cause damages to structures on the surface. Since downbursts are much more frequent than tornadoes, they are reported to be the most destructive winds in inland North America (Fujita, 1990; Holmes, 2002).

In many parts of the world, downburst is the dominant wind type for structural design because of the strong wind close to the ground and their higher frequency of occurrence compared to tornadoes (Solari et al., 2015). Many full scale measurement campaigns have been performed over the last 50 years with the goal to better understand the formation, dynamics, evolution and predictability of downbursts. Some of the well-known field campaigns are the Northern Illinois Meteorological Research on Downbursts (NIMROD) (Fujita, 1978), the Joint Airports Wind Shear (JAWS) (Wilson and Wakimoto, 2001), the Microburst and Severe Thunderstorm (MIST) (Fujita, 1990), the Winds and Ports (Solari et al., 2012), the Severe Convective Outflow in Thunderstorms (SCOUT) (Gunter and Schroeder, 2015), and the Wind, Ports, and Sea (Repetto et al., 2017). Although the carefully conducted full scale measurements are the most reliable method to investigate downbursts, these measurements are often difficult to conduct and require vast technological resources. Namely, downbursts are characterized with the short duration (up to approximately 20 min) and the high degree of uncertainty of their occurrence in both space and time, which all result in challenging full scale measurements of these events. Consequently, this difficulty to measure downbursts using either anemometers or Doppler radars results in the limited number of wind speed records which are often characterized with low spatial and temporal resolutions. Moreover, the full scale events are one-of-a-kind and their intensities vary from one event to the other, making it almost impossible for a parametric analysis.

Aside from full scale field measurements, a number of numerical simulations and physical experiments were carried out by researchers to further understand the downburst outflow and its characteristics. Numerical simulations of downbursts are usually performed by employing either a cooling source (CS) model using negatively-buoyant thermodynamic cooling from a pre-defined source to produce downdrafts (Anderson et al., 1992; Mason et al., 2009; Vermeire et al., 2011; Zhang et al., 2013; Orf et al., 2014; Oreskovic et al., 2018) or an impinging jet model using axisymmetric continuous or impulsively driven impinging jet flows to simulate downbursts (Kim and Hangan, 2007; Sengupta and Sarkar, 2008; Vermeire et al., 2011). One of the main advantages of CS model is that it produces the downdraft using gradual density perturbation that closely matches the physics of the downburst formation in nature (Anderson et al., 1992). However, one of the major

drawbacks of CS model is that it requires large domains (usually 10's of kilometers) resulting in very high number of grid points for reasonable spatial resolution close to the ground. For example, Orf et al. (2014) employed 717 million grid points in the computational domain of  $92 \times 92 \times 14 \text{ km}^3$  with the first vertical grid point at 2.5 m above ground. Therefore, CS models could be computationally expensive especially for parametric studies.

Downbursts have also been modelled numerically using impinging jets. Impulsively driven impinging jets are often used by researchers as steady flowing impinging jets fail to model the vortex dynamics at the downburst outflow (Proctor, 1988; Kim and Hangan, 2007; Zhang et al., 2013). Reynolds Averaged Navier-Stokes (RANS) turbulence modelling approach has been adopted by many researchers to simulate impinging jets (Hangan et al., 2004; Chay et al., 2006; Kim and Hangan, 2007; Sengupta and Sarkar, 2008; Li et al., 2012; Zhang et al., 2013), as this approach is computationally less demanding compared to other numerical approaches, e.g., Direct Numerical Simulation (DNS) or Large Eddy Simulation (LES). However, RANS modelling can only predict mean (or ensemble averaged) wind speed, but not wind gusts. With the increasing affordability of computational power these days, more often than not, LES turbulence modelling approach is used to simulate impinging jets for downburst applications in wind engineering (Sengupta and Sarkar, 2008; Sengupta et al., 2008; Aboshosha et al., 2015; Haines and Taylor, 2018). After comparing the wind flow field from LES with the full scale field measurements and/or wind tunnel experiments, which is still one of the essential requirements for the reliable numerical solutions, studies have reported the matching as “quite good” (Haines and Taylor, 2018) or “agree well” (Sengupta and Sarkar, 2008; Aboshosha et al., 2015) without quantifying the agreement.

To experimentally simulate a downburst outflow in a wind simulator, Lin et al. (2007) and Lin and Savory (2010) used slot jet or wall jet techniques. These experimental methods are only capable of producing a portion of the whole downburst outflow and they result in a two-dimensional (2-D) simulation of a three-dimensional (3-D) real event (McConville et al., 2009). Therefore, the impinging jet approach is more popular in comparison to other experimental methods and widely adopted in research community due to the simpler



mechanism of downburst generation, easy scalability, capability to satisfactorily replicate the vortex structure of real downbursts, and the ability to provide reasonable spatial and temporal resolutions in the surface layer (Landreth and Adrian, 1990; Wood et al., 2001; Chay and Letchford, 2002; Sarkar et al., 2006; Xu and Hangan, 2008; McConville et al., 2009; Zhang et al., 2013; Jubayer et al., 2016). Although impinging jet approach has been criticized for not being able to capture the buoyancy driven nature of downbursts in the real atmosphere (Vermeire et al., 2011), this method is capable of producing successive primary, secondary and trailing (intermediate) vortices that are also observed in the real downbursts (Mason et al., 2005). Considering the advantages and disadvantages of different downburst simulation techniques, experimental impinging jet (impulsively driven) technique has been adopted in this study.

Over the past two decades, several downburst simulators have emerged with the goal to reproduce downburst events in a laboratory environment using impinging jets (Mason et al., 2005; McConville et al., 2009; Sengupta and Sarkar, 2008; Xu and Hangan, 2008). These simulators vary in size, shape, fan configurations and wind speeds. A brief description of these downburst simulators is provided in Hangan et al. (2017). To date, the largest downburst simulator using impinging jet is the WindEEE Dome at Western University (Jubayer et al., 2016; Hangan et al., 2017). This facility can produce downdrafts of up to 4.5 m in diameter with a height of 3.8 m.

In the present study, 6 downbursts are simulated in the WindEEE Dome with the objective to characterize the downburst outflow. This study analyzes the wind speed time histories from experimentally simulated downbursts similar to an approach used for full scale downburst records (Solari et al., 2015). Moreover, this study also investigates the important turbulence characteristics (e.g., spectra, probability density function, gust factor) relevant to wind loading of structures and compares them against full scale downbursts for a range of Reynolds numbers ( $1.82 \times 10^6$  to  $4.24 \times 10^6$ ) and two downburst height ( $H$ ) to diameter ( $D$ ) ratios ( $H/D < 1$  and  $> 1$ ). In addition, particle image velocimetry (PIV) measurement technique is employed to analyze the primary vortex structure for the same range of Reynolds numbers ( $1.82 \times 10^6$  to  $4.24 \times 10^6$ ) and  $H/D$  ratios ( $< 1$  and  $> 1$ ). For the first time,

an effort has been made to compare the primary vortex structure and its evolution with the limited full scale downburst records obtained using Doppler radar measurements.

## 3.2 Experimental setup and test cases

### 3.2.1 Test chamber (WindEEE Dome)

The WindEEE Dome at Western University in London, Ontario, Canada is a 3-D wind testing chamber designed to physically replicate tornadoes, thunderstorm downbursts, sheared and veering flows, gusts, and atmospheric boundary layer (ABL) winds at different intensities and scales (Hangan et al., 2017). The test chamber at the WindEEE Dome has a hexagonal footprint of 25 m in diameter and 3.8 m in height. The facility can replicate a variety of winds in large scales and therefore it allows testing of large-scale models at high spatiotemporal resolution of measurement.

The WindEEE Dome has a total of 106 fans, among which 100 fans are mounted on peripheral walls and 6 larger fans are situated above the test chamber ceiling. 100 fans on the peripheral walls distributed as follows: 8 fans are installed on five walls and 60 fans are mounted on one wall in a matrix of 15 columns and 4 rows. Each of the 100 fans in the test chamber has a diameter of 0.8 m with a nominal power of 25 kW and the 6 larger fans in the upper chamber have a diameter of 2 m each with a nominal power of 220 kW. The air from the upper plenum is fed to the test chamber through a circular opening with a bell mouth and mechanically operated louvers. It takes approximately 2 s to open the louvers from fully closed to fully opened position. The diameter of the circular opening can be varied from 1.6 m to 4.5 m using annular rings of different diameters.

To simulate a downburst in the WindEEE Dome, the 6 fans in the upper plenum are run with the bell mouth louvers initially closed in order to develop the internal pressure in the upper chamber in respect to the testing chamber. With the buildup of approximately 3.5 Pa pressure difference between the upper plenum and testing chamber, the louvers are opened to create a sudden downdraft that impinges to the testing chamber floor and consequently produces a downburst-like outflow. In the present study, three different fan speeds (FS)

(20, 30 and 50% of the rated RPM of the fans) of the upper plenum fans were tested in combination with two different downdraft jet diameters ( $D$ ) (3.2 and 4.5 m). A schematic of the downburst flow at the WinDEE Dome is shown in **Figure 3.1**.

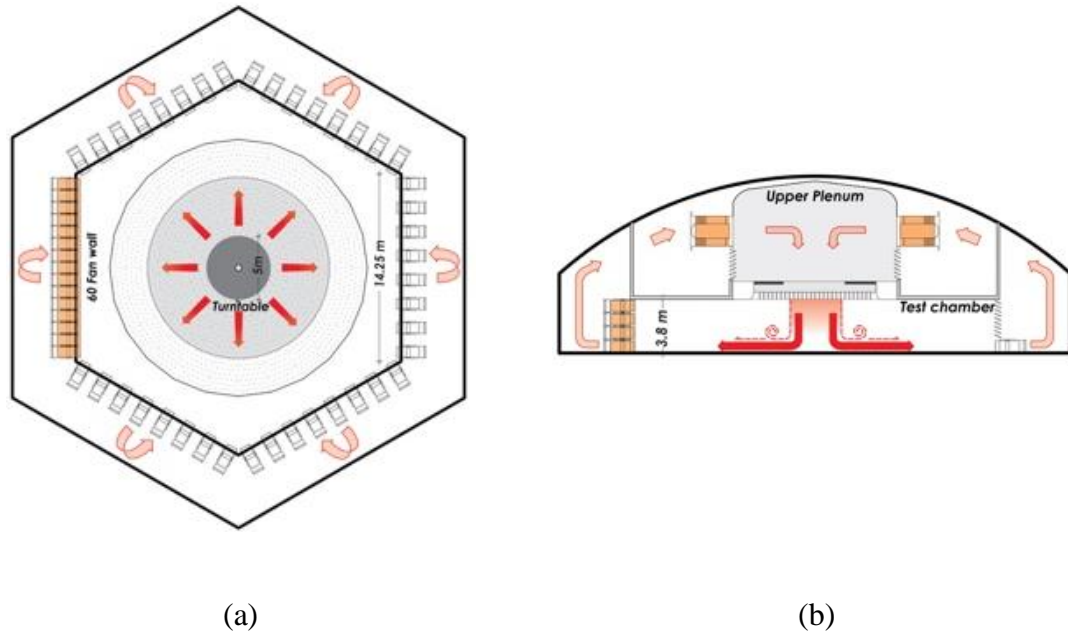


**Figure 3.1: Schematic of (a) horizontal and (b) vertical sections of the WinDEE Dome downburst mode.**

### 3.2.2 Cobra probe setup

A total of 12, 4-hole Cobra probes (developed by Turbulent Flow Instrumentation Pty Ltd.) were placed in a vertical mast to measure the downburst outflow velocities. The heights of the Cobra probes are in the range between 0.01 and 0.86 m with the higher spatial resolution of the probes closer to the ground. For each of the tested downbursts, the mast was placed at 6 different radial distances from the downburst centre ( $R$ ). The setup of the Cobra probes is shown in **Figure 3.2**. As indicated in **Figure 3.2b**, these 6 locations ranged from  $R/D = 0.7$  to  $R/D = 1.2$ . The measurements were performed for two jet diameters (i.e.,  $D = 3.2$  m and  $D = 4.5$  m) and three upper fan speeds (i.e., 20, 30 and 50% of the nominal fan RPM).

Therefore, the total number of investigated cases is 6. The sampling time was 60 s with the sampling frequency of 1250 Hz. Data were processed only for the initial few seconds that contained the transient gust. The details of determining the initial processing time are described in Section 3.3.1. Lastly, the accuracy of Cobra probes is generally within  $\pm 0.5$  m/s and the probes are capable of capturing the flow within a cone of  $\pm 45^\circ$  in respect to the axis of the installed probe.

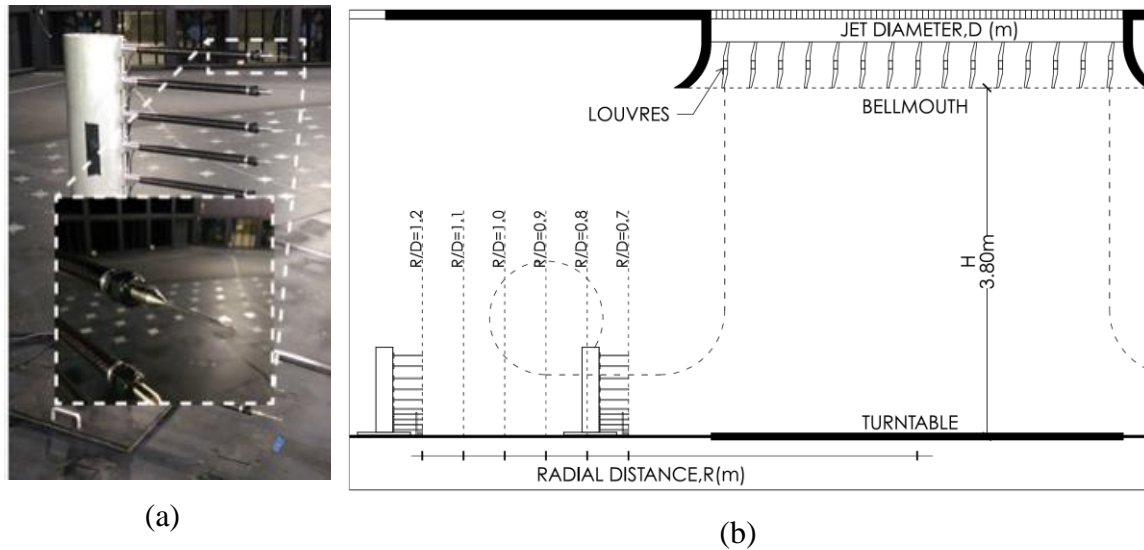


**Figure 3.2: (a) Mast equipped with 12 Cobra probes (b) Schematics of the location of the measuring mast and Cobra probes in the WindEEE Dome testing chamber**

In this study, Reynolds numbers ( $Re$ ) of the impinging jets are calculated based on the mean speed of the continuous jets at the centre of the bell mouth exit and jet diameters. The values of  $Re$  for the six investigated cases are listed in Table 3.1 .

**Table 3.1:  $Re$  for different jet diameters and fan speeds**

Jet diameter, $D$ (m)	3.2	3.2	3.2	4.5	4.5	4.5
$H/D$	1.2 (>1)	1.2 (>1)	1.2 (>1)	0.8 (<1)	0.8 (<1)	0.8 (<1)
Fan speed, FS (% of nominal RPM)	20	30	50	20	30	50

---

Reynolds						
Number, $Re$	$1.83 \times 10^6$	$2.62 \times 10^6$	$4.24 \times 10^6$	$1.82 \times 10^6$	$2.68 \times 10^6$	$4.09 \times 10^6$

---

### 3.2.3 PIV setup

In addition to the point velocity measurements conducted using Cobra probes, downburst outflow in a vertical plane was also measured using PIV technique. A total of 6 CMOS cameras (Flare 12M125-CL by IO industries) were used in the vertical plane in order to capture a region of 2.7 m (width) by 1.4 m (height) of the downburst outflow. Each camera has a resolution of 12 megapixels. The pixel to meter conversion was performed using a calibration board (Refan and Hangan, 2018). A dual head, pulsed laser generator (nd: YAG; Nano TRL 425 by Litron) with a wavelength of 532 nm was used to illuminate the particles. The repetition rate for the laser heads can be up to 15 Hz and each head has an output energy of 425 mJ/pulse. A combination of spherical and cylindrical lenses was used to achieve the uniform 5 mm laser sheet from the laser beam. In order to capture this large field of view with high spatial resolution, the camera frame rate was set to 18 fps, which resulted in the PIV sampling frequency of 9 Hz. A schematic of the PIV setup in the WindEEE Dome is shown in **Figure 3.3**.

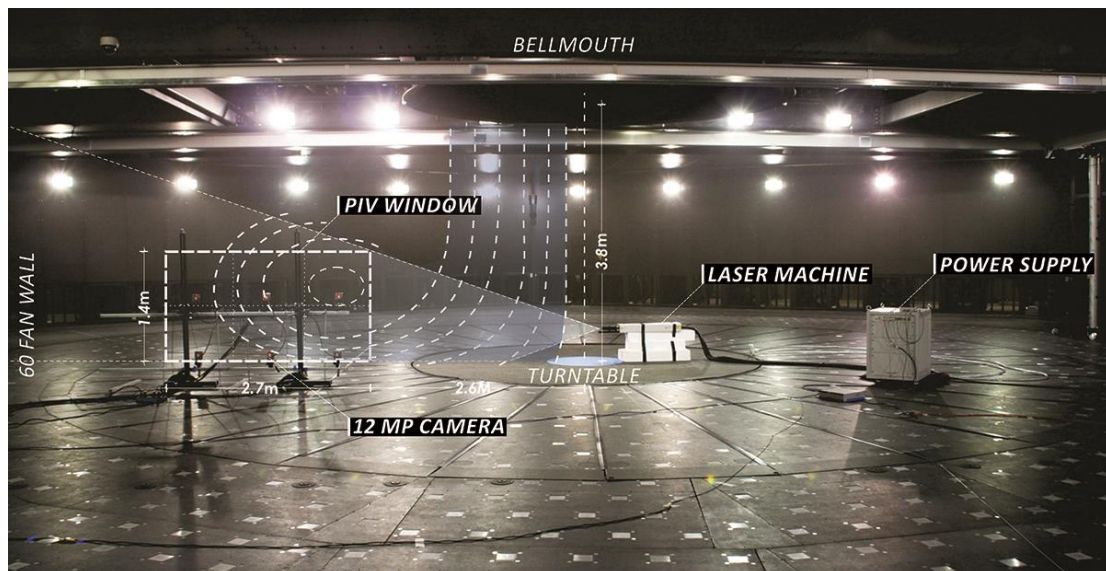


**Figure 3.3: PIV setup**

The cameras were connected to six image acquisition systems (CORE-DVR by IO Industries) that stored 8-bit raw images. A synchronizer (ILA Synchronizer 2011 by ILA GmbH) was used to control the time interval between the laser pulses and to synchronize them with the camera exposure time. An industrial fog machine (Power Fog Industrial 9D by Ultratec Special Effects) was deployed to disperse the seeding particles throughout the chamber. It was assured that the uniformity of particles in the region of interest was well established prior to the data acquisition. The utilized fog machine uses Di-Ethyl-Hexyl-Sebacate,  $(\text{CH}_2)_8(\text{COOC}_8\text{H}_{17})_2$ , as seeding particles with an average diameter of 1–5  $\mu\text{m}$ . Errors due to PIV experiment is shown in Appendix B.

### 3.3 Results

#### 3.3.1 Downburst records analysis and the proper value of moving average period ( $T_{avg}$ )

Each Cobra probe measures the radial ( $u$ ), lateral ( $v$ ) and axial (or vertical) ( $w$ ) components of velocity. The radial component of downburst outflows is the critical one for inflicting damages on structures (Fujita, 1990). Time histories of  $u$ ,  $v$  and  $w$  from the Cobra probe that captured the maximum instantaneous value of  $u$  for different  $Re$  (see Table 3.2) are plotted in **Figure 3.4**.

Although the sampling time was 60 s, time histories are plotted only up to 15 s to emphasize on the initial gust front and the peak of the downburst velocity. **Figure 3.4** shows that  $u$  is the dominating velocity components in downburst outflows. This velocity component (i.e.,  $u$ ) has been taken into consideration for further investigation of the downburst outflow. Table 3.2 shows the maximum instantaneous radial velocity ( $u_{max,i}$ ), as well as its radial location ( $R/D$ ) and height ( $Z_{max,i}$ ) from the impinging surface for all  $H/D$  and  $Re$  cases analyzed in this article.

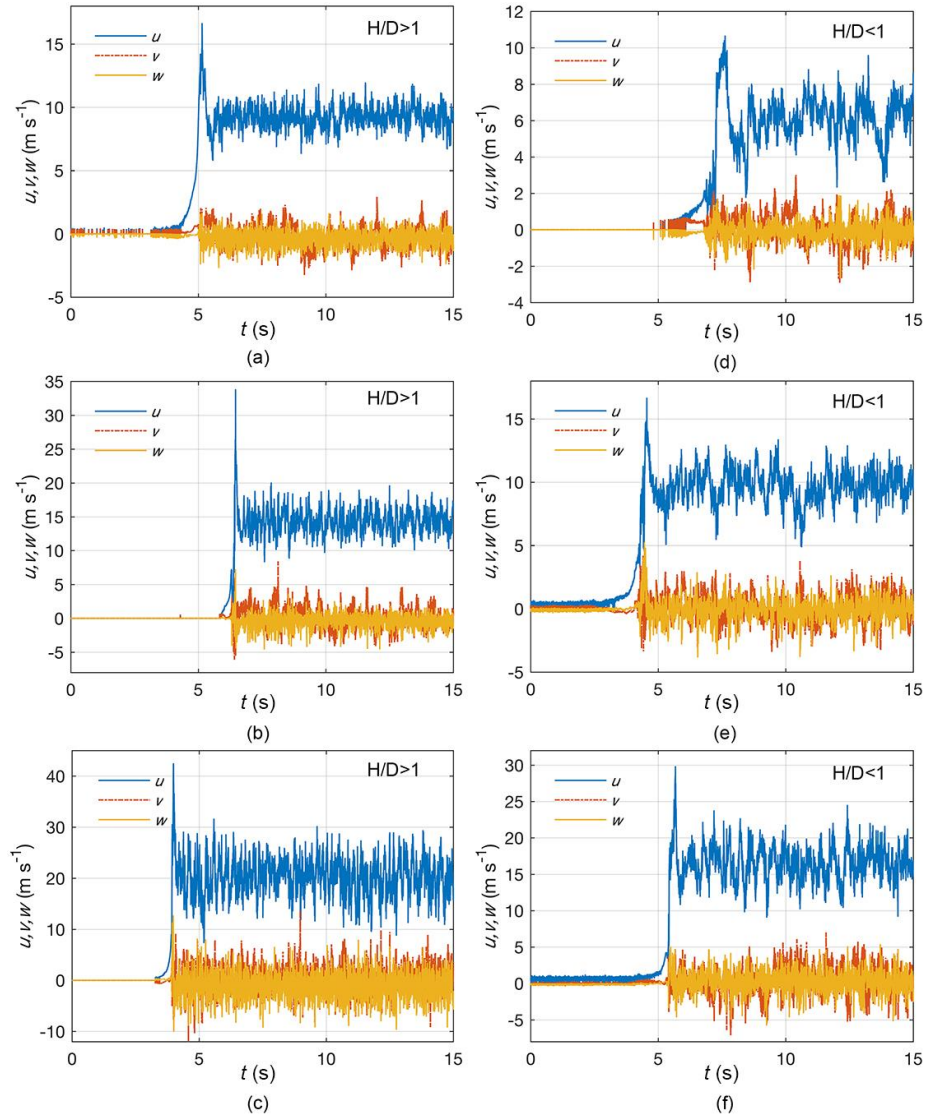


**Figure 3.4: Radial ( $u$ ), lateral ( $v$ ) and vertical ( $w$ ) components of instantaneous velocity for  $Re$  (a)  $1.83 \times 10^6$ , (b)  $2.62 \times 10^6$ , (c)  $4.24 \times 10^6$ , (d)  $1.82 \times 10^6$ , (e)  $2.68 \times 10^6$  and (f)  $4.09 \times 10^6$**

**Table 3.2: The maximum instantaneous radial velocity ( $u_{max,i}$ ) and its location for each of the investigated cases**

$H/D$	1.2 (>1)	1.2 (>1)	1.2 (>1)	0.8 (<1)	0.8 (<1)	0.8 (<1)
$Re$	$1.83 \times 10^6$	$2.62 \times 10^6$	$4.24 \times 10^6$	$1.82 \times 10^6$	$2.68 \times 10^6$	$4.09 \times 10^6$

$u_{max,i}$ (m/s)	16.66	33.84	42.51	10.67	16.68	29.85
$R/D$	0.8	1	1.1	1.2	1.1	1.1
$Z_{max,i}$ (m)	0.05	0.05	0.151	0.05	0.151	0.1

Since data sampling started with the bell mouth louvres closed, this resulted in a near zero velocities at the beginning of the wind speed records. A method proposed by Lavielle (2005) and Killick et al. (2012) was used to discard this noise at the beginning of the records and to objectively determine the starting point of the downburst signal. Since downburst winds are transient in nature, turbulent fluctuations in downbursts are more pronounced before and after the downburst. Romanic et al. (2018) applied this method for the detection of abrupt changes in velocity time series in a downburst. The method identifies the abrupt changes in a signal based on the mean value of two segments of the data. In simple words, if the statistical properties (i.e., mean) of two adjacent segments around a point in the record are significantly (statistically) different from each other, then the point is assigned as the change point in the time series. The statistical significance of the difference is prescribed as the minimum threshold value that guards against overfitting. The detailed explanations and mathematical expressions of this method are provided in Lavielle (2005) and Killick et al. (2012). **Figure 3.5** depicts the detected change points for a couple of time histories. The first change point was chosen as the starting point of the downburst. The data was processed for the next 3 s after the first change point, which was always ensured to be long enough to capture the initial gust. The same process was applied for all  $Re$  in order to discard the near zero values (i.e., noise) at the beginning of the time series as well as to identify the ramp-up portion of the downburst segment.



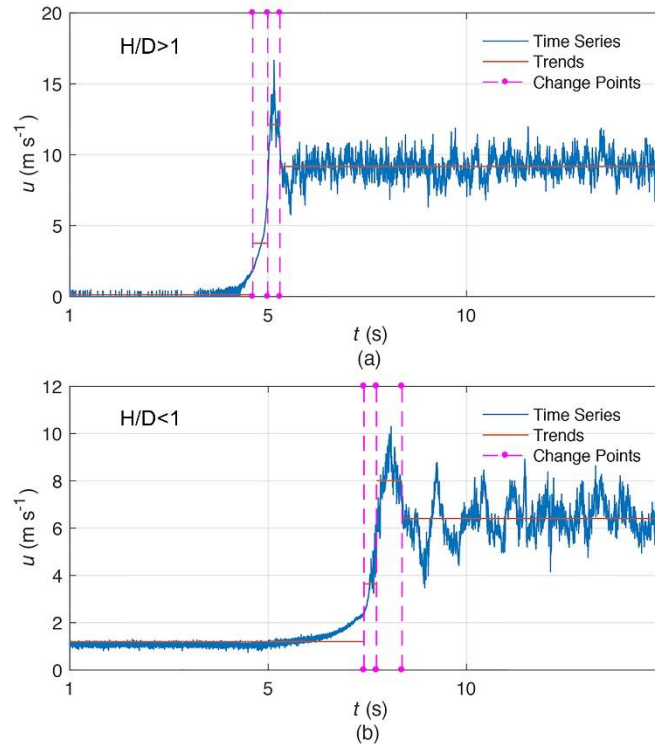


**Figure 3.5: Abrupt changes in the signal (dashed lines) used to determine the initial point of the gust front (first dashed line) for (a)  $Re=1.83 \times 10^6$  and (b)  $Re=1.82 \times 10^6$**

In general, temporal analyses applicable for the ABL winds cannot be directly applied to downbursts. One example is the hourly mean wind speed that is widely used in the analysis of ABL winds, but such a value is meaningless in the analysis of downbursts that last for not longer than 20–30 min (Holmes, 2002). Moreover, using a fixed averaging time for thunderstorm events might be questionable because of the rapid changes in wind speeds and directions. In this study, the  $u$  velocity component from the Cobra probes are decomposed following a similar approach as in the full scale events analyzed by Choi and Hidayat (2002), Chen and Letchford (2004), Holmes et al. (2008), McCullough et al. (2014), Lombardo et al. (2014) and Solari et al. (2015). Here, however, the goal is to obtain the proper averaging time ( $T_{avg}$ ) in the experimentally-produced downbursts. In their investigation of thunderstorm wind loads on buildings, Choi and Hidayat (2002) proposed a decomposition of the wind velocity into the running mean and fluctuating parts. This

approach was later also adopted by Holmes et al. (2008), McCullough et al. (2014), Solari et al. (2015), among others. Namely, wind velocity has been decomposed as per Eq. (3.1):

$$u(t) = \bar{u}(t) + u'(t) \quad (3.1)$$

Here,  $u(t)$  is the radial velocity as a function of time ( $t$ ),  $\bar{u}(t)$  is the moving average of  $u(t)$  and  $u'(t)$  is the high-frequency residual fluctuations. For instance, Solari et al. (2015) showed that  $u'(t)$  can further be decomposed into the standard deviation and reduced turbulent fluctuations via:

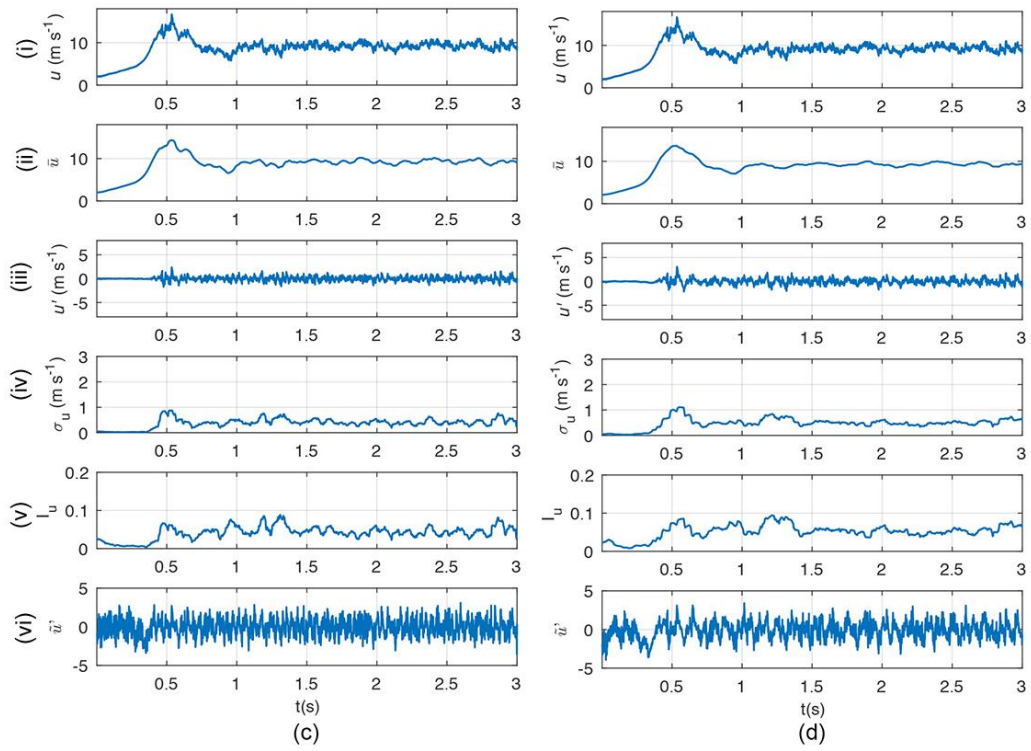
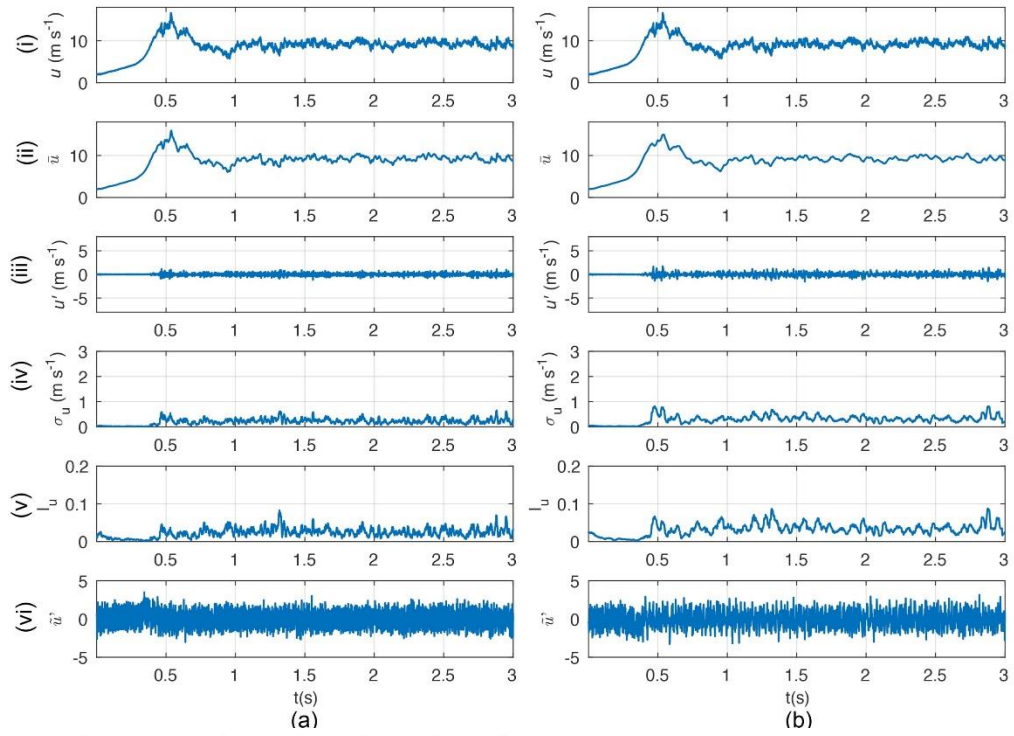
$$u'(t) = \sigma_u(t)\tilde{u}'(t) \quad (3.2)$$

where  $\sigma_u(t)$  is the slowly varying standard deviation and  $\tilde{u}'(t)$  is the reduced turbulent fluctuations. The fluctuating component of the residual turbulence can be treated as a zero-mean stationary Gaussian random process (McCullough et al., 2014; Solari et al., 2015; Burlando et al., 2017).

Furthermore, notice that a time-dependent turbulence intensity,  $I_u(t)$ , can be expressed as:

$$I_u(t) = \frac{\sigma_u(t)}{\bar{u}(t)} \quad (3.3)$$

**Figure 3.6** shows the time history of  $u$  and its decomposition at  $u_{max,i}$  (also see Table 3.2) for different values of  $T_{avg}$ . For  $Re=1.83 \times 10^6$  and  $H/D>1$ , **Figure 3.6** shows: (i) radial velocity,  $u$  (ii) running mean,  $\bar{u}$  (iii) residual fluctuation,  $u'$  (iv) standard deviation of the residual fluctuation,  $\sigma_u$  (v) turbulence intensity,  $I_u$  and (vi) reduced turbulent fluctuation



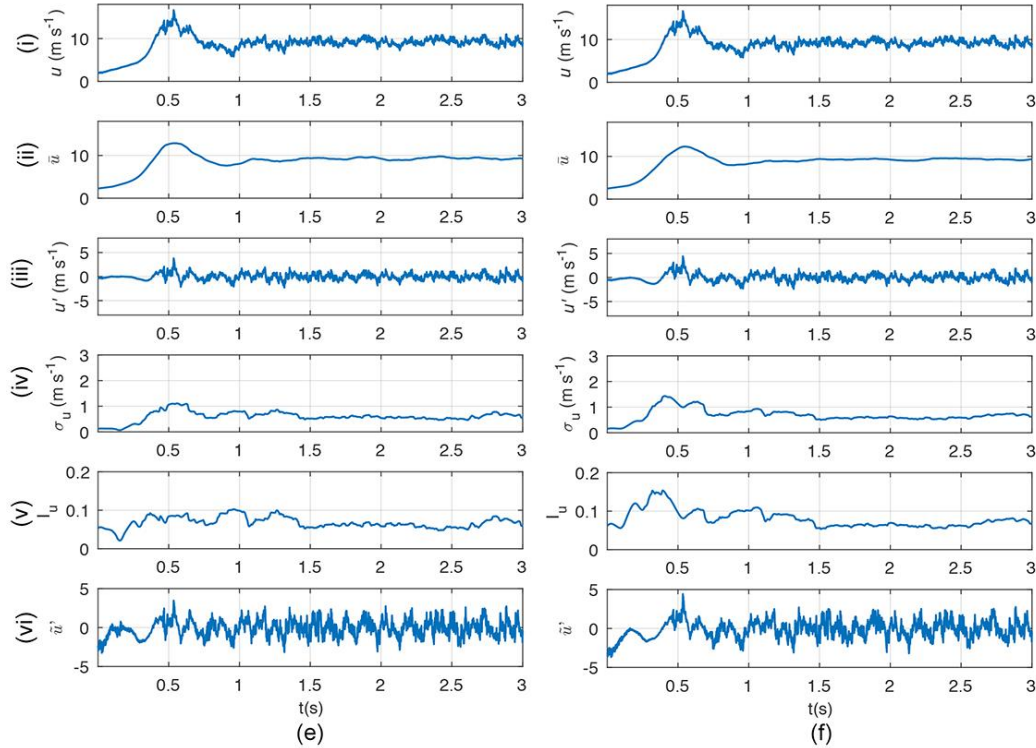


**Figure 3.6: Time history of the  $u$  velocity component and its decomposition for the case of  $Re = 1.83 \times 10^6$  and  $H/D > 1$  obtained by using different values of  $T_{avg}$ : (a) 0.01 s, (b) 0.025 s, (c) 0.05 s, (d) 0.1 s, (e) 0.2 s, and (f) 0.3 s.**

Six different values of  $T_{avg}$ —0.01, 0.025, 0.05, 0.1, 0.2 and 0.3 s—are investigated herein to determine the appropriate value of  $T_{avg}$  that matches the criteria proposed by Holmes et al. (2008) and Solari et al. (2015). In all cases, **Figure 3.6** demonstrates a clear dependency of  $\bar{u}(t)$  and  $u'(t)$  on  $T_{avg}$ . For larger values of  $T_{avg}$ ,  $u'(t)$  tends to contain the large-scale flow structures, whereas for smaller values of  $T_{avg}$ ,  $\bar{u}(t)$  includes the high-frequency fluctuation content of the signal. A concluding discussion on the proper value of  $T_{avg}$  is carried out in the following three paragraphs.

Firstly, the appropriate value of  $T_{avg}$  is analyzed by subjectively investigating the decomposed time series in **Figure 3.6**. For the smallest averaging periods (i.e.,  $T_{avg} = 0.01$  and 0.025 s), **Figure 3.6** a and b show that  $\bar{u}(t)$  still contains some of the high-frequency fluctuations thereby indicating that these averaging times seem to be too short. With the further increase of  $T_{avg}$  (**Figure 3.6** c-f),  $\bar{u}(t)$  becomes flatter and  $u'(t)$  starts to depict

some of the large-scale flow fluctuations. Consequently, for the largest averaging times, such as  $T_{avg} = 0.2$  and  $0.3$  s (**Figure 3.6** e and f), the downburst ramp-up, which is the main features of any downburst outflow, is largely attenuated in the time series of  $\bar{u}(t)$ . Therefore, these averaging times are considered too long to be an appropriate value of  $T_{avg}$ . Following the subjective criteria proposed by Holmes et al. (2008) and Solari et al. (2015),  $T_{avg} = 0.05$  and  $0.1$  s seem to provide reasonable results for which  $\bar{u}(t)$  retains the main features of a downburst record and  $u'(t)$  possesses a near zero mean value. The same analysis has been applied to all  $Re$  cases and  $T_{avg} = 0.05$  and  $0.1$  s are found to provide the most satisfactory results.

Secondly, an objective analysis for determining the appropriate value of  $T_{avg}$  is also conducted. This analysis is based on the Fourier transform of  $\bar{u}(t)$  and  $u'(t)$  into the frequency domain. **Figure 3.7** a–e show the functions  $n|F_{\bar{u}}|^2$ ,  $n|F_{u'}|^2$  and  $n|F_{\bar{u}}||F_{u'}|$  for  $Re=1.83 \times 10^6$  ( $H/D>1$ ) at the location of  $u_{max,i}$  (**Table 3.2**) and for  $T_{avg} = 0.01, 0.025, 0.05, 0.1, 0.2$  and  $0.3$  s. Here,  $n$  is the frequency, and  $F_{\bar{u}}$  and  $F_{u'}$  are the Fourier transforms of  $\bar{u}(t)$  and  $u'(t)$ , respectively. According to Solari et al. (2015), the frequency content of  $\bar{u}(t)$  and  $u'(t)$  should be distinct, as in the cases of synoptic and stationary ABL wind events. If the frequency contents are completely disjoint, then  $n|F_{\bar{u}}||F_{u'}| = 0$ . **Figure 3.7** demonstrates that  $n|F_{\bar{u}}||F_{u'}|$  has the lower values for the smaller  $T_{avg}$  (e.g.,  $0.01, 0.025, 0.05, 0.1$  s) and results in an almost flat line (**Figure 3.7** a–d). With the increase of  $T_{avg}$ , in particular for the values greater than  $0.1$  s,  $n|F_{\bar{u}}||F_{u'}|$  increases significantly thereby indicating that the frequency contents are not disjoint (**Figure 3.7** e–f). Therefore, both quantitative and qualitative analyses of the proper value of  $T_{avg}$  for the experimentally produced downbursts show that  $T_{avg} = 0.2$  and  $0.3$  s are not the appropriate choices for  $T_{avg}$ .

A third criterion for deriving the proper value of  $T_{avg}$  is to consider the statistics of reduced turbulent fluctuations,  $\tilde{u}'(t)$ . As mentioned above, this quantity is analyzed as a stationary random Gaussian process. That being said, by definition the running mean of  $\tilde{u}'(t)$  should have a mean  $\mu_{\tilde{u}'} = 0$ , the standard deviation  $\sigma_{\tilde{u}'} \cong 1$ , skewness  $\gamma_{\tilde{u}'} \cong 0$ , and kurtosis  $\kappa_{\tilde{u}'} \cong 3$ . **Table 3.3** shows the average values of these parameters for all cases analyzed in

this study. Notice that all values of  $T_{avg}$  somewhat satisfy the condition that  $\mu_{\bar{u}'} = 0$  and  $\gamma_{\bar{u}'} \cong 0$ . However,  $T_{avg} = 0.025$  to  $0.3$  s show better results in terms of  $\sigma_{\bar{u}'} \cong 1$  when compared to  $T_{avg} = 0.01$  s. On the other hand, the mean of  $\kappa_{\bar{u}'}$  generally increases with increasing  $T_{avg}$  and the higher values of  $T_{avg}$  better match the condition of  $\kappa_{\bar{u}'} \cong 3$ .

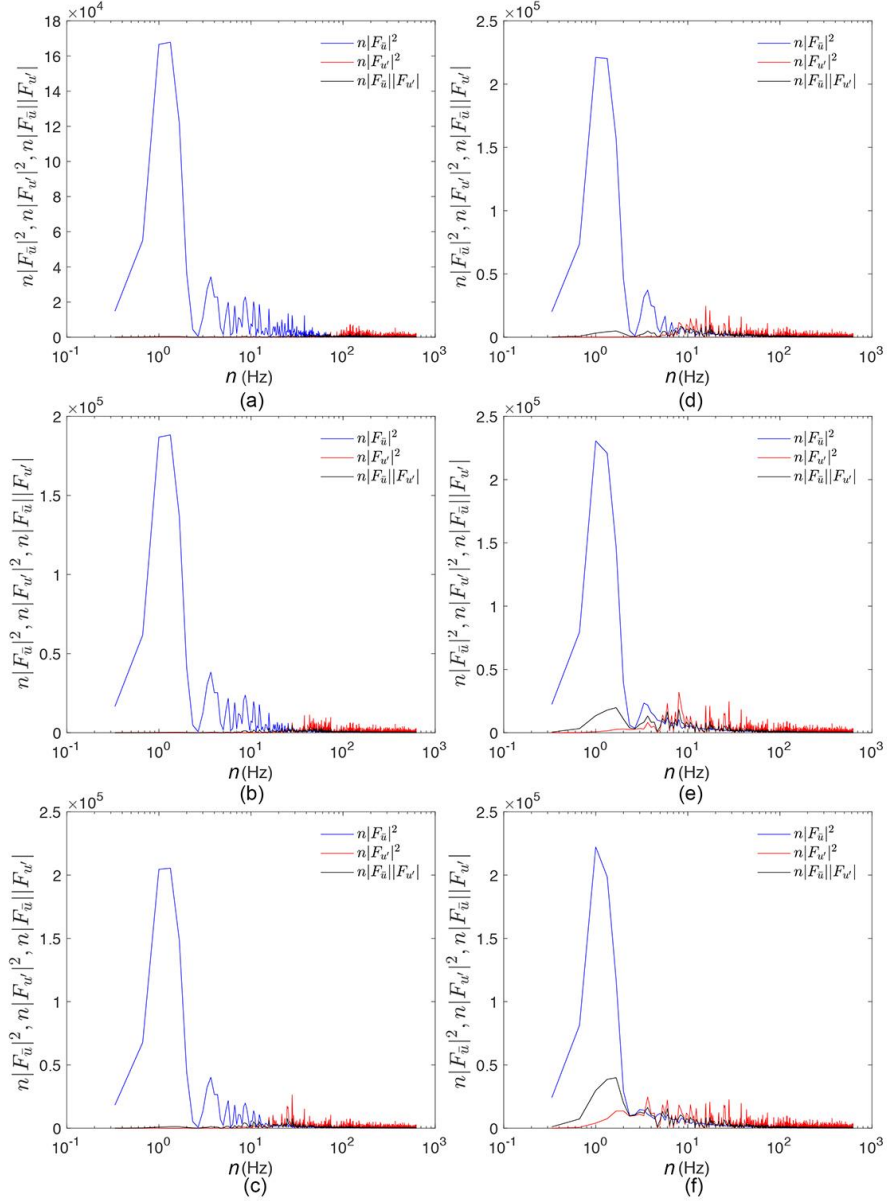


**Figure 3.7: Derived functions based on the Fourier transform of  $\bar{u}(t)$  and  $u'(t)$ ,  $n|F_{\bar{u}}|^2$ ,  $n|F_{u'}|^2$  and  $n|F_{\bar{u}}||F_{u'}|$ , for  $Re = 1.83 \times 10^6$  and  $H/D > 1$ . The panels indicate**

**different values of  $T_{avg}$  that were used to obtain  $\bar{u}(t)$  and  $u'(t)$ : (a) 0.01 s, (b) 0.025 s, (c) 0.05 s, (d) 0.1 s, (e) 0.2s and (f) 0.3 s**

**Table 3.3: Average values of  $\mu_{\tilde{u}'}$ ,  $\sigma_{\tilde{u}'}$ ,  $\gamma_{\tilde{u}'}$ ,  $\kappa_{\tilde{u}'}$  from all six cases**

$T_{avg}$ (s)	0.01	0.025	0.05	0.1	0.2	0.3
$\bar{\mu}_{\tilde{u}'}$	0.00	-0.01	-0.02	-0.05	-0.08	-0.06
$\bar{\sigma}_{\tilde{u}'}$	0.83	1.00	1.02	1.03	1.02	1.04
$\bar{\gamma}_{\tilde{u}'}$	-0.04	0.01	0.03	0.03	0.07	0.07
$\bar{\kappa}_{\tilde{u}'}$	2.52	2.67	2.77	2.88	2.83	2.92

To sum up, based on the above three criteria—namely, (1) the characteristics of  $\bar{u}(t)$  and  $u'(t)$ , (2) the joint Fourier transforms (i.e.,  $n|F_{\bar{u}}||F_{u'}|$ ), and (3) the statistical properties of  $\tilde{u}'(t)$ —it can be concluded that the values of  $T_{avg} = 0.05$  and 0.1 s are the proper values for the decomposition analysis of experimentally produced downburst outflows. In a concurrent study by Romanic et al. (2018), a range of time scales was proposed for the downburst outflows in the WindEEE Dome. The values span from 1:15 to 1:405 and their results are obtained by comparing the model downbursts in the WindEEE Dome with full scale downburst events from the field measurements reported in Solari et al. (2012) and Repetto et al. (2018). Based on the proposed time scales in Romanic et al. (2018), the proper  $T_{avg}$  for the experimentally produced downbursts in the WindEEE Dome could be from 0.07 to 2 s. The proper value of  $T_{avg} = 0.1$  s is independently obtained in both studies (i.e., Romanic et al. (2018) and this paper) and therefore this value is chosen over the value of 0.05 s for all further analysis of Cobra probe data in this article.

### 3.3.2 Downburst velocity profiles

The vertical profiles of  $\bar{u}(t)$  for all  $Re$  cases ( $T_{avg} = 0.1$  s) are investigated at the radial location and the instance of the maximum of the time varying mean velocity ( $\bar{u}_{max}$ ). The values of  $\bar{u}_{max}$  for all  $Re$  cases, as well as its radial distance ( $R/D$ ) and the height from the impinging surface ( $Z_{max}$ ) are listed in Table 3.4. The profiles of  $\bar{u}$  are shown in **Figure 3.8 a**. It is observed that the profiles corresponding to  $H/D > 1$  produce larger radial velocities and have a more pronounced “nose” shape when compared to the ones for  $H/D < 1$  at similar Reynolds numbers. The case of  $H/D > 1$  corresponds to the situation when the annular vortex has the time to fully develop (Xu and Hangan, 2008). In addition, **Figure 3.8 b** portrays the normalized profiles of  $\bar{u}$ , where the velocity and height ( $Z$ ) are normalized with  $\bar{u}_{max}$  and  $Z_{max}$ , respectively.

**Table 3.4: The maximum value of the time varying mean radial velocity,  $\bar{u}_{max}$  and its location**

$H/D$	>1	>1	>1	<1	<1	<1
$Re$	$1.83 \times 10^6$	$2.62 \times 10^6$	$4.24 \times 10^6$	$1.82 \times 10^6$	$2.68 \times 10^6$	$4.09 \times 10^6$
$\bar{u}_{max}$ (m/s)	14.17	23.02	32.76	9.87	14.2	24.24
$R/D$	1.1	0.9	1	1.2	1.0	1.1
$Z_{max}$ (m)	0.1	0.1	0.05	0.05	0.05	0.1



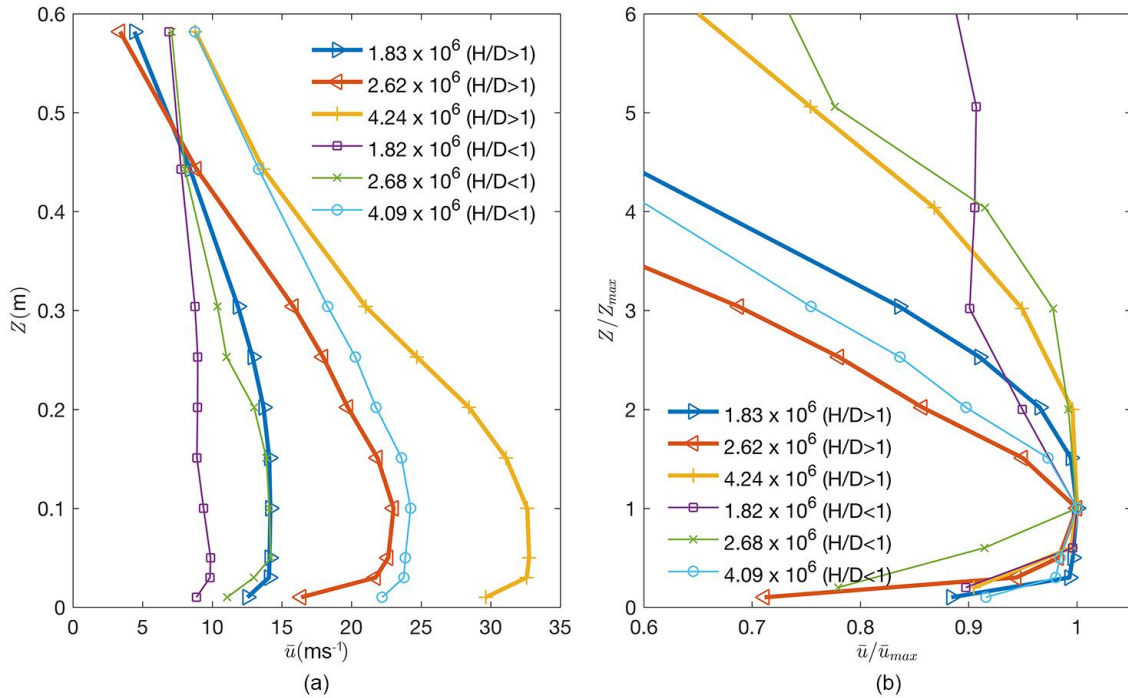


**Figure 3.8: Downburst radial velocity profiles at the radial location of  $\bar{u}_{max}$  (a) without normalization and (b) normalized**

Lastly, **Figure 3.9** shows the comparison of the current experiments with the previous full scale events. The full scale data shown in **Figure 3.9** are from four events captured during the JAWS campaign in Denver, Colorado (Hjelmfelt, 1988) and one event from the NIMROD campaign in Chicago (Fujita, 1978) using doppler radar. Velocity profiles from the full scale events shown in **Figure 3.9** were captured at the location of the maximum radial velocity observed during the downburst events. Despite the rather large variability of these profiles it appears that the profiles corresponding to the case of  $H/D > 1$ , especially at lower  $Re$  ( $1.82 \times 10^6$  to  $2.68 \times 10^6$ ) show better comparison with full scale data. For these cases, the main annular vortex is fully formed before it touches the surface (Xu and Hangan, 2008).

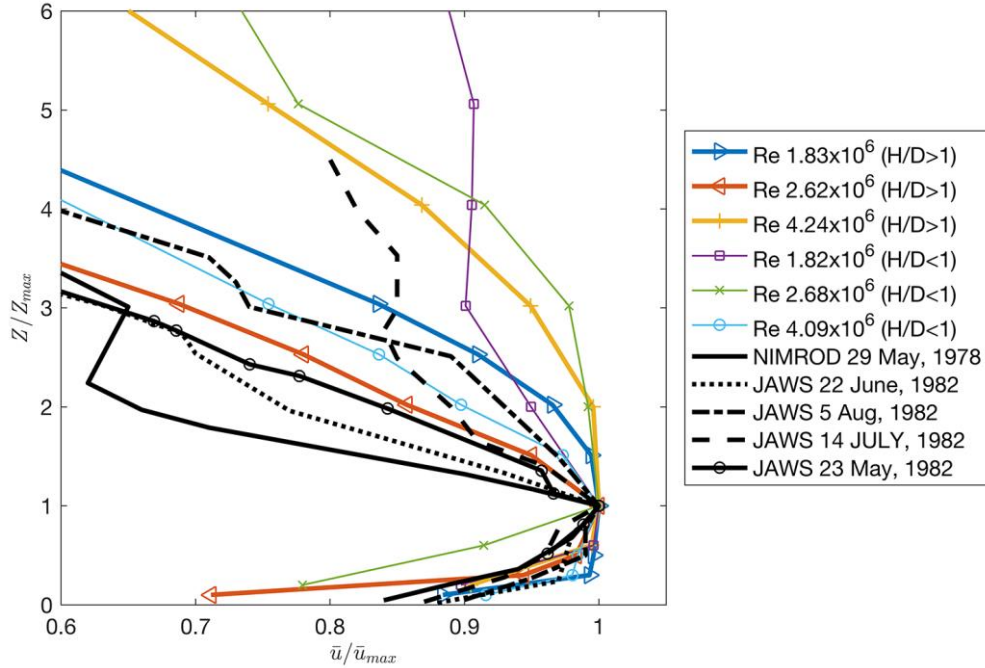


**Figure 3.9: Normalized velocity profiles from full scale events are plotted against the experimentally generated downbursts in the WindEEE Dome**

Evolution of the vertical profiles of  $\bar{u}(t)$  at the location of  $\bar{u}_{max}$  for one of the six cases (i.e.,  $Re = 2.62 \times 10^6$  and  $H/D > 1$ ) is further investigated and the results are shown in **Figure 3.10**. It is worth mentioning that the investigated case has the best match between the normalized radial velocity profile and the full scale event. At the instance of  $t = 0.46$  s in the model time, Figure 10(iv) shows that the ramp-up interval is completed and the value of  $\bar{u}_{max}$  is achieved. At this time, the typical nose-shape downburst profile is well developed (**Figure 3.10 b, iv**). Interestingly, somewhat developed nose-shape velocity profile is also observed prior to  $\bar{u}_{max}$ , at the time instance  $t = 0.42$  s (**Figure 3.10 b, iii**). The nose shape profile quickly disappears after the end of the ramp-up segment (**Figure 3.10 b, v**).

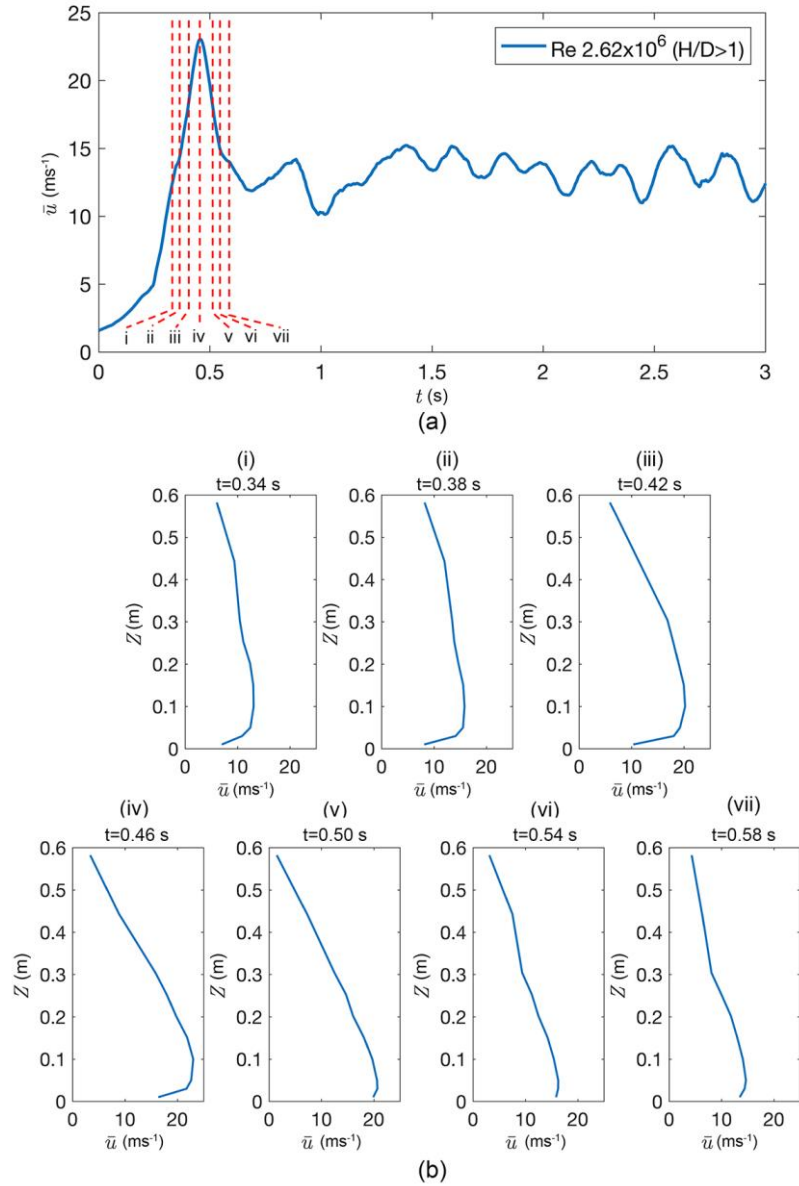


**Figure 3.10: Vertical profiles of  $\bar{u}(t)$  at different time instances in the time series and at the radial location of  $\bar{u}_{max}$ . The investigated case is for  $\text{Re}=2.62 \times 10^6$  and  $H/D > 1$ . (a) Moving mean time series and (b) vertical profiles at different time instances,  $t=0.34$  to  $0.58$  s (i)–(vii)**

### 3.3.3 Statistical Analysis of Turbulence

In this section, turbulence characteristics of the downburst outflow at the spatial location of  $\bar{u}_{max}$  for six cases using  $T_{avg} = 0.1$  s are analyzed. Form the Kolmogorov's similarity

hypothesis, the energy cascade in the inertial subrange is proportional to  $n^{-\frac{5}{3}}$ , where  $n$  is the frequency. Analyzing the power spectral density (PSD) of the reduced turbulent fluctuations from downburst events, McCullough et al. (2014) and Burlando et al. (2017) demonstrated that the  $-5/3$  law holds for both thunderstorm downbursts as well as synoptic ABL winds. Holmes et al. (2008) also showed the matching of the  $n^{-\frac{5}{3}}$  profile with PSD of the downburst events in Lubbock-Reese. Similar results were also obtained by Solari et al. (2015) for several downbursts events in the Mediterranean. **Figure 3.11** shows the PSD of  $\tilde{u}'(t)$  for different  $Re$  produced in the WindEEE Dome. It is evident that the high frequency end of the spectra has the similar slope to  $n^{-\frac{5}{3}}$ , which, in turn, is in accordance with the inertial subrange of ABL winds at full scale. However, the slope of  $n^{-\frac{5}{3}}$  matches better with the empirical spectra for the higher values of  $Re$  ( $\geq 2.62 \times 10^6$ ). The lower  $Re$  cases ( $< 2.62 \times 10^6$ ) have milder slope compared to the theoretical  $n^{-\frac{5}{3}}$ . Effectively the larger Reynolds number and the  $H/D > 1$  cases correspond to a fuller vortex formation and capture a larger range of scales and therefore show a better match with the typical inertial range behavior.

A comparison between the PSD of  $\tilde{u}'(t)$  and the analytical model proposed by Solari and Piccardo (2001) is shown in **Figure 3.12**. The theoretical model of Solari and Piccardo (2001) is given by:

$$nS_{\tilde{u}'}(n) = \frac{f/f_m}{\left(1 + \frac{1.5f}{f_m}\right)^{5/3}} \quad (3.4)$$

where,  $S_{\tilde{u}'}$  is the PSD of  $\tilde{u}'(t)$ ,  $f = nz/\bar{u}_{max}$  is the reduced frequency in which the radial mean wind velocity,  $\bar{u}$ , is substituted with its maximum value  $\bar{u}_{max}$  (Choi and Hidayat, 2002),  $f_m = 0.1456/L_v$  is the value of  $f$  for which  $nS_{\tilde{u}'}$  takes the maximum value and  $L_v$  is the integral length scale. **Figure 3.12d** demonstrates that the least accurate match with the analytical model is found for  $Re = 1.83 \times 10^6$  and  $H/D < 1$ . Moreover, **Figure 3.12** shows that the best match with the analytical model is obtained for the highest  $Re$  cases (i.e.,  $4.09 \times 10^6$  and  $4.24 \times 10^6$ ) regardless of the  $H/D$  values (**Figure 3.12 c,f**).

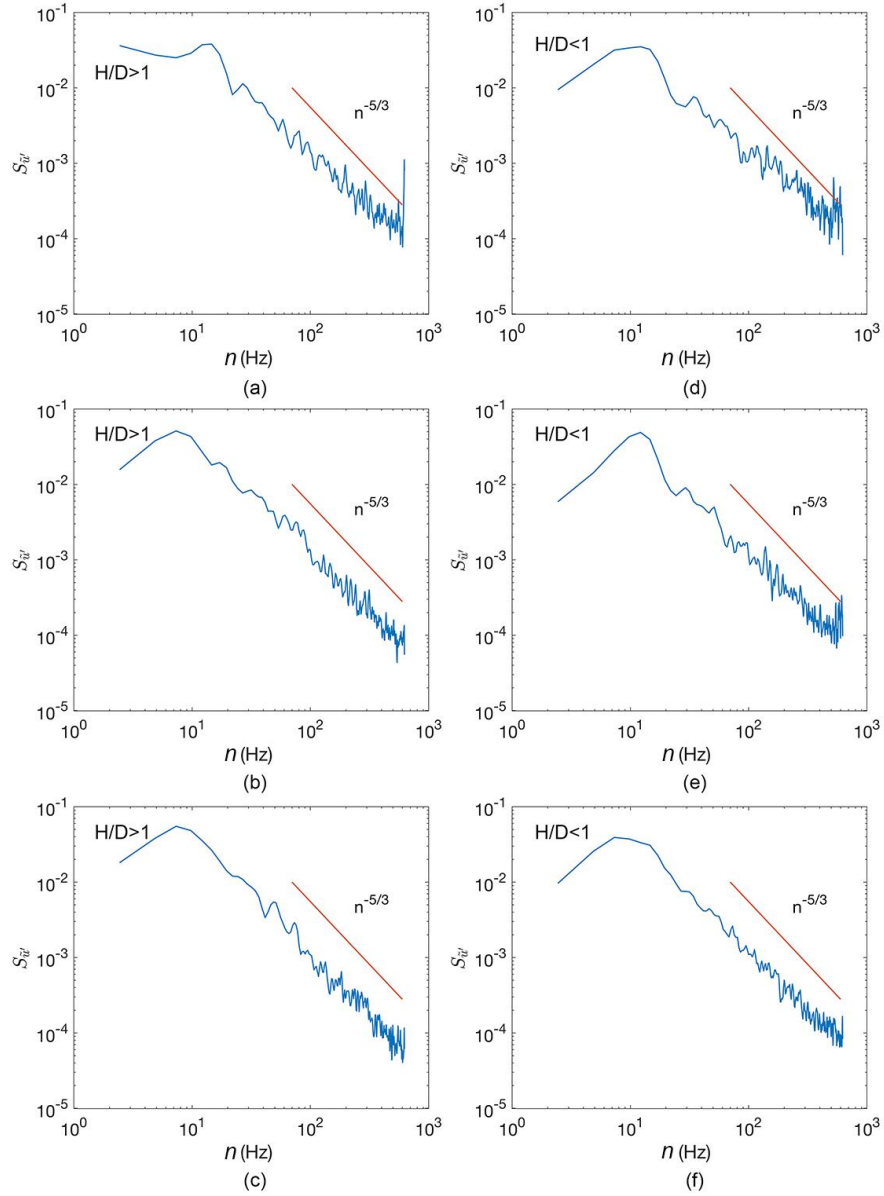


**Figure 3.11: PSD of the reduced turbulence fluctuations matched with  $n^{-\frac{5}{3}}$  profile (red line) using  $T_{avg} = 0.1$  s for Re, (a)  $1.83 \times 10^6$ , (b)  $2.62 \times 10^6$ , (c)  $4.24 \times 10^6$ , (d)  $1.82 \times 10^6$ , (e)  $2.68 \times 10^6$  and (f)  $4.09 \times 10^6$**

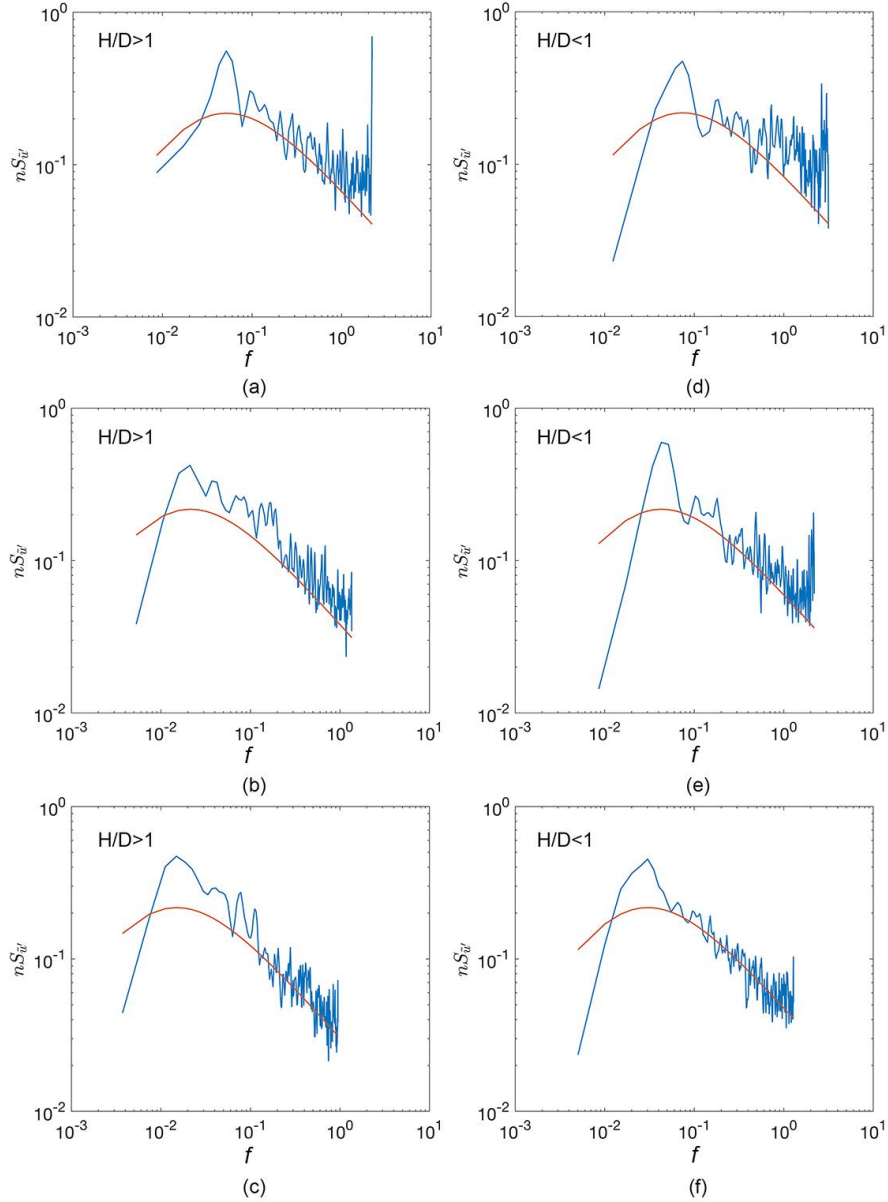


**Figure 3.12: PSD of the reduced turbulence fluctuations ( $T_{avg} = 0.1$  s) matched against the analytical model proposed by Solari and Piccardo (2001) (red line) for  $Re$  (a)  $1.83 \times 10^6$ , (b)  $2.62 \times 10^6$ , (c)  $4.24 \times 10^6$ , (d)  $1.82 \times 10^6$ , (e)  $2.68 \times 10^6$  and (f)  $4.09 \times 10^6$**

**Figure 3.13** shows the probability density function (PDF) of  $\tilde{u}'(t)$  for all cases. To quantify the Gaussianity of the PDFs, negentropy ( $N$ ) for each of the six cases is reported in **Figure 3.13**. Negentropy measures the deviation of PDF of a signal from a Gaussian distribution based on the differences in entropy between the PDF of the signal and Gaussian distribution

(Comon, 1994). The larger the value  $N$ , the more the PDF deviates from Gaussian distribution. Mean ( $\mu$ ), standard deviation ( $\sigma$ ), skewness ( $\gamma$ ) and kurtosis ( $k$ ) are also reported in each of the plots in **Figure 3.13**. Although downburst events are a non-stationary and non-Gaussian process (De Gaetano et al., 2014), **Figure 3.13** confirms that the PDF of the reduced turbulence (equation 3.2)  $\tilde{u}'(t)$  is indeed Gaussian even for the properly produced downbursts in wind simulators. The same holds for the full scale downburst events (Burlando et al., 2017). Qualitatively, the PDFs of  $\tilde{u}'(t)$  of the experimentally produced downbursts in this study are similar to full scale downburst events recently reported by Solari et al., (2015) and Burlando et al., (2017).

Solari et al. (2015) demonstrated that gust factors for the synoptic (i.e., ABL) winds are significantly different from thunderstorms due to the non-stationarity of the latter. Similarly, the averaging periods for synoptic winds and downbursts cannot be the same due to the small duration of downbursts in comparison to the ABL winds. Gust factor for synoptic events is defined as the ratio between the peak wind speed ( $\hat{u}$ ) averaged over a short time interval ( $\tau$ ) and the mean wind speed averaged over 10 to 60 min (Davenport, 1961). For thunderstorm winds, Solari et al. (2015) defined three wind speed ratios that are of importance to structural loading and response in downburst winds, i.e.:

$$\hat{R} = \frac{u_{max}}{\hat{u}} \quad (3.5)$$

$$G_{max} = \frac{u_{max}}{\bar{u}_{max}} \quad (3.6)$$

$$\hat{G} = \frac{\hat{u}}{\bar{u}_{max}} \quad (3.7)$$

Here,  $u_{max}$  is the instantaneous maximum of the downburst wind speed,  $\hat{u}$  is the 1-s peak wind speed and  $\bar{u}_{max}$  is the maximum of the time varying mean. In order to calculate  $\hat{u}$  for the experimental data in this study, a simple method is used to infer the time scale between the experimental downbursts generated in the WinDEEE Dome and full scale downburst events.

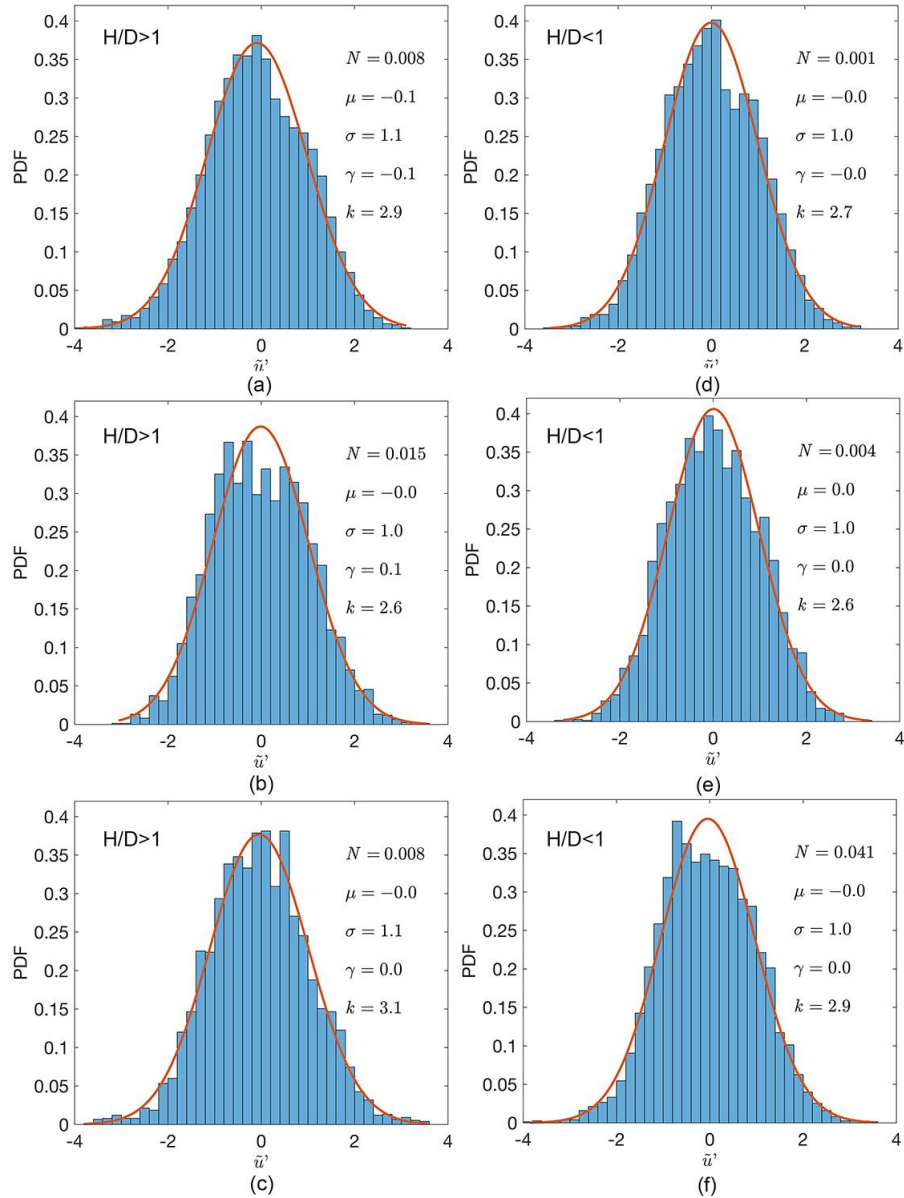


**Figure 3.13: PDF of the reduced turbulent fluctuations ( $T_{avg} = 0.1$  s) for Re (a)  $1.83 \times 10^6$ , (b)  $2.62 \times 10^6$ , (c)  $4.24 \times 10^6$ , (d)  $1.82 \times 10^6$ , (e)  $2.68 \times 10^6$  and (f)  $4.09 \times 10^6$ . Red line represents a Gaussian PDF.**

Here, the time scale is calculated from the ratio of  $T_{avg}$  between full scale and WindEEE downburst records. In literature, different  $T_{avg}$  values have been suggested for different full scale downburst events. Some of the values of  $T_{avg}$  for full scale events are: 17 s (Lombardo et al., 2014), 30 s (Solari et al., 2015; Burlando et al., 2017), 40 s (Holmes et



al., 2008), 60 s (Choi and Hidayat, 2002) and 120 s (Orwig and Schroeder, 2007). Given the chosen  $T_{avg}$  of 0.1 s for the simulated downbursts in the WindEEE Dome, a time scale range of 1:170 to 1:1200 can be inferred based on these full scale data  $T_{avg}$  values. Since the aforementioned wind ratios are going to be compared between the ratios reported in Solari et al. (2015) and the simulated downbursts in the WindEEE Dome, a time scale of 1:300 is found based on  $T_{avg} = 30$  s. This scale is further used to calculate the 1-s peak wind speed,  $\hat{u}$ , in Eq. (3.7). Table 3.5 shows the three wind speed ratios (equations 3.5 to 3.7) for each of the investigated cases as well as the ratios for full scale events reported in Solari et al. (2015). The wind speed ratios of the experimentally produced downbursts in this study match closely (<10% difference) with the full scale downburst events (Table 3.5). The observed similarity is of particular importance for the reliable estimates of wind actions of experimentally generated downbursts.

**Table 3.5: The values of  $\hat{R}$ ,  $G_{max}$ ,  $\hat{G}$  using  $T_{avg} = 0.1$  s for all  $Re$  cases in this study**

$Re$	$H/D$	$\hat{R}$	$G_{max}$	$\hat{G}$
$1.83 \times 10^6$	>1	1.03	1.14	1.10
$2.62 \times 10^6$	>1	1.00	1.18	1.17
$4.24 \times 10^6$	>1	1.01	1.17	1.16
$1.82 \times 10^6$	<1	1.03	1.09	1.06
$2.68 \times 10^6$	<1	1.01	1.13	1.11
$4.09 \times 10^6$	<1	1.04	1.25	1.21
Average		1.02	1.16	1.14
Average of 93 downburst records from Solari et al. (2015)		1.06	1.27	1.20

### 3.3.4 Vortex dynamics using Particle Image Velocimetry

Particle Image Velocimetry (PIV) measurements were performed with the goal to analyze the dynamics of the vortex structures of the experimentally simulated downbursts in a 2D ( $r, z$ ) plane. **Figure 3.14** shows the evolution and movement of the leading downburst annular vortex for the case of  $Re = 2.68 \times 10^6$  at the instances after the downdraft has impinged on the surface. As mentioned in the PIV setup description (Section 3.2.3), this setup includes six cameras that had to be combined in order to cover an area of 2.7 m (height)  $\times$  1.4 m (width). Images from six cameras were patched together in order to capture the domain depicted in **Figure 3.14**. The right-hand edge of the PIV domain was about 2.6 m away from the centre of the downburst. As the two jet diameters used ( $D$ ) were 4.5 m and 3.2 m, the region captured by PIV was always outside of the direct downdraft from the bell mouth. The bottom edge of the PIV window was at about 13.5 mm from the chamber floor. The distance from the floor was introduced in order to avoid laser reflections from the floor. Although the measurement window was 2.7 m  $\times$  1.4 m, an area of 0.5 m  $\times$  1.4 m towards the furthest end from the jet was discarded due to the low intensity of the laser, which ultimately resulted in bad data (i.e., bad vectors). The radial distance of  $R = 0$  is assigned at the downdraft centre on the chamber floor (also the turntable centre) and negative  $R$  is in the leftward direction from the downdraft centre (see **Figure 3.14**). Therefore in **Figure 3.14**, the downdraft jet is on the right and the flow is going from right to left.

**Figure 3.14** shows 4 instances of the vortex evolution in subplots (a)–(d). The time interval between the instances is 0.11 s as the sampling rate for the experiment was 9 Hz. The first instance in the figure (**Figure 3.14 a**) is approximately 2.8 seconds after the downburst was initiated. The time when the vortex enters the camera field of view is defined as initial instance time,  $T_{ii}$  and the instance when the primary vortex has passed the camera field of view is the ending instance time,  $T_{ei}$ . The value of  $T_{int}$  is defined as the time interval of the primary vortex passing the camera field of view, hence:  $T_{int} = T_{ei} - T_{ii}$ . Table 3.6 shows the values of  $T_{ii}$ ,  $T_{ei}$  and  $T_{int}$  for different  $Re$ . As expected, with the increase of  $Re$ , the value of  $T_{int}$  decreases as the vortex moves faster across the camera frames at the higher  $Re$ . Lundgren et al. (1992) and Alahyari and Longmire (1994) noted that the maximum

velocity in a downburst outflow is approximately five times higher than the propagation speed of the vortex core. Table 6 shows the convective speed of the vortex core,  $u_{co}$ , and the ratio between the maximum radial velocity in the flow field  $\bar{u}_{max}$  for different  $Re$ . We observe that the ratio  $\bar{u}_{max}/u_{co}$  for all  $Re$  cases investigated in this study resulted in the values in the range between 4.0 and 6.4 which is somewhat in agreement with the observation of Lundgren et al. (1992).

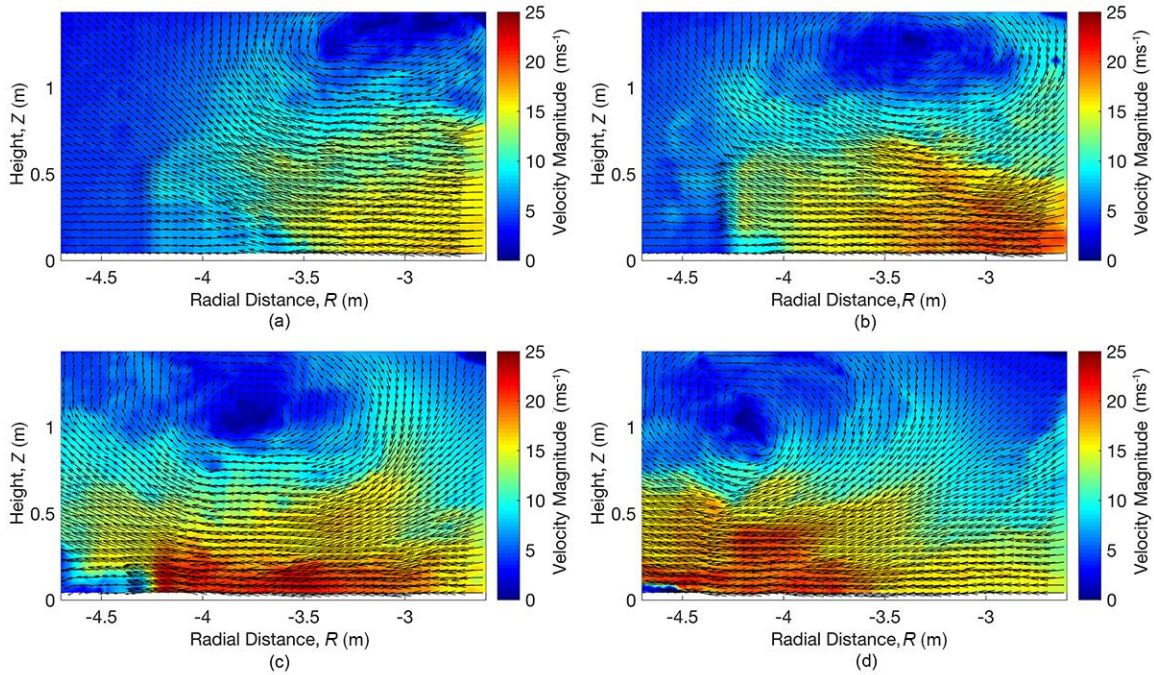


**Figure 3.14: PIV vectors and velocity magnitude contours for  $H/D < 1$  and  $Re = 2.68 \times 10^6$  at different time instances. Time interval between two consecutive instances is 0.11s.**

**Table 3.6: The values of  $T_{ii}$ ,  $T_{ei}$  and  $T_{int}$  observed at for different values of  $Re$**

$Re$	$1.82 \times 10^6$	$1.83 \times 10^6$	$2.62 \times 10^6$	$2.68 \times 10^6$	$4.09 \times 10^6$	$4.24 \times 10^6$
$H/D$	>1	>1	>1	<1	<1	<1
$T_{ii}$ (s)	2.75	2.09	2.09	1.87	0.99	1.87
$T_{ei}$ (s)	3.33	2.88	2.64	2.42	1.32	2.20

$T_{int}(s)$	0.58	0.77	0.55	0.55	0.33	0.33
$u_{co}(m/s)$	2.06	2.85	4	3.63	6.66	6.66
$\bar{u}_{max}/u_{co}$	4.86	5.2	6.4	4	4	5.38

As soon as the downdraft hits the ground, the primary annular vortex that was initially generated due to the Kelvin-Helmholtz instability at the bell mouth level changes its propagation velocity from the initial vertical descent to a radial movement. The primary vortex is intensified and stretched as it spreads along the ground surface (Yao and Lundgren, 1996). In the present PIV experiment, the evolution a fully formed primary vortex is clearly visible in **Figure 3.15**. This figure shows the fully formed primary vortex and the location of the maximum velocity in comparison to the centre of the vortex that was previously portrayed in **Figure 3.14**. Analyzing a large set of downburst data from the JAWS field campaign, Hjelmfelt (1988) demonstrated that the maximum velocity in a downburst occurs near the ground as well as underneath and slightly after the centre of the vortex in the radial flow direction (see **Figure 3.15 c**). The location of the centre of the vortex and the maximum velocity for the investigated downbursts in this paper are marked in **Figure 3.15 a,b**. The location of the maximum velocity relative to the primary vortex centre in the experimentally simulated downburst at WindEEE is comparable with full scale events reported in Hjelmfelt (1988).

Streamlines resulting from the PIV measurements are depicted in **Figure 16**. The dominant feature in the figure are the primary vortex structure and its radial movement across the PIV field of view. The primary vortex centre entered the PIV field of view at the time  $T_{ii} = 1.87$  s and afterwards it continued developing and advancing radially. Densely packed streamlines are observed between the vortex core and the ground. This funneling-like effect results in flow speedups underneath the vortex. A small region of recirculation, forming below and in front of the main annular vortex, is visible in **Figure 3.16 c**. This dynamic region of separation and reattachment moves radially with the convection of the main vortex. At approximate  $R/D = 0.9$  (**Figure 3.16 d**), the primary vortex is at its peak



**schematic of the downburst flow field and the location of the maximum velocity obtained using the full scale data from the JAWS campaign (Hjelmfelt, 1988)**

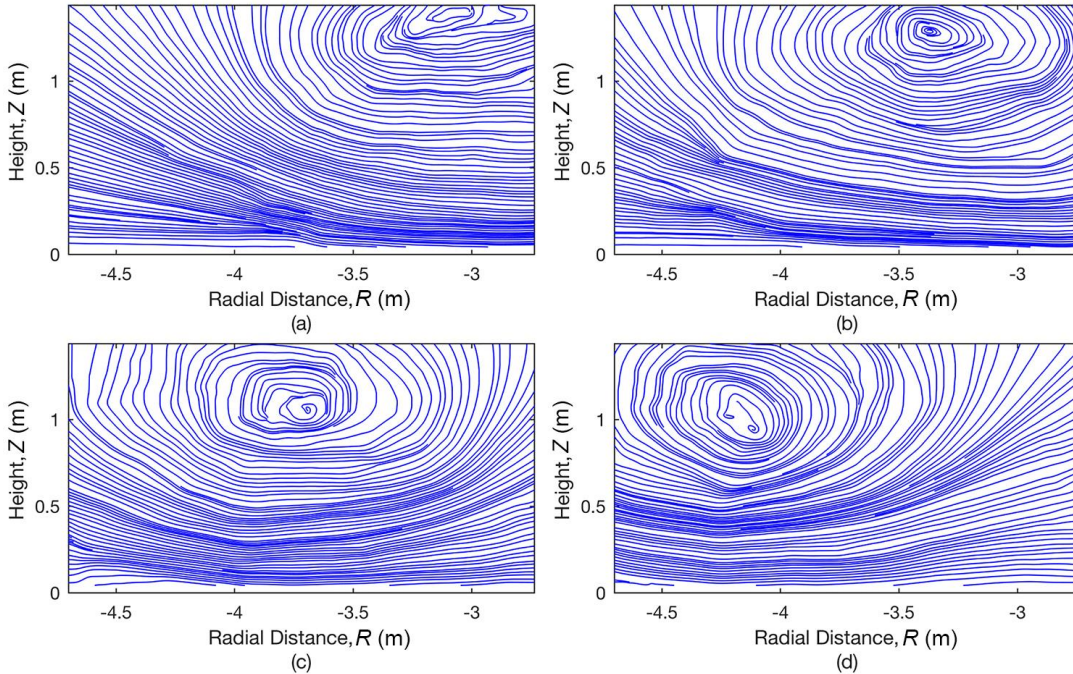


**Figure 3.16: Streamline plots showing the primary vortex at different instances for  $H/D < 1$  and  $Re = 2.68 \times 10^6$**

A second vortex, which is also due to the initial Kelvin-Helmholtz instability that develops earlier in the descent phase of the downburst (Kim and Hangan, 2007), has been observed after the passage of the primary vortex (**Figure 3.17**). However, the second vortex is smaller and less organized when compared to the primary vortex. This is because the primary vortex formed at the initial opening of the bell-mouth louvers benefits from maximum initial shear. The interval between each of the four consecutive time instances in **Figure 3.17** a–d is 0.11 s.

The convective velocity of the primary vortex core in the full scale downburst events that were observed on June 16 and 17, 1978 by are found to be 9.7 and 1.47 m s<sup>-1</sup> respectively. On the other hand, the convective velocity of the primary vortex core for the experimentally simulated downbursts in the WindEEE Dome are in the range from 2.06 to 6.66 m s<sup>-1</sup> (Table 3.6) based on the scales detailed above.

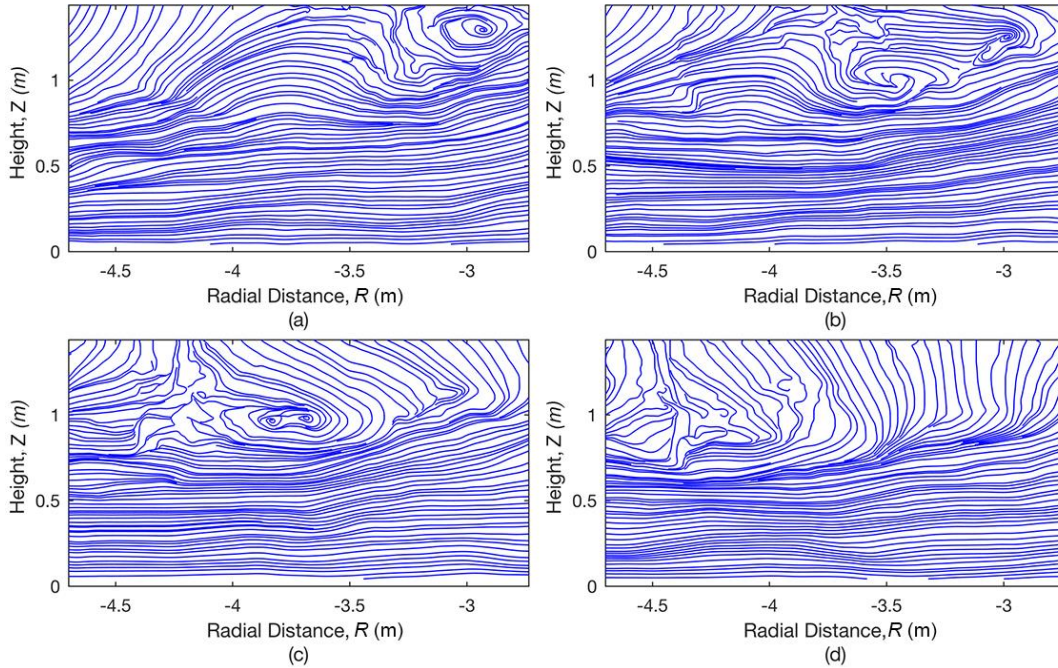


**Figure 3.17: Streamlines showing the second vortex after passing of the primary vortex for  $H/D < 1$  and  $Re = 2.68 \times 10^6$**

The height of the vortex core is another important parameter for accurately assessing downburst wind actions on ground mounted structures since the maximum wind speed in a downburst event occurs below this height (Fujita, 1990; Alahyari and Longmire, 1994). **Figure 3.18** shows the trajectory of the vortex centre for all  $Re$  cases for the vortex advancing from right to left. Overall, the vortex centre firstly tends to move down to the position of a minimum height and only afterwards it moves upward creating an arch-like trajectory. For  $H/D < 1$  and for the lower values of  $Re$  (i.e.,  $1.82 \times 10^6$ ,  $2.68 \times 10^6$ ), the centre of the primary vortex enters into the PIV field of view at the higher elevations than in the cases when  $H/D > 1$ . This tendency could be due to the difference in vortex structure for different  $H/D$  ratios (Xu and Hangan, 2008).

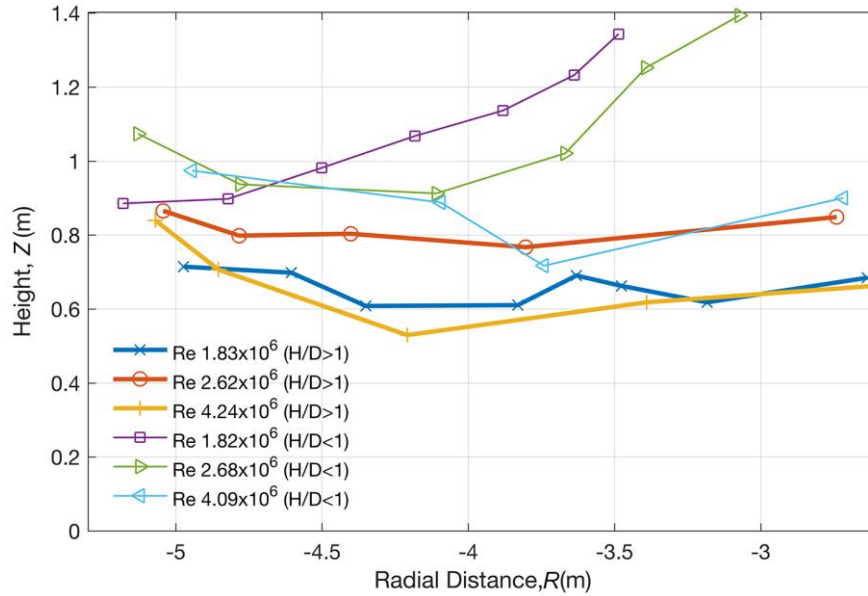


**Figure 3.18: Trajectory of the vortex centre for different values of  $Re$ .**

The heights of the vortex centre for all six  $Re$  cases are compared in **Figure 3.19** with two full scale downburst records obtained from a Doppler radar and reported in Wakimoto (1982). A proper length scale of the WindEEE Dome downbursts is simply calculated based on the previously adopted time and velocity scales. Namely, the proper velocity scale is calculated by comparing  $\bar{u}_{max}$  between the experimentally simulated downbursts in this study and full scale events in Wakimoto (1982). This comparison resulted in velocity scales ranging from 1:0.4 to 1:2.6. Therefore, with the adopted time scale of 1:600 (see Section 3.3.3), the length scales range from 1:230 to 1:1500. Radial distance of the vortex centre from downburst centre for the full scale events could not be calculated due to the spatiotemporal limitations of full scale measurements. **Figure 3.19** indicates that both real events considered in this paper have the heights of the vortex centres within the range of the vortex centre heights from the experimentally simulated downbursts. **Figure 3.20** compares the normalized vortex trajectories between full scale and experimentally simulated downbursts. Here, the heights of the vortex centre is normalized with the minimum height in the trajectory ( $Z_{cm}$ ) and the radial distances are normalized with the radial distance at  $Z_{cm}$  (i.e.,  $R_{cm}$ ). Overall, a similar trend is observed between the full scale event on 17 June, 1978 and the experimentally simulated downburst in this study. These



simple comparisons of the vortex trajectory and their heights between full scale and experimental data are the first efforts in this direction and add credibility to the simulations.

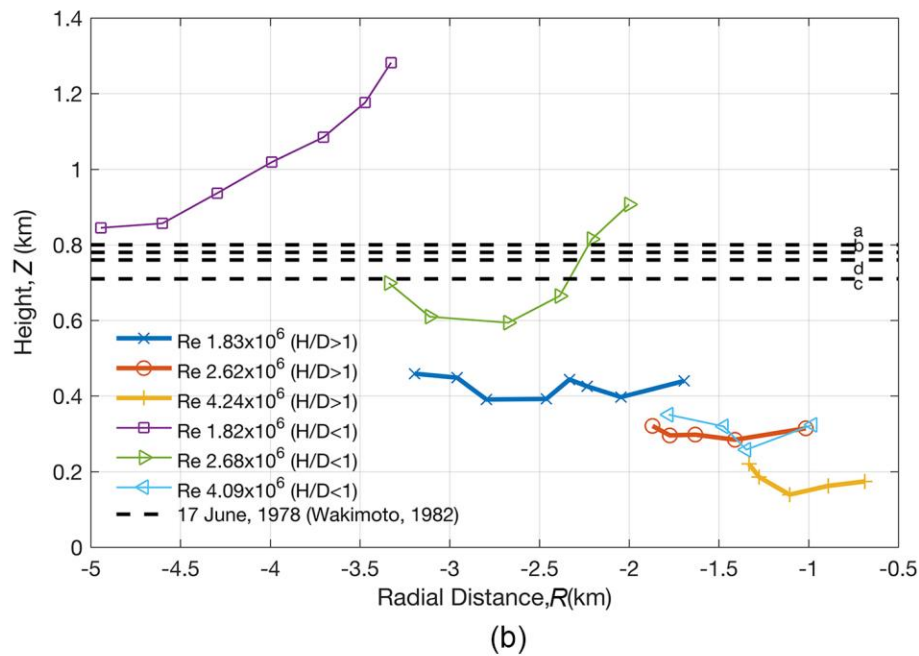
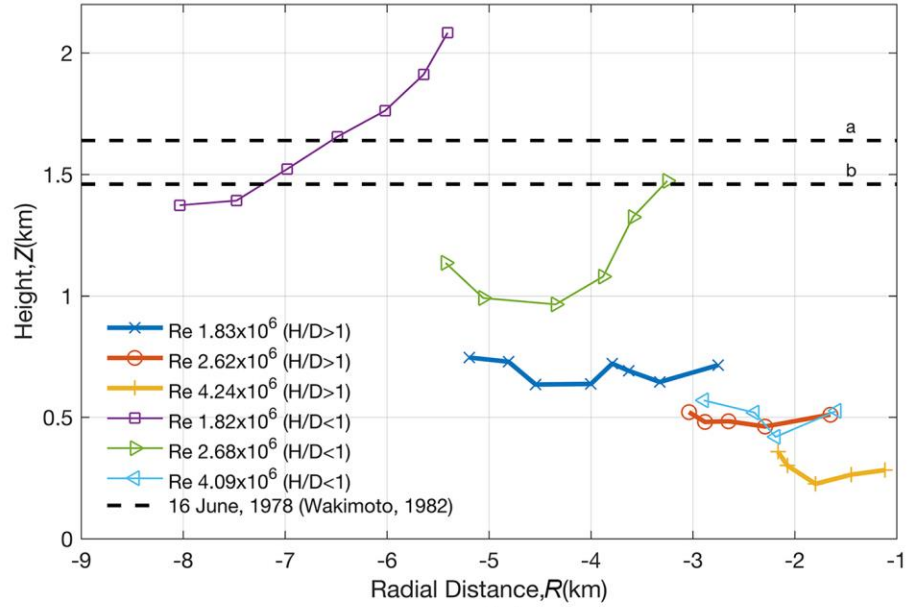


**Figure 3.19: Comparison of vortex centre heights from the WindEEE Dome downbursts and full scale events on (a) 16 June 1978 (b) 17 June 1978 (Wakimoto, 1982)**

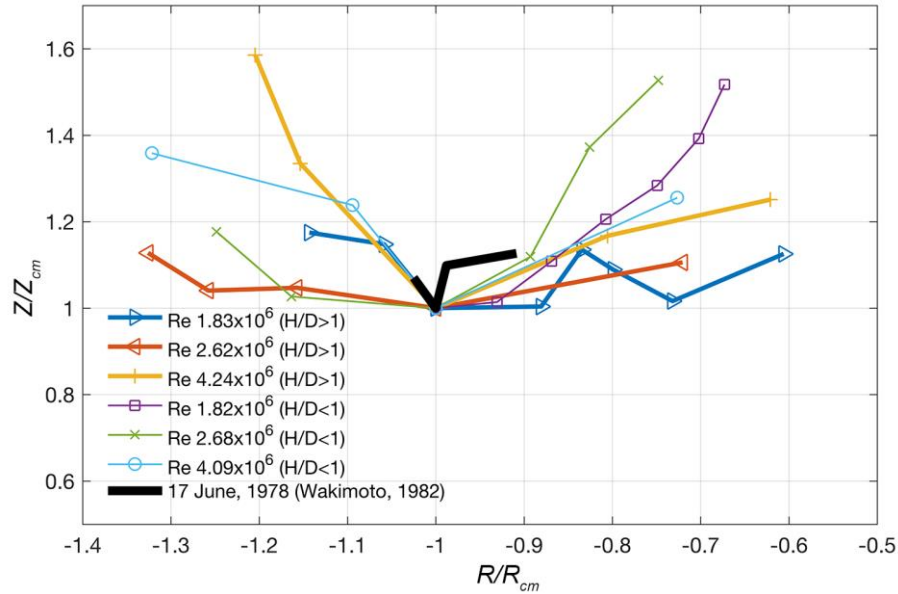


**Figure 3.20: Normalized vortex trajectories from the WindEEE Dome downbursts compared with full scale event on 17 June, 1978 (Wakimoto, 1982)**

### 3.4 Summary and Conclusions

This study investigates the mean and the turbulent features of the experimentally produced downbursts with respect to height-to-diameter ( $H/D$ ) ratios and Reynolds numbers ( $Re$ ). Point velocity measurements with high temporal resolution are obtained using Cobra probes for  $H/D = 1.2$  and  $H/D = 0.8$ , as well as for a range of the values of  $Re$  (between  $Re = 1.82 \times 10^6$  and  $Re = 4.24 \times 10^6$ ). In addition, 2D planar velocity measurements using large-scale particle image velocimetry (PIV) technique were conducted. Wind velocity data were decomposed into the transient mean and transient turbulence components based on the criteria set by Holmes et al. (2008) and Solari et al. (2015), among others. A wide range of proper values for the moving average times ( $T_{avg}$ )—from 0.01 to 0.3 s—was investigated with respect to several criteria: (1) characteristics of running mean and residual fluctuations, (2) joint Fourier transforms of running mean and residual fluctuations, and (3) mean, standard deviation, skewness and kurtosis of reduced turbulent

fluctuations. Based on this analysis,  $T_{avg} = 0.1$  s was deemed to be the proper averaging time for the simulated downbursts in the WindEEE Dome.

Profiles of time varying means of radial velocities with height are calculated for different values of  $Re$  and normalized profiles are compared against previously published full scale data. At similar Reynolds number, the profiles corresponding to  $H/D > 1$  have a more pronounced “nose” shape when compared to the ones for  $H/D < 1$ . Overall, the profiles corresponding to the case of  $H/D > 1$ , especially at lower  $Re$  ( $1.82 \times 10^6$  to  $2.68 \times 10^6$ ) show better comparison with the existing full scale data.

This study analyzes the turbulence characteristics of laboratory simulated downbursts similarly with full scale downburst data analysis (Solari et al., 2015). Probability distribution function of the reduced turbulent fluctuations for all cases matches reasonably well with Gaussian distribution. The similar matching is observed in the full scale downburst events. Spectra of the reduced turbulent fluctuations for the experimentally simulated downbursts has a  $-5/3$  slope in the inertial subrange, in particular for  $Re \geq 2.62 \times 10^6$ . Spectra of the reduced turbulent fluctuation is also matched with the analytical model proposed by Solari and Piccardo (2001) and good agreement is found for all cases except for  $H/D < 1$  with  $Re = 1.82 \times 10^6$ . In the simulated downbursts in this study, the wind speed ratios that are of importance for the proper assessment of thunderstorm wind actions on buildings, as defined in Solari et al. (2015), are found to be within 10% of their average values of the 93 real downburst records reported in Solari et al. (2015).

Lastly, the vortex dynamics obtained from the PIV measurements for the experimentally simulated downbursts in the WindEEE Dome is compared with the available full scale data. For the first time, the relative location of the primary vortex centre with respect to the maximum radial velocity, convective velocity of the primary vortex, heights and trajectory of the primary vortex centre are compared between laboratory simulated downbursts and full scale downburst records, and promising agreement is found.

### 3.5 Acknowledgements

This research has been made possible through funding from Natural Sciences and Engineering Research Council of Canada (NSERC) Discovery Grant and Canada Foundation of Innovation (CFI) WindEEE Dome Grant.

### 3.6 References

- Aboshosha, H., Bitsuamlak, G., El Damatty, A., 2015. Turbulence characterization of downbursts using LES. *Journal of Wind Engineering and Industrial Aerodynamics* 136, 44–61. <https://doi.org/10.1016/j.jweia.2014.10.020>
- Alahyari, A., Longmire, E.K., 1994. Particle image velocimetry in a variable density flow: application to a dynamically evolving microburst. *Experiments in Fluids* 17, 434–440. <https://doi.org/10.1007/BF01877047>
- Anderson, J.R., Orf, L.G., Straka, J.M., 1992. A 3-D model system for simulating thunderstorm microburst outflows. *Meteorol. Atmos. Phys.* 49, 125–131. <https://doi.org/10.1007/BF01025404>
- Burlando, M., Romanić, D., Solari, G., Hangan, H., Zhang, S., 2017. Field Data Analysis and Weather Scenario of a Downburst Event in Livorno, Italy, on 1 October 2012. *Monthly Weather Review* 145, 3507–3527. <https://doi.org/10.1175/MWR-D-17-0018.1>
- Byers, H.R., Braham, R.R., 1948. Thunderstorm structure and circulation. *J. Meteor.* 5, 71–86. [https://doi.org/10.1175/1520-0469\(1948\)005<0071:TSAC>2.0.CO;2](https://doi.org/10.1175/1520-0469(1948)005<0071:TSAC>2.0.CO;2)
- Chay, M.T., Albermani, F., Wilson, R., 2006. Numerical and analytical simulation of downburst wind loads. *Engineering Structures* 28, 240–254. <https://doi.org/10.1016/j.engstruct.2005.07.007>
- Chay, M.T., Letchford, C.W., 2002. Pressure distributions on a cube in a simulated thunderstorm downburst—Part A: stationary downburst observations. *Journal of Wind Engineering and Industrial Aerodynamics* 90, 711–732. [https://doi.org/10.1016/S0167-6105\(02\)00158-7](https://doi.org/10.1016/S0167-6105(02)00158-7)
- Chen, L., Letchford, C.W., 2004. A deterministic–stochastic hybrid model of downbursts and its impact on a cantilevered structure. *Engineering Structures* 26, 619–629. <https://doi.org/10.1016/j.engstruct.2003.12.009>
- Choi, E.C., Hidayat, F.A., 2002. Dynamic response of structures to thunderstorm winds. *Progress in Structural Engineering and Materials* 4, 408–416. <https://doi.org/10.1002/pse.132>

- Choi, E.C.C., Hidayat, F.A., 2002. Gust factors for thunderstorm and non-thunderstorm winds. *Journal of Wind Engineering and Industrial Aerodynamics*, Fifth Asia-Pacific Conference on Wind Engineering 90, 1683–1696. [https://doi.org/10.1016/S0167-6105\(02\)00279-9](https://doi.org/10.1016/S0167-6105(02)00279-9)
- Comon, P., 1994. Independent component analysis, A new concept? *Signal Processing, Higher Order Statistics* 36, 287–314. [https://doi.org/10.1016/0165-1684\(94\)90029-9](https://doi.org/10.1016/0165-1684(94)90029-9)
- Cook, N.J., Ian Harris, R., Whiting, R., 2003. Extreme wind speeds in mixed climates revisited. *Journal of Wind Engineering and Industrial Aerodynamics* 91, 403–422. [https://doi.org/10.1016/S0167-6105\(02\)00397-5](https://doi.org/10.1016/S0167-6105(02)00397-5)
- Cowen, E.A., Monismith, S.G., 1997. A hybrid digital particle tracking velocimetry technique. *Experiments in Fluids* 22, 199–211. <https://doi.org/10.1007/s003480050038>
- Davenport, A.G., 1961. The Application of Statistical Concepts to the Wind loading of Structures. *Proceedings of the Institution of Civil Engineers* 19, 449–472. <https://doi.org/10.1680/iicep.1961.11304>
- De Gaetano, P., Repetto, M.P., Repetto, T., Solari, G., 2014. Separation and classification of extreme wind events from anemometric records. *Journal of Wind Engineering and Industrial Aerodynamics* 126, 132–143. <https://doi.org/10.1016/j.jweia.2014.01.006>
- Fujita, 1978. Manual of downburst identification for Project NIMROD. SMRP Res. Paper, 156 104.
- Fujita, T., 1990. Downbursts: meteorological features and wind field characteristics. *Journal of Wind Engineering and Industrial Aerodynamics*, The Sixth U.S. National Conference on Wind Engineering 36, 75–86. [https://doi.org/10.1016/0167-6105\(90\)90294-M](https://doi.org/10.1016/0167-6105(90)90294-M)
- Fujita, T.T., 1985. *The Downburst: Microburst and MacRoburst*. University of Chicago.
- Fujita, T.T., 1974. Jumbo Tornado Outbreak of 3 April 1974. *Weatherwise* 27, 116–126. <https://doi.org/10.1080/00431672.1974.9931693>
- Fujita, T.T., Byers, H.R., 1977. Spearhead Echo and Downburst in the Crash of an Airliner. *Mon. Wea. Rev.* 105, 129–146. [https://doi.org/10.1175/1520-0493\(1977\)105<0129:SEADIT>2.0.CO;2](https://doi.org/10.1175/1520-0493(1977)105<0129:SEADIT>2.0.CO;2)
- Fujita, T.T., Wakimoto, R.M., 1981. Five Scales of Airflow Associated with a Series of Downbursts on 16 July 1980. *Mon. Wea. Rev.* 109, 1438–1456. [https://doi.org/10.1175/1520-0493\(1981\)109<1438:FSOAAW>2.0.CO;2](https://doi.org/10.1175/1520-0493(1981)109<1438:FSOAAW>2.0.CO;2)

- Gomes, L., Vickery, B.J., 1978. Extreme wind speeds in mixed wind climates. *Journal of Wind Engineering and Industrial Aerodynamics* 2, 331–344. [https://doi.org/10.1016/0167-6105\(78\)90018-1](https://doi.org/10.1016/0167-6105(78)90018-1)
- Gunter, W.S., Schroeder, J.L., 2015. High-resolution full-scale measurements of thunderstorm outflow winds. *Journal of Wind Engineering and Industrial Aerodynamics* 138, 13–26. <https://doi.org/10.1016/j.jweia.2014.12.005>
- Haines, M., Taylor, I., 2018. Numerical investigation of the flow field around low rise buildings due to a downburst event using large eddy simulation. *Journal of Wind Engineering and Industrial Aerodynamics* 172, 12–30. <https://doi.org/10.1016/j.jweia.2017.10.028>
- Hangan, H., Refan, M., Jubayer, C., Parvu, D., Kilpatrick, R., 2017a. Big Data from Big Experiments. The WindEEE Dome, in: *Whither Turbulence and Big Data in the 21st Century?* Springer, Cham, pp. 215–230. [https://doi.org/10.1007/978-3-319-41217-7\\_12](https://doi.org/10.1007/978-3-319-41217-7_12)
- Hangan, H., Refan, M., Jubayer, C., Romanic, D., Parvu, D., LoTufo, J., Costache, A., 2017b. Novel techniques in wind engineering. *Journal of Wind Engineering and Industrial Aerodynamics* 171, 12–33. <https://doi.org/10.1016/j.jweia.2017.09.010>
- Hangan, Kim J.-D., Xu Z., n.d. *The Simulation of Downbursts and its Challenges*. (2004), Proceedings. [https://doi.org/10.1061/40700\(2004\)170](https://doi.org/10.1061/40700(2004)170)
- Hjelmfelt, M.R., 1988. Structure and Life Cycle of Microburst Outflows Observed in Colorado. *J. Appl. Meteor.* 27, 900–927. [https://doi.org/10.1175/1520-0450\(1988\)027<0900:SALCOM>2.0.CO;2](https://doi.org/10.1175/1520-0450(1988)027<0900:SALCOM>2.0.CO;2)
- Holmes, J. d., 2002. A Re-analysis of Recorded Extreme Wind Speeds in Region A. *Australian Journal of Structural Engineering* 4, 29–40. <https://doi.org/10.1080/13287982.2002.11464905>
- Holmes, J.D., Hangan, H.M., Schroeder, J.L., Letchford, C.W., Orwig, K.D., 2008. A forensic study of the Lubbock-Reese downdraft of 2002. *Wind and Structures* 11, 137–152. <https://doi.org/10.12989/was.2008.11.2.137>
- Holmes, J.D., Oliver, S.E., 2000. An empirical model of a downburst. *Engineering Structures* 22, 1167–1172. [https://doi.org/10.1016/S0141-0296\(99\)00058-9](https://doi.org/10.1016/S0141-0296(99)00058-9)
- Järvi, L., Punkka, A.-J., Schultz, D.M., Petäjä, T., Hohti, H., Rinne, J., Pohja, T., Kulmala, M., Hari, P., Vesala, T., 2007. Micrometeorological observations of a microburst in southern Finland, in: *Atmospheric Boundary Layers*. Springer, New York, NY, pp. 187–203. [https://doi.org/10.1007/978-0-387-74321-9\\_13](https://doi.org/10.1007/978-0-387-74321-9_13)
- Jesson, M., Haines, M., Singh, N., Sterling, M., Taylor, I., 2013. Numerical and Physical Simulation of a Thunderstorm Downburst. Research Publishing Services, pp. 1139–1148. [https://doi.org/10.3850/978-981-07-8012-8\\_P3](https://doi.org/10.3850/978-981-07-8012-8_P3)

- Jesson, M., Sterling, M., 2018. A simple vortex model of a thunderstorm downburst – A parametric evaluation. *Journal of Wind Engineering and Industrial Aerodynamics* 174, 1–9. <https://doi.org/10.1016/j.jweia.2017.12.001>
- Jubayer, C., Elatar, A., Hangan, H., 2016. Pressure distributions on a low-rise building in a laboratory simulated downburst, 8th International Colloquium on Bluff Body Aerodynamics and Applications. Presented at the 8th International Colloquium on Bluff Body Aerodynamics and Applications, Boston, Massachusetts, USA.
- Killick, R., Fearnhead, P., Eckley, I.A., 2012. Optimal Detection of Changepoints With a Linear Computational Cost. *Journal of the American Statistical Association* 107, 1590–1598. <https://doi.org/10.1080/01621459.2012.737745>
- Kim, J., Hangan, H., 2007. Numerical simulations of impinging jets with application to downbursts. *Journal of Wind Engineering and Industrial Aerodynamics* 95, 279–298. <https://doi.org/10.1016/j.jweia.2006.07.002>
- Landreth, C.C., Adrian, R.J., 1990. Impingement of a low Reynolds number turbulent circular jet onto a flat plate at normal incidence. *Experiments in Fluids* 9, 74–84. <https://doi.org/10.1007/BF00575338>
- Lavielle, M., 2005. Using penalized contrasts for the change-point problem. *Signal Processing* 85, 1501–1510. <https://doi.org/10.1016/j.sigpro.2005.01.012>
- Letchford, C.W., Chay, M.T., 2002. Pressure distributions on a cube in a simulated thunderstorm downburst. Part B: moving downburst observations. *Journal of Wind Engineering and Industrial Aerodynamics* 90, 733–753. [https://doi.org/10.1016/S0167-6105\(02\)00163-0](https://doi.org/10.1016/S0167-6105(02)00163-0)
- Letchford, C.W., Mans, C., Chay, M.T., 2002. Thunderstorms—their importance in wind engineering (a case for the next generation wind tunnel). *Journal of Wind Engineering and Industrial Aerodynamics, Fifth Asia-Pacific Conference on Wind Engineering* 90, 1415–1433. [https://doi.org/10.1016/S0167-6105\(02\)00262-3](https://doi.org/10.1016/S0167-6105(02)00262-3)
- Li, C., Li, Q.S., Xiao, Y.Q., Ou, J.P., 2012. A revised empirical model and CFD simulations for 3D axisymmetric steady-state flows of downbursts and impinging jets. *Journal of Wind Engineering and Industrial Aerodynamics* 102, 48–60. <https://doi.org/10.1016/j.jweia.2011.12.004>
- Lin, W.E., Orf, L.G., Savory, E., Novacco, C., 2007. Proposed large-scale modelling of the transient features of a downburst outflow. *Wind and Structures* 10, 315–346. <https://doi.org/10.12989/was.2007.10.4.315>
- Lin, W.E., Savory, E., 2010. Physical modelling of a downdraft outflow with a slot jet. *Wind and Structures* 13, 385–412. <https://doi.org/10.12989/was.2010.13.5.385>

- Lin, W.E., Savory, E., 2006. Large-scale quasi-steady modelling of a downburst outflow using a slot jet. *Wind and Structures* 9, 419–440. <https://doi.org/10.12989/was.2006.9.6.419>
- Lombardo, F.T., Smith, D.A., Schroeder, J.L., Mehta, K.C., 2014. Thunderstorm characteristics of importance to wind engineering. *Journal of Wind Engineering and Industrial Aerodynamics* 125, 121–132. <https://doi.org/10.1016/j.jweia.2013.12.004>
- Lundgren, T.S., Yao, J., Mansour, N.N., 1992. Microburst modelling and scaling. *Journal of Fluid Mechanics* 239, 461–488. <https://doi.org/10.1017/S002211209200449X>
- Mason, M.S., Letchford, C.W., James, D.L., 2005. Pulsed wall jet simulation of a stationary thunderstorm downburst, Part A: Physical structure and flow field characterization. *Journal of Wind Engineering and Industrial Aerodynamics* 93, 557–580. <https://doi.org/10.1016/j.jweia.2005.05.006>
- Mason, M.S., Wood, G.S., Fletcher, D.F., 2009. Numerical simulation of downburst winds. *Journal of Wind Engineering and Industrial Aerodynamics* 97, 523–539. <https://doi.org/10.1016/j.jweia.2009.07.010>
- McConville, A.C., Sterling, M., Baker, C.J., 2009. The physical simulation of thunderstorm downbursts using an impinging jet. *Wind and Structures An International Journal* 12, 133–149. <https://doi.org/10.12989/was.2009.12.2.133>
- McCullough, M., Kwon, D.K., Kareem, A., Wang, L., 2014. Efficacy of Averaging Interval for Nonstationary Winds. *Journal of Engineering Mechanics* 140, 1–19. [https://doi.org/10.1061/\(ASCE\)EM.1943-7889.0000641](https://doi.org/10.1061/(ASCE)EM.1943-7889.0000641)
- Oreskovic, C., Orf, L.G., Savory, E., 2018. A parametric study of downbursts using a full-scale cooling source model. *Journal of Wind Engineering and Industrial Aerodynamics* 180, 168–181. <https://doi.org/10.1016/j.jweia.2018.07.020>
- Orf, L.G., Oreskovic, C., Savory, E., Kantor, E., 2014. Circumferential analysis of a simulated three-dimensional downburst-producing thunderstorm outflow. *Journal of Wind Engineering and Industrial Aerodynamics* 135, 182–190. <https://doi.org/10.1016/j.jweia.2014.07.004>
- Orwig, K.D., Schroeder, J.L., 2007. Near-surface wind characteristics of extreme thunderstorm outflows. *Journal of Wind Engineering and Industrial Aerodynamics* 95, 565–584. <https://doi.org/10.1016/j.jweia.2006.12.002>
- Panneer Selvam, R., Holmes, J.D., 1992. Numerical simulation of thunderstorm downdrafts. *Journal of Wind Engineering and Industrial Aerodynamics, Special Issue 8th International Conference on Wind Engineering 1991* 44, 2817–2825. [https://doi.org/10.1016/0167-6105\(92\)90076-M](https://doi.org/10.1016/0167-6105(92)90076-M)



- Prasad, A.K., Adrian, R.J., Landreth, C.C., Offutt, P.W., 1992. Effect of resolution on the speed and accuracy of particle image velocimetry interrogation. *Experiments in Fluids* 13, 105–116. <https://doi.org/10.1007/BF00218156>
- Proctor, F.H., 1988. Numerical Simulations of an Isolated Microburst. Part I: Dynamics and Structure. *J. Atmos. Sci.* 45, 3137–3160. [https://doi.org/10.1175/1520-0469\(1988\)045<3137:NSOAIM>2.0.CO;2](https://doi.org/10.1175/1520-0469(1988)045<3137:NSOAIM>2.0.CO;2)
- Refan, M., Hangan, H., 2018. Near surface experimental exploration of tornado vortices. *Journal of Wind Engineering and Industrial Aerodynamics* 175, 120–135. <https://doi.org/10.1016/j.jweia.2018.01.042>
- Repetto, M.P., Burlando, M., Solari, G., De Gaetano, P., Pizzo, M., 2017. Integrated tools for improving the resilience of seaports under extreme wind events. *Sustainable Cities and Society* 32, 277–294. <https://doi.org/10.1016/j.scs.2017.03.022>
- Repetto, M.P., Burlando, M., Solari, G., De Gaetano, P., Pizzo, M., Tizzi, M., 2018. A web-based GIS platform for the safe management and risk assessment of complex structural and infrastructural systems exposed to wind. *Advances in Engineering Software, Special Section - CIVIL-COMP 2017* 117, 29–45. <https://doi.org/10.1016/j.advengsoft.2017.03.002>
- Romanic, D., LoTufo, J., Hangan, H., 2018. Transient behavior in impinging jets in crossflow with application to downburst flows - ScienceDirect [WWW Document]. URL <https://www.sciencedirect.com.proxy1.lib.uwo.ca/science/article/pii/S0167610518303854?dgcid=author> (accessed 12.6.18).
- Sarkar, P.P., Haan, J.F.L., Balaramudu Vasanth, Sengupta Anindya, 2006. Laboratory Simulation of Tornado and Microburst to Assess Wind Loads on Buildings. Structures Congress 2006. [https://doi.org/10.1061/40889\(201\)11](https://doi.org/10.1061/40889(201)11)
- Schultz, T.A., 1990. Multiple vortex ring model of the DFW microburst. *Journal of Aircraft* 27, 163–168. <https://doi.org/10.2514/3.45913>
- Sengupta, A., Haan, F.L., Sarkar, P.P., Balaramudu, V., 2008. Transient loads on buildings in microburst and tornado winds. *Journal of Wind Engineering and Industrial Aerodynamics, 4th International Symposium on Computational Wind Engineering (CWE2006)* 96, 2173–2187. <https://doi.org/10.1016/j.jweia.2008.02.050>
- Sengupta, A., Sarkar, P.P., 2008. Experimental measurement and numerical simulation of an impinging jet with application to thunderstorm microburst winds. *Journal of Wind Engineering and Industrial Aerodynamics* 96, 345–365. <https://doi.org/10.1016/j.jweia.2007.09.001>
- Sherman, D.J., 1987. The Passage of a Weak Thunderstorm Downburst over an Instrumented Tower. *Mon. Wea. Rev.* 115, 1193–1205. [https://doi.org/10.1175/1520-0493\(1987\)115<1193:TPOAWT>2.0.CO;2](https://doi.org/10.1175/1520-0493(1987)115<1193:TPOAWT>2.0.CO;2)

- Solari, G., Burlando, M., De Gaetano, P., Repetto, M.P., 2015. Characteristics of thunderstorms relevant to the wind loading of structures. *Wind and Structures* 20, 763–791. <https://doi.org/10.12989/was.2015.20.6.763>
- Solari, G., Piccardo, G., 2001. Probabilistic 3-D turbulence modeling for gust buffeting of structures. *Probabilistic Engineering Mechanics* 16, 73–86. [https://doi.org/10.1016/S0266-8920\(00\)00010-2](https://doi.org/10.1016/S0266-8920(00)00010-2)
- Solari, G., Repetto, M.P., Burlando, M., De Gaetano, P., Pizzo, M., Tizzi, M., Parodi, M., 2012. The wind forecast for safety management of port areas. *Journal of Wind Engineering and Industrial Aerodynamics*, 13th International Conference on Wind Engineering 104–106, 266–277. <https://doi.org/10.1016/j.jweia.2012.03.029>
- Srivastava, R.C., 1985. A Simple Model of Evaporatively Driven Downdraft: Application to Microburst Downdraft [WWW Document]. [http://dx.doi.org/10.1175/1520-0469\(1985\)042<1004:ASMOED>2.0.CO;2](http://dx.doi.org/10.1175/1520-0469(1985)042<1004:ASMOED>2.0.CO;2). URL [https://journals.ametsoc.org/doi/abs/10.1175/1520-0469\(1985\)042%3C1004:ASMOED%3E2.0.CO%3B2](https://journals.ametsoc.org/doi/abs/10.1175/1520-0469(1985)042%3C1004:ASMOED%3E2.0.CO%3B2) (accessed 8.6.18).
- Srivastava, R.C., Srivastava, R.C., 1987. A Model of Intense Downdrafts Driven by the Melting and Evaporation of Precipitation [WWW Document]. [http://dx.doi.org/10.1175/1520-0469\(1987\)044<1752:AMOIDD>2.0.CO;2](http://dx.doi.org/10.1175/1520-0469(1987)044<1752:AMOIDD>2.0.CO;2). URL [https://journals.ametsoc.org/doi/abs/10.1175/1520-0469\(1987\)044%3C1752:AMOIDD%3E2.0.CO;2](https://journals.ametsoc.org/doi/abs/10.1175/1520-0469(1987)044%3C1752:AMOIDD%3E2.0.CO;2) (accessed 8.6.18).
- Vermeire, B.C., Orf, L.G., Savory, E., 2011. Improved modelling of downburst outflows for wind engineering applications using a cooling source approach. *Journal of Wind Engineering and Industrial Aerodynamics* 99, 801–814. <https://doi.org/10.1016/j.jweia.2011.03.003>
- Wakimoto, R.M., 1985. Forecasting Dry Microburst Activity over the High Plains. *Mon. Wea. Rev.* 113, 1131–1143. [https://doi.org/10.1175/1520-0493\(1985\)113<1131:FDMAOT>2.0.CO;2](https://doi.org/10.1175/1520-0493(1985)113<1131:FDMAOT>2.0.CO;2)
- Wakimoto, R.M., 1982. The Life Cycle of Thunderstorm Gust Fronts as Viewed with Doppler Radar and Rawinsonde Data. *Mon. Wea. Rev.* 110, 1060–1082. [https://doi.org/10.1175/1520-0493\(1982\)110<1060:TLCOTG>2.0.CO;2](https://doi.org/10.1175/1520-0493(1982)110<1060:TLCOTG>2.0.CO;2)
- Wilson, J.W., Roberts, R.D., Kessinger, C., McCarthy, J., 1984. Microburst Wind Structure and Evaluation of Doppler Radar for Airport Wind Shear Detection. *J. Climate Appl. Meteor.* 23, 898–915. [https://doi.org/10.1175/1520-0450\(1984\)023<0898:MWSAEO>2.0.CO;2](https://doi.org/10.1175/1520-0450(1984)023<0898:MWSAEO>2.0.CO;2)
- Wilson, J.W., Wakimoto, R.M., 2001. The Discovery of the Downburst: T. T. Fujita's Contribution. *Bulletin of the American Meteorological Society* 82, 49–62. [https://doi.org/10.1175/1520-0477\(2001\)082<0049:TDOTDT>2.3.CO;2](https://doi.org/10.1175/1520-0477(2001)082<0049:TDOTDT>2.3.CO;2)
- Wolfson, M.M., 1988. Characteristics of Microbursts in the Continental United States.

- Wood, G.S., Kwok, K.C.S., Motteram, N.A., Fletcher, D.F., 2001. Physical and numerical modelling of thunderstorm downbursts. *Journal of Wind Engineering and Industrial Aerodynamics* 89, 535–552. [https://doi.org/10.1016/S0167-6105\(00\)00090-8](https://doi.org/10.1016/S0167-6105(00)00090-8)
- Xu, Z., Hangan, H., 2008. Scale, boundary and inlet condition effects on impinging jets. *Journal of Wind Engineering and Industrial Aerodynamics* 96, 2383–2402. <https://doi.org/10.1016/j.jweia.2008.04.002>
- Yao, J., Lundgren, T.S., 1996. Experimental investigation of microbursts. *Experiments in Fluids* 21, 17–25. <https://doi.org/10.1007/BF00204631>
- Zhang, Y., Hu, H., Sarkar, P.P., 2013. Modeling of microburst outflows using impinging jet and cooling source approaches and their comparison. *Engineering Structures* 56, 779–793. <https://doi.org/10.1016/j.engstruct.2013.06.003>

## Chapter 4

### 4 Conclusions and Recommendations

The scope of the present study is two-folded. First, it uses an objective time-series analysis method to evaluate the different stages and the transient nature of downburst events. This method divides the downburst time histories into statistically significant segments and is applied on full scale downburst events spanning three continents. Second, the study performs a comprehensive parametric analysis on large scale downburst experiments conducted in the WindEEE Dome. The velocity data from these experiments are analyzed for the first time in a similar way as for full scale events. Comparisons between mean and most importantly turbulent characteristics of downbursts between laboratory experiments and full scale events are presented. Concluding remarks as well as recommendations for future work are included at the end of this chapter.

#### 4.1 Summary

Chapter 2 of this thesis presents the analysis of transient nature of full scale downburst events. In total 37 downburst records from 14 downburst events from 3 different continents (North America, Europe and Australia) are investigated. An objective method is introduced here to find different stages of downbursts by detecting the change points in their time series based on different statistical properties such as Mean (M), Standard deviation (D) and Linear trend (LT) (Lavielle, 2005; Killick et al., 2012). This method of identifying change points has been implemented to segment different stages of downburst events.

In the following chapter, Chapter 3, experimental simulation of large-scale model downbursts in the WindEEE Dome is described to investigate the characteristics of downburst outflows. Experiments are conducted for two  $H/D$  ratios ( $H/D=0.8$  and  $H/D=1.2$ ) and six Reynolds numbers ( $Re = 1.82 \times 10^6$ ,  $1.83 \times 10^6$ ,  $2.62 \times 10^6$ ,  $2.68 \times 10^6$ ,  $4.09 \times 10^6$ ,  $4.24 \times 10^6$ ) based on two downdraft jet diameters and three downdraft intensities

(20, 30 and 50% of the rated RPM of the fans). Point measurements for downburst outflows are captured using 12 4-hole pressure probes (TFI-Cobra probes) in a vertical mast positioning over 6 radial locations from the centre of the downdraft. In addition, planar measurements of downburst flow field are performed using Particle Image Velocimetry (PIV) technique in a vertical plane of  $2.7 \text{ m} \times 1.4 \text{ m}$ . Wind velocity data is decomposed into a deterministic low frequency moving mean and a residual fluctuation. Statistical analysis on reduced turbulent fluctuation is conducted to find the similarities between the experimentally simulated model downbursts and the full scale downburst events. In addition, three wind ratios ( $R, G_{max}, \hat{G}$ ) of importance for wind loading on structures are compared with full scale downburst data from Solari et al. (2015). Vortex dynamics obtained from the PIV experiment are compared with the available full scale data.

## 4.2 Conclusions

Based on the overall findings of this thesis, the following major conclusions are stated below. Major findings from Chapter 2 are:

- The objective methodology separates the downburst time series into 3-4 segments using statistical parameter mean (M) and linear trend (LT), and 2-3 segments using standard deviation (SD). Sub-division of multiple peaks in downburst time history is found using M and LT approaches whereas SD tends to isolate the whole thunderstorm
- The penalty constant function,  $\gamma$  is dependent on the sampling frequency,  $f_s$ . For the M model, the relation between  $\gamma$  and anemometer sampling frequency,  $f_s$  is linear with the proportionately constant being 1200. Using the M method, the best results in respect of segmentation of time series are achieved with  $\gamma$  to be 12400-15000 for  $f_s = 10 \text{ Hz}$ , 2600-3160 for  $f_s = 1 \text{ Hz}$  and 400 for  $f_s < 1 \text{ Hz}$ . Similarly, better results are found  $\gamma$  to be 3000-8000, 300-1250 and 250 for  $f_s = 10 \text{ Hz}$ , 1 Hz or  $f_s < 1 \text{ Hz}$ , respectively. In the case of using LT method, the values of  $\gamma$  are 9000-11000, 1220-1970 and 250, respectively for similar values of  $f_s$

- The duration of the first downburst peak (ramp up time to first peak plus ramp down time) is typically shorter than 5 min. Duration of the ramp up time (interval between the start of the downburst and the moment of peak velocity) is much shorter compared to downburst duration, typically less than 1 min
- Background winds prior to the downburst peak are about 2-3 times weaker than the mean wind speed in 60% of the analyzed cases. In general, mean wind speed prior to the downburst peak is higher than the mean wind speed after the downburst peak
- Standard deviation of the wind speed during the downburst peak is twice compared to that of before and after the peak event. Turbulence fluctuations in background winds are always smaller compared to the downburst event

Major findings from Chapter 3 are:

- Considering different criteria (characteristics of running mean, residual fluctuation, joint Fourier transforms of running mean and residual fluctuation, mean, standard deviation, skewness and kurtosis of reduced turbulent fluctuations),  $T_{avg} = 0.1$  s is selected as a reasonable averaging time for the simulated downbursts in WindEEE Dome
- At similar Reynolds number, the profiles corresponding to  $H/D > 1$  have a more pronounced “nose” shape when compared to the ones for  $H/D < 1$ .
- The probability density function of the reduced turbulent fluctuation ( $\tilde{u}'$ ) is found to be a random stationary gaussian process, similar to the full scale downburst records
- Spectral analysis of the reduced turbulent fluctuation ( $\tilde{u}'$ ) shows that the dissipation of the kinetic energy in the inertial sub-range has a slope of  $-5/3$ , similar to the slope of spectra in the inertial sub-range of synoptic events, in particular for  $Re \geq 2.62 \times 10^6$

- Power Spectral Density of the reduced turbulent fluctuation ( $\tilde{u}'$ ) is in fair agreement with the analytical model proposed by Solari and Piccardo (2001)
- The values of three wind speed ratios ( $R, G_{max}, \hat{G}$ ), important to loading and response of structures to downburst winds, match within 10% of their average values of the 93 real downburst records reported in Solari et al. (2015).
- The ratio  $\bar{u}_{max}/u_{co}$  for all  $Re$  cases investigated in this study resulted in the values in the range between 4.0 and 6.4 which is somewhat in agreement with the observation of Lundgren et al. (1992). Here,  $\bar{u}_{max}$  is the maximum of the time averaged mean velocity and  $u_{co}$  is the convective velocity of the vortex centre
- The location of the maximum velocity relative to the primary vortex centre in the experimentally simulated downburst at WindEEE is comparable with full scale events reported in Hjelmfelt (1988).
- When the normalized heights of the vortex centre trajectories are compared with the full scale event on 17 June, 1978 (Wakimoto (1982), a similar trend is observed between WindEEE downbursts and full scale downburst events. This type of vortex dynamics comparison between simulated and full scale events are the first efforts in this direction

### 4.3 Recommendation and future work

In spite of the extensive analysis on the topics stated in this thesis, there is still room for further development and improvement on the current body of knowledge. In this regard, following recommendations for future works can be made:

- The objective segmentation method proposed here can be coupled with a downburst detection algorithm which can automatically extract and analyze downburst characteristics such as ramp-up and downburst duration

- Scaling of the downburst is possible using this segmentation method. Velocity scale can be achieved by comparing peak velocity with full scale events whereas time and length scales can be determined based on duration of the downburst or ramp up time to the peak velocity and velocity scale
- To capture a large field of view, PIV is performed with low sampling frequency and therefore turbulent characteristics of the flow could not be analyzed from the PIV data. PIV with high sampling frequency using high speed camera and laser could provide detailed information on the turbulent characteristics of the downburst flow at high spatial resolution
- The high speed PIV is of most interest when potentially used to analyze the effects of roughness.

## 4.4 References

- Hjelmfelt, M.R., 1988. Structure and Life Cycle of Microburst Outflows Observed in Colorado. *J. Appl. Meteorol.* 27, 900–927. [https://doi.org/10.1175/1520-0450\(1988\)027<0900:SALCOM>2.0.CO;2](https://doi.org/10.1175/1520-0450(1988)027<0900:SALCOM>2.0.CO;2)
- Killick, R., Fearnhead, P., Eckley, I.A., 2012. Optimal Detection of Change-points With a Linear Computational Cost. *J. Am. Stat. Assoc.* 107, 1590–1598. <https://doi.org/10.1080/01621459.2012.737745>
- Lavielle, M., 2005. Using penalized contrasts for the change-point problem. *Signal Process.* 85, 1501–1510. <https://doi.org/10.1016/j.sigpro.2005.01.012>
- Lundgren, T.S., Yao, J., Mansour, N.N., 1992. Microburst modelling and scaling. *J. Fluid Mech.* 239, 461–488. <https://doi.org/10.1017/S002211209200449X>
- Solari, G., Burlando, M., De Gaetano, P., Repetto, M.P., 2015. Characteristics of thunderstorms relevant to the wind loading of structures. *Wind Struct.* 20, 763–791. <https://doi.org/10.12989/was.2015.20.6.763>
- Solari, G., Piccardo, G., 2001. Probabilistic 3-D turbulence modeling for gust buffeting of structures. *Probabilistic Eng. Mech.* 16, 73–86. [https://doi.org/10.1016/S0266-8920\(00\)00010-2](https://doi.org/10.1016/S0266-8920(00)00010-2)



Wakimoto, R.M., 1982. The Life Cycle of Thunderstorm Gust Fronts as Viewed with Doppler Radar and Rawinsonde Data. *Mon. Weather Rev.* 110, 1060–1082.  
[https://doi.org/10.1175/1520-0493\(1982\)110<1060:TLCOTG>2.0.CO;2](https://doi.org/10.1175/1520-0493(1982)110<1060:TLCOTG>2.0.CO;2)

## Appendices

### Appendix A: Figures presented here are in support of the Chapter 3.

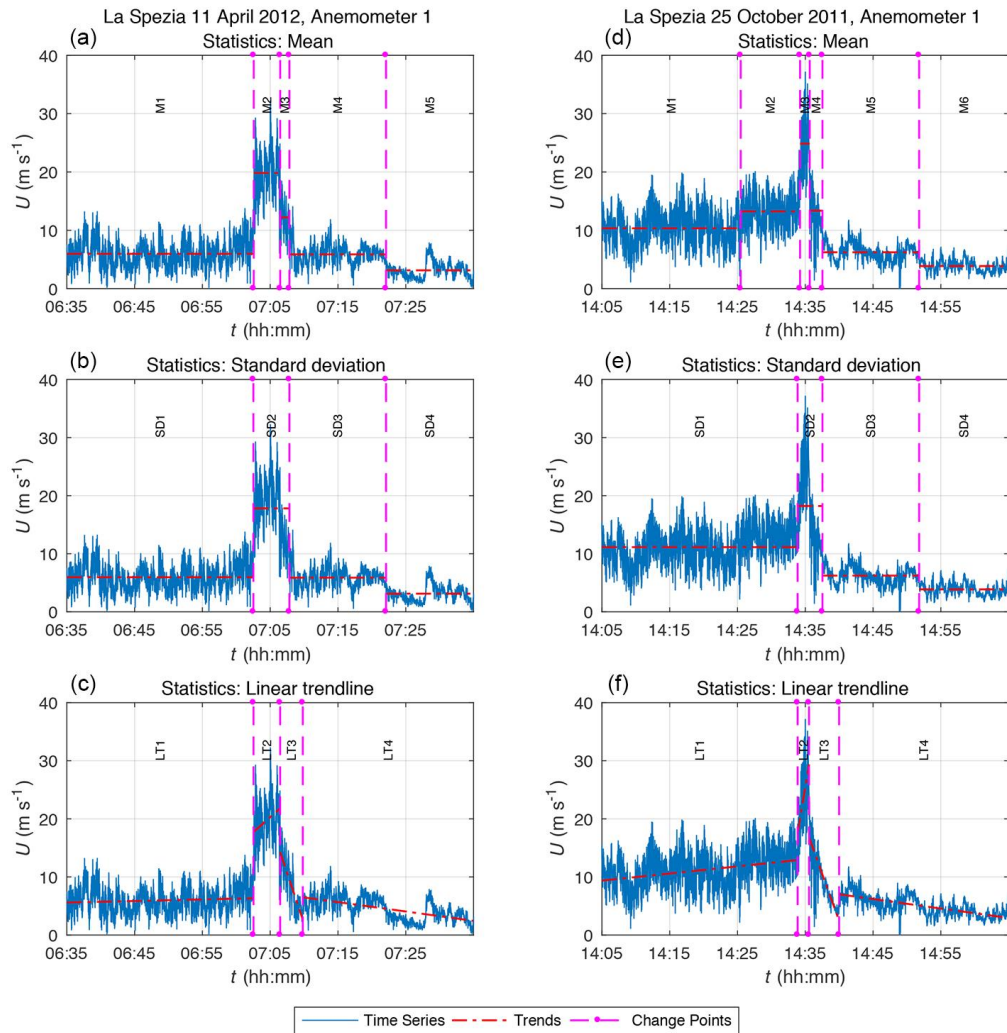


**Figure A 1: Three segmentation methods applied to a downburst records from La Spezia**

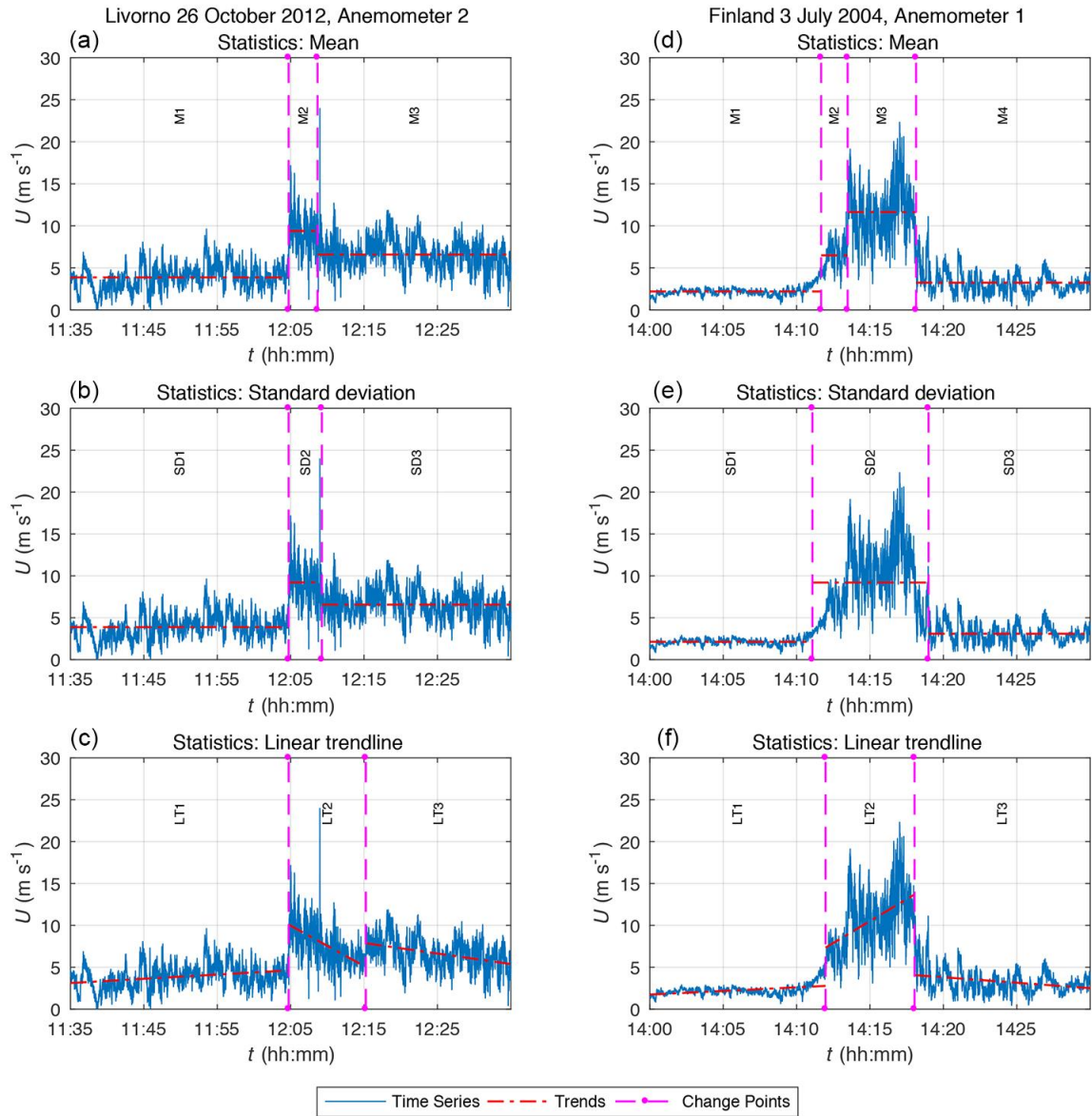


**Figure A 2: Three segmentation methods applied to a downburst records from Livorno (left panels) and Finland (right panels)**

## Appendix B: PIV error correction

According to Cowen and Monismith (1997) the total error of particle Image Velocimetry depends on the sum of errors originating from seeding particles diameter, density, out of plane motion of particles, velocity gradient, dynamic range, peak locking and Adaptive gaussian Window interpolation. The mean and RMS error of various sources of error are obtained by using graphs from Cowen and Monismith (1997). Total error are calculated based on this errors. RMS error is defined by Cowen and Monismith (1997) which is caused by random noise during imaging process.

### Particle size:

Figure 5a. in Cowen and Monismith (1997) provides a graph where errors due to particle size is presented. For the experiment in this thesis Ultratec power 9D industrial fog machine is used which uses Di-Ethyl-Hexyl-Sebacate (C<sub>26</sub>H<sub>50</sub>O<sub>4</sub>) as seeding particle that has an average diameter of 1  $\mu$ m. Coverting 1  $\mu$ m to pixels is equivalent to 0.00998 pixels. From Figure 5. In Cowen and Monismith (1997) the smallest particle diameter is 1 pixel. So the error based on 1 pixel diameter particle size is used here.

$$\text{Error related to particle size, } \varepsilon_{ps} = (-0.03) + 0.095 = 0.065 \text{ pixels}$$

For better estimation of the error due to the particle size of 0.00998 pixel diameter, Figure 13. In Prasad et al. (1992) is used. From this Figure the bias and peak locking errors of a particle is found. For the particle size 00098 pixel diameter a 43% larger error is found when compared to the error associated with a particle of 1 pixel in diameter. Additional error in particle diameter was estimated to be 30%, that means,

$$\varepsilon_{ps} = 0.065 \times 1.3 = 0.0845 \text{ pixels}$$

### Velocity gradient:

Mean and RMS error due to velocity gradient is calculated based on Figure 5e. from Cowen and Monismith (1997). The maximum radial and axial velocity gradient ( $\partial u_r / \partial r$  and

$\partial u_{ax}/\partial r$  respectively) is found here  $27.46 \text{ s}^{-1}$  and  $20.76 \text{ s}^{-1}$  for  $Re$   $4.24 \times 10^6$  and  $2.68 \times 10^6$  respectively. The error corresponding to velocity gradients can be approximated as follows

$$\varepsilon_{g,u_r} = (-0.005) + 0.01 = 0.005 \text{ pixels}$$

$$\varepsilon_{g,u_{ax}} = (-0.002) + 0.015 = 0.013 \text{ pixels}$$

### **Adaptive Gaussian Window:**

To calculate error associated with Adaptive Gaussian Window (AGW) interpolation Figure 5f. from Cowen and Monismith (1997) was used. Only RMS error was reported in Figure 5f. as the mean results were unaffected. The dynamic range for 8-bit CCD cameras varies in between 100 and 150 counts. Therefore, the AGW averaging error is approximately,

$$\text{Error related to Adaptive Gaussian Window, } \varepsilon_{AGW} = 0.08 \text{ pixels}$$

### **Seeding density:**

Error due to seeding density changes from one image to another. So the number of particles from one image to another is also changed in  $32 \times 32$  window. Assuming that there is an approximate 30 particles in a  $32 \times 32$  window, error from Figure 5c. from Cowen and Monismith (1997) is given below.

$$\text{Error related to seeding density, } \varepsilon_{sd} = (-0.03) + 0.05 = 0.02 \text{ pixels}$$

### **Out of plane motions:**

In the measurement area, the thickness of the laser sheet was about 2mm which is equivalent to 19.96 pixels. The maximum in plane displacement in this experiment was about 17.25 pixels which is lower than the thickness of the laser sheet. Therefore, the error due to the out of plane motion of particles is considered negligible.

Therefore the total error is calculated by adding all the aforementioned error, which is,

$$\text{Total error, } \varepsilon_T, u_r = .01895 \text{ pixels}$$

$$\text{Total error, } \varepsilon_T, u_{ax} = 0.1975$$

So, the total error of measurement for the radial velocity is  $0.23 \text{ ms}^{-1}$  or 1.53% of the maximum moving mean radial velocity and for axial velocity  $0.27 \text{ ms}^{-1}$  or 2.7% of the maximum moving mean axial velocity.

## References

- Cowen, E.A., Monismith, S.G., 1997. A hybrid digital particle tracking velocimetry technique. *Experiments in Fluids* 22, 199–211. <https://doi.org/10.1007/s003480050038>
- Prasad, A.K., Adrian, R.J., Landreth, C.C., Offutt, P.W., 1992. Effect of resolution on the speed and accuracy of particle image velocimetry interrogation. *Experiments in Fluids* 13, 105–116. <https://doi.org/10.1007/BF00218156>

## Curriculum Vitae

**Name:** **Chowdhury Md Junayed**

**Post-secondary Education and Degrees:** **University of Western Ontario**  
London, Ontario, Canada  
M.E.Sc. (2016-Present)

**Bangladesh University of Engineering and Technology**  
Dhaka, Bangladesh  
B.Arch. (2007-2013)

**Honours and Awards:** **1<sup>st</sup> Prize Winner**  
Third Earth Architecture Competition by NKA Foundation, USA  
2015

**3<sup>rd</sup> Prize Winner**  
National Competition for Designing a Green Commercial High Rise Building, Dhaka, Bangladesh  
2014

**Work Experience** **Lecturer**  
University of Asia Pacific, Dhaka  
Department of Architecture  
May 2014- September 2016

**Associate Architect**  
Aesthetes Architectural Company, Dhaka  
January 2014- August-2016

**Related Work Experience** **Teaching Assistant**  
Engineering Statistics (Winter 2017, Fall 2017, Winter 2018)  
University of Western Ontario  
2016-2018

### Conference Proceedings:

1. Junayed C, Jubayer C, Parvu D, Hangan H. (2017) Simulation and characterization of wind flow in large-scale laboratory produced downbursts. In: Thousand Islands Fluids Dynamics Conference 2017, Gananoque, Ontario, Canada.
2. Junayed C. Jubayer C, Parvu D, Karami M, Hangan H. (2018) Wind Flow Characteristics of a model downburst. In: Proceedings of the ASME 2018 5<sup>th</sup> joint US-European Fluids Engineering Division Summer Conference, Montreal, Canada, FEDSM2018-83443.